MECHANISTIC ANALYSIS OF CLUSTER TRANSFER TO APO-ACCEPTORS IN ISC PATHWAY

A Dissertation

by

DEEPIKA DAS

Submitted to the Office of Graduate and Professional Studies of
Texas A&M University
in partial fulfillment of the requirements for the degree of

DOCTOR OF PHILOSOPHY

Chair of Committee,	David Barondeau
Committee Members,	Frank Raushel
	Paul Lindahl
	Hays Rye
Head of Department,	Simon North

May 2018

Major Subject: Chemistry

ABSTRACT

Iron-sulfur (Fe-S) clusters are ubiquitous protein cofactors that are required for some of the most important reactions in nature, including nitrogen fixation, oxidative phosphorylation, and photosynthesis. Multiple biosynthetic pathways have evolved for assembling Fe-S clusters and delivering them to protein targets. The ISC (Iron-Sulfur Cluster assembly) pathway is found in many prokaryotes and in eukaryotic mitochondria. A central component of the pathway is a cysteine desulfurase, which uses a pyridoxal phosphate (PLP) cofactor to convert cysteine to alanine and functions as a sulfur source. The scaffold protein IscU combines this sulfur with ferrous iron and electrons to synthesize Fe-S clusters. The Fe-S clusters can then be transferred to acceptor proteins such as the monothiol glutaredoxins (Grx4 in bacteria, GRX5 in humans) and ferredoxin (Fdx). The chaperone co-chaperone pair (HscA-HscB) accelerate cluster transfer reactions from holo-IscU to Grx4 and Fdx. In eukaryotes, Fe-S cluster biosynthesis is stimulated by frataxin (FXN), which is associated with the neurodegenerative disease Friedreich's ataxia (FRDA). To gain a mechanistic understanding into these processes, we employed stopped-flow kinetic analysis and developed visible circular dichroism, fluorescence reporter, and radioactivity-based assays. Importantly, we develop the first complete functional assay in which Fe-S clusters are built and then transferred to a target protein. Here, studies will be presented that show (1) FXN accelerates specific steps in the PLP-associated chemistry of the cysteine desulfurase, interprotein sulfur transfer, and intermediate Fe-S cluster formation on the scaffold protein; (2) a FXN suppressor mutant identified on the scaffold

protein functions differently than FXN, accelerating cluster transfer from the scaffold protein to GRX5; (3) glutaredoxin functions as an intermediate carrier in cluster transfer reactions from IscU to apo acceptor proteins Fdx and HcaC; and (4) chaperones accelerate cluster transfer reactions from IscU to Grx4 and do not appear to assist in the folding or unfolding of the target proteins. Overall, this work provides new mechanistic insight into specific steps of Fe-S cluster assembly and transfer and may provide new opportunities for drug discovery to treat FRDA.

To my parents, teachers and my husband….

ACKNOWLEDGEMENTS

I would like to thank my research advisor, Dr. David Barondeau for providing freedom to pursue work of my choice and his constant support through the ups and downs of the course of my research. I would like to thank my committee members, Dr. Raushel, Dr. Lindahl, and Dr. Rye for their guidance and insight t throughout different presentations and meetings.

I would like to thank Dr. Begley for letting us use the CD spectrometer and other facilities at his research laboratory. I would also like to thank Dr. Lindahl for working with us on the collection and analysis of Mössbauer spectroscopy performed on High molecular weight species (HMWS).

I will be forever thankful to Barondeau lab members for their constant support, criticism, help and providing a nurturing environment. I would especially like to thank former lab members, Dr. Nicholas Fox, Dr. James Vranish and Dr. Darell J. Martin for their mentoring and guidance and Robert, Melissa, Hyeran for their support. I would like to acknowledge the current lab members Shachin Patra, Seth Cory, Seth Van Andel and Steven Havens for their useful suggestions and letting me use and misplace their pipets. I would like to thank Shachin Patra for being a great support-system both inside and outside lab all through my graduate life.

I am grateful to my parents for their unconditional trust and encouragement all along. I would like to thank the friends and colleagues at Texas A&M University for a great experience and helping me make a home away from home at College Station.

Lastly, I would like to thank my husband, Dr. Atanu Acharya who has been making my worst days bad and good days best since we are together. He has been my worst critic and biggest fan all along and I hope we can keep on exploring the highs and lows together forever.

CONTRIBUTORS AND FUNDING SOURCES

This work was supervised by a dissertation committee consisting of Professor David Barondeau (advisor), Professor Frank Raushel and Professor Paul Lindahl of the Department of Chemistry and Professor Hays Rye of the Department of Biochemistry and Biophysics.

In Chapter II, the isolation and characterization of High Molecular Weight Species (HMWS) were performed by Dr. Nicholas Fox. Collection and analysis of Mössbauer spectra were performed by Dr. Nickelous Fox and Dr. Mrinmoy Chakrabarti respectively under supervision of Prof. Paul Lindahl and Dr. David Barondeau and was published in 2015. In Chapter III, studies on the effect of CyaY on i) quinonoid formation and decay ii) formation and transfer of persulfide intermediate on IscS and were performed by Shachin Patra. In Chapter IV, assay for persulfide detection and quantification was developed and run by Shachin Patra along with stopped flow studies on intermediate species in cluster assembly. In Chapter V, fluorescence quenching experiments and global fit kinetic analysis were carried out by Dr. James Vranish and was published in 2016.

All other work conducted for the dissertation was completed by the student independently.

Graduate study was supported by Teaching Assistantship from department of Chemistry at Texas A&M University. This work was made possible in part by funding from National Science Foundation (NSF) under Grant Number 444431-00001, National

Institutes of Health (NIH) under Grant Number 412561-00001 and Robert A. Welch Foundation under Grant Number 456460-20000.

TABLE OF CONTENTS

LIST OF FIGURES

LIST OF TABLES

CHAPTER I

INTRODUCTION

Iron sulfur clusters are one of the earliest protein cofactors used by living systems [1]. They are abundant in diverse life forms from prokaryotes (i.e. *E. coli*) to eukaryotes ranging from yeast to humans [2]. Iron can switch between oxidation states of +3 and +2 which enables iron-sulfur clusters to accept or donate electrons in complex enzymatic reactions [3]. In addition, iron-sulfur clusters can exist in different stoichiometries, flexible geometries and have a wide range of reduction potentials. These properties make them well-suited to participate in wide variety of processes like electron-transfer, substrate activation and gene regulation [4-6]. Hence, multiple biosynthetic pathways have evolved for the assembly of iron-sulfur clusters and their delivery to different Fe-S containing proteins [7-9]. Though widely studied, mechanistic details of the cluster biosynthesis and delivery process remain poorly understood along with the protein-protein interactions involved therein.

Iron-sulfur Clusters

Fe-S clusters consist of ferrous or ferric ions coordinated by bridging sulfide and, typically cysteine thiolates from proteins. However, histidine, aspartate, serine and amides from protein backbone have also been observed to serve as ligands [10]. Different forms of iron-sulfur clusters are observed in Nature with distinct properties and functions (Fig. 1.1). Though, [2Fe-2S] and [4Fe-4S] are the most common forms, additional iron sulfur clusters with varying number of iron and sulfides such as [3Fe-4S], [4Fe-3S], [5Fe-5S] and [8Fe-7S] are also known.

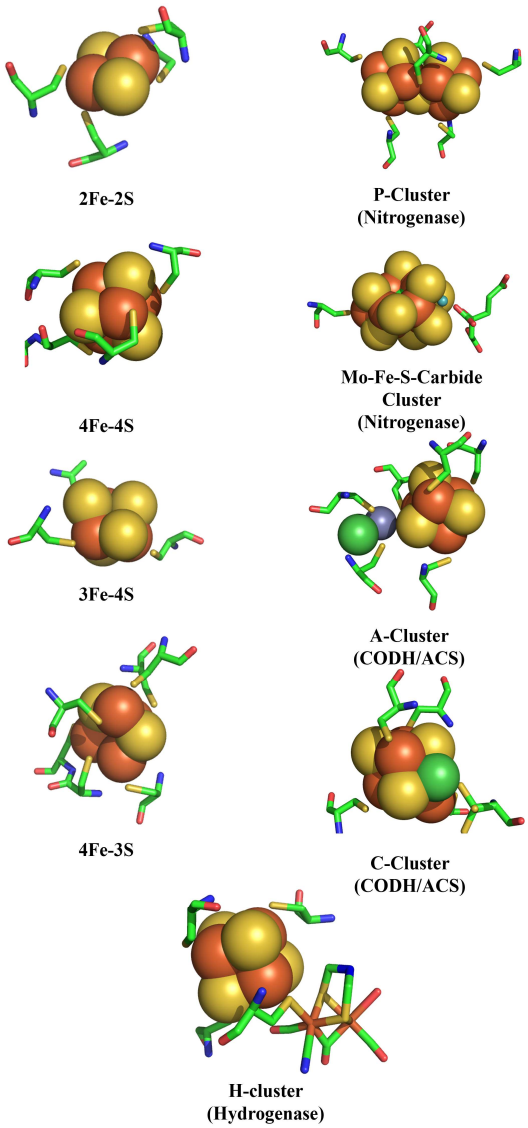

Figure 1.1. Iron-sulfur cluster protein cofactors found in nature. Orange and yellow spheres represent iron and sulfur ions, respectively. The small blue sphere in the Mo-Fe-S-Carbide is a molybdenum ion and the green center ion is a carbide. The green spheres in the CODH/ACS metal complexes are nickel ions and the grey sphere is a zinc ion (this is inactive form of the enzyme. The active form contains Ni^{2+} instead of Zn^{2+}). Coordinating cysteine ligands are shown.

Clusters bound to metal ions other than iron are also found in Nature. For example, carbon monoxide dehydrogenase has two separate iron-sulfur clusters coupled to a Ni ion [11]. Nitrogenase harbors a Mo-Fe-S cluster that consists of one Mo, seven Fe, a carbide, and nine sulfide ions, and is bound with a molecule of homo-citrate [12]. Many enzymes rely on ferredoxin, which typically contain a [2Fe-2S] cluster, to channel electrons into or out of their active site and catalyze chemical reactions [13]. [4Fe-4S] clusters pair with S-adenosylmethionine to catalyze an array of chemical reactions in the radical-SAM superfamily [14]. DNA binding proteins, such as IscR, bind Fe-S clusters as negative feedback transcriptional regulators [15]. More recently, DNA repair enzymes have been implicated in using Fe-S clusters to sense DNA damage [16]. The wide variety of functions for Fe-S proteins requires a robust Fe-S cluster maturation system that can incorporate clusters into hundreds of different protein targets that can tailor their orientations, ligands, redox properties and substrate access [17].

Iron-sulfur Cluster Biosynthesis Pathways

Though iron sulfur clusters can readily self-assemble from free sulfide and iron [18], it is non-feasible to use this as an *in vivo* strategy for their formation due to the toxic effects of free iron and sulfide [19]. Hence, several multi-component pathways were evolved to ensure regulated iron-sulfur cluster biosynthesis in cells. Defects in these pathways result in complications including iron trafficking problems, mitochondrial dysfunction and onset of several diseases [20]. Four biosynthetic pathways known as NIF, ISC, SUF and CIA have been identified. The first pathway to be discovered was NIF (Nitrogen Fixation Pathway). NIF is found in prokaryotes and is associated with cluster

biosynthesis for nitrogenase [7]. The Iron sulfur cluster assembly pathway (ISC), the second pathway discovered, is present in both prokaryotes and eukaryotic mitochondria. It is responsible for iron sulfur cluster biogenesis for multiple targets under normal growth conditions [21]. Another specialized pathway in prokaryotes is sulfur mobilization pathway (SUF) which often functions to assemble clusters under conditions of oxidative stress [8]. Eukaryotes also have cytosolic iron-sulfur protein assembly pathway (CIA) that is involved in maturation of iron-sulfur protein clusters in the nucleus and cytosol which is fundamentally different than the other pathways and will not be discussed here [9]. The NIF, ISC and SUF pathways are similar in having a cysteine desulfurase enzyme that converts cysteine to alanine thereby providing the sulfur required for cluster assembly and a scaffold protein on which the cluster is assembled (Fig. 1.2). Chemically, the cluster assembly reaction can be represented as:

$$2\ \text{L-cysteine} + 2\ Fe^{2+} + 2\ e^{-} \rightarrow [2Fe\text{-}2S]^{2+} + 2\ \text{L-alanine}$$

The source of iron and electrons for the reaction remains controversial with many possible candidates suggested in the literature. These pathways are essential and hence knock-outs are lethal except in case of organisms with multiple operative pathways. For example, *E. coli* contains both SUF and ISC pathways and deletion of one system is not lethal. However, in humans, impaired cluster biosynthesis in the mitochondria, which only has the ISC pathway, leads to several disorders like Friedreich's ataxia, sideroblastic anemia and myopathy [22]. Hence, a deeper mechanistic understanding of ISC pathway would facilitate targeting the diseases resulting from defects associated with cluster assembly machinery.

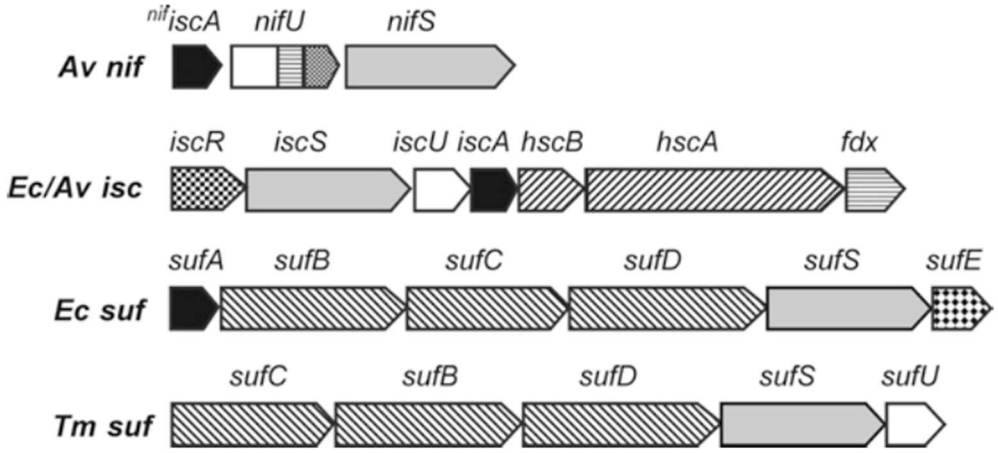

Figure 1.2. Operon structure of Fe-S biosynthetic systems. NIF, ISC, and SUF operons are shown for *Azotobacter vinelandii* (Av), *Escherichia coli* (Ec), and *Thermotoga maritima* (Tm). Cysteine desulfurases are indicated by solid gray genes. U-type scaffold proteins/domains are indicated by white genes. Reproduced with permission from Bandyopadhyay S, Chandramouli K, Johnson MK. 2008. Biochem Soc Trans. 36 (Pt 6), 1112-9. [193]© The Biochemical Society.

ISC Pathway

The ISC pathway is the only pathway shared between humans and prokaryotes. In *E. coli*, most of the genes for the pathway are encoded in a single operon [21]. The operon encodes genes for IscS, IscU, HscA, HscB, IscA, Fdx, IscR and IscX. IscS is cysteine desulfurase that converts cysteine to alanine and provides sulfur for cluster assembly. IscU is the scaffold protein on which [2Fe-2S] and possibly [4Fe-4S] clusters are assembled [23]. Electrons required for cluster synthesis may be provided by Fdx [24]. IscA has been proposed to function as an iron donor and as an alternate scaffold protein responsible for synthesis of [2Fe-2S] and [4Fe-4S] clusters [25]. HscA-HscB form the chaperone/co-chaperone pair that have been shown to accelerate the cluster transfer from IscU to apo-Fdx [26] IscS is cysteine desulfurase that converts cysteine to alanine and provides sulfur for cluster assembly. IscU is the scaffold protein on which [2Fe-2S] and possibly [4Fe-4S] clusters are assembled [23]. Electrons required for cluster synthesis may be provided by Fdx [24]. IscA has been proposed to function as an iron donor and as an alternate scaffold protein responsible for synthesis of [2Fe-2S] and [4Fe-4S] clusters [25]. HscA-HscB form the chaperone/co-chaperone pair that have been shown to accelerate the cluster transfer from IscU to apo-Fdx [26]. IscR acts as the negative feedback regulator for the ISC operon [27]. IscX is suggested to be an iron-donor or to have regulatory role [28, 29]. Additional proteins outside the ISC operon are also involved in cluster biosynthesis via the ISC pathway. For example, monothiol glutaredoxins function in the cluster transfer process [30] and frataxin (FXN) has been shown to be crucial in cluster biosynthesis for eukaryotes [31].

Major Players in ISC Pathway

IscS is PLP dependent cysteine desulfurase that converts L-cysteine to L-alanine and generates a persulfide intermediate on an absolutely conserved cysteine residues that resides on a mobile loop near the active site [32]. The persulfide can be transferred to the scaffold protein, IscU, for cluster synthesis or cleaved by reductants like DTT to generate sulfide for monitoring cysteine desulfurase activity. Importantly, cleavage of the persulfide with reductants generates sulfide, which can readily combine with iron in a chemical reaction, and can seriously cripple the ability to monitor physiological (enzymatic) reactions using *in vitro* Fe-S assembly assays.

IscU serves as the scaffold protein for cluster assembly. The Fe-S cluster is ligated by three conserved cysteine residues from IscU. The identity of the physiologically relevant fourth ligand is still unclear [33-35]. Fe-S clusters can be assembled on IscU in the presence of IscS, iron and cysteine. A crystal structure of a [2Fe-2S] cluster bound to the IscU-IscS complex revealed the cluster can be ligated by the three cysteines from IscU and the mobile loop cysteine of IscS [36]. There is also evidence of [2Fe-2S] cluster bound by cysteine residues of the two subunits in an IscU dimer [23]. In spite of this available information, the identity of the species responsible for transferring the clusters to downstream apo-acceptors is still not clear. In addition, although IscU clearly functions as the scaffold to build Fe-S clusters, the order of events, including whether iron or sulfur is incorporated first, has not been firmly established.

Fdx is a [2Fe-2S] containing protein which is believed to behave as an electron source for the cluster biosynthesis. This stems from the observation that reduced

ferredoxin is oxidized in the presence of IscS and cysteine leading them to propose formation of persulfide radical in the process as there was no exogenous iron present [24]. There have been multiple studies on interaction of Fdx with other proteins. Ferredoxin and IscU have been shown to independently bind to IscS [24, 191]. NMR data show that conformation of IscU was perturbed on addition of Fdx into IscU-IscS complex. This data could be interpreted as dissociation of IscU from IscS in presence of Fdx or conformational change of iscU in presence of Fdx due to the formation of a ternary complex. Another puzzling observation is the competition of CyaY and Fdx for binding to IscS [192]. The significance of the interactions remains unclear.

HscA is an ATPase and belongs to the Hsp70 (Heat Shock Protein 70) class of proteins but differs from its homologues like DnaK in having high 'substrate' specificity and selectively binding to specific client proteins [37]. Substrates for the chaperones are defined as proteins that bind in a nucleotide-dependent manner, have different affinities for different nucleotide-bound forms, and undergo conformational changes upon binding. HscA recognizes and binds IscU, the only substrate currently known, via a highly conserved LPPVK motif [38]. The basal ATPase activity of HscA is low but enhanced synergistically in the presence of IscU and HscB. HscB is a co-chaperone that recruits IscU and has recognition motifs for both HscA and IscU. Details of the mechanism by which the chaperones accelerate cluster transfer are poorly understood. The working model is that ATP-bound HscA binds to IscU with low affinity (T-state) and hydrolysis of ATP to ADP causes a conformational change on HscA, which leads to tighter binding

of ADP-bound HscA (D-state) to IscU and facilitates cluster transfer to the apo-acceptor [39] (Fig. 1.3).

Glutaredoxins have been proposed to function in Fe-S cluster storage, transfer and sensing [40]. Monothiol glutaredoxins (Grx4) are known to bind [2Fe-2S], [3Fe-4S] and [4Fe-4S] clusters [41]. Preliminary evidence supports monothiol glutaredoxins as intermediate cluster carriers that function downstream of IscU in cluster biosynthesis [144].

Frataxin (FXN) plays an important role in cluster biosynthesis as evident from FXN deletion phenotypes resulting in iron accumulation in mitochondria, increased oxidative stress and loss of activity of Fe-S enzymes [42]. Proposals for the role of FXN include an iron chaperone [43], iron donor for Fe-S cluster and heme biosynthesis [44] and detoxification of ROS [45]. Strong evidence was later obtained to support the role of FXN as an allosteric activator for the cysteine desulfurase in the presence of ISCU2 [31].

Comparison of Bacterial & Eukaryotic ISC Machinery

As the ISC pathway is conserved between prokaryotes and eukaryotes, homology is expected between the analogous components in *E. coli*. Human cysteine desulfurase (NFS1) is 59% identical to IscS, ISCU2 (human scaffold protein) is 70% identical to *E. coli* IscU and CyaY (FXN homolog in E.coli) is 20% identical to human FXN [46]. In spite of the high sequence identities, there are many functional differences between the proteins in the *E. coli* and human pathways. For example, eukaryotic NFS1 by itself has very low basal activity as compared to IscS and requires an accessory protein ISD11 for its structural stability and exists as an NFS1-ISD11 complex (SD) [47]. FXN acts as an

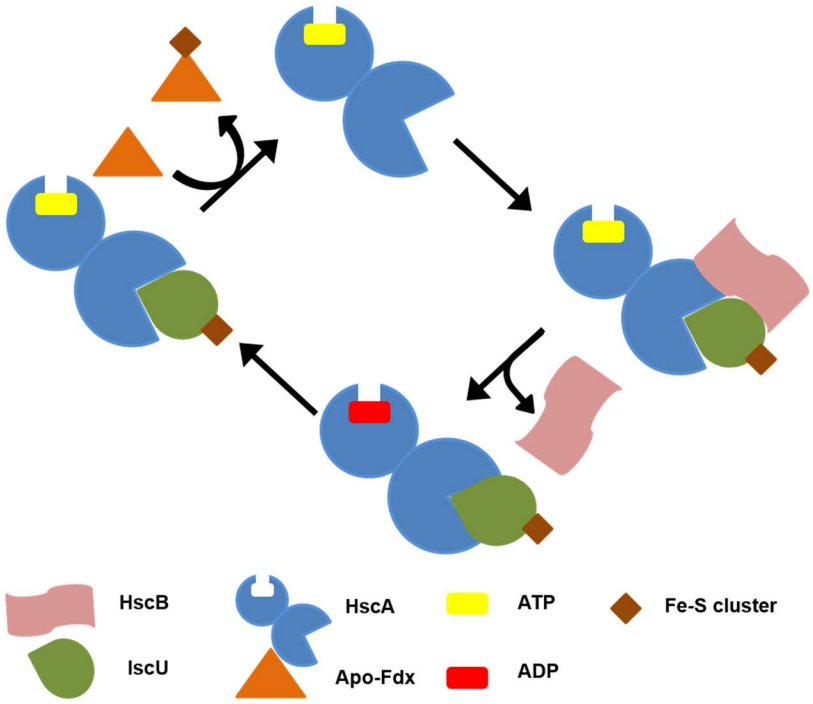

Figure 1.3. Model of chaperone-dependent acceleration of cluster transfer from holo-IscU to apo-Fdx. HscA has differential affinities for holo-IscU in ATP and ADP bound states. ATP hydrolysis to ADP is coupled to cluster transfer from holo-IscU. Adapted with permission from Hoff, K.G., J.J. Silberg, and L.E. Vickery, Proc Natl Acad Sci USA, 2000. **97**(14), 790-5. [39]

allosteric activator of cysteine desulfurase whereas CyaY, the bacterial homolog, is observed to inhibit cluster assembly on IscU. It has been observed that the functional difference of FXN and CyaY are dependent on the identity of cysteine desulfurase [46]. Both FXN and CyaY inhibit the rate of cluster assembly in assays containing the bacterial cysteine desulfurase, IscS, whereas they both accelerate the rate of cluster assembly in assays containing the human cysteine desulfurase complex, SD [46]. This is consistent with the recent discovery that the eukaryotic cysteine desulfurase complex exhibits a fundamentally different architecture compared to the IscS dimer [48, 49]. However, the mechanistic details of FXN activation and CyaY inhibition remain unclear.

Proteins Involved in Cluster Transfer

The next step of the cluster biogenesis is transfer of the cluster assembled on IscU to the downstream apo-acceptors (Fig. 1.4). The process needs to be highly fine-tuned for a multitude of reasons. First, iron-sulfur cluster intermediates need to be protected to prevent non-specific and possibly toxic side reactions. Moreover, ensuring specificity is critical as the ligating residues of different acceptors are amenable to coordinating other Fe-S cluster stoichiometries ([2Fe-2S] vs. [4Fe-4S] cluster) and metal ions (Cu and Zn in particular).

Monothiol glutaredoxins have been shown to accept clusters from holo-IscU in a chaperone-dependent fashion [50]. Cluster transfer from holo-glutaredoxin to apo ferredoxin has also been demonstrated [51]. Monothiol glutaredoxins have been proposed to function as intermediate cluster carriers for redistribution of clusters or as cluster-storage proteins [30]. Monothiol glutaredoxins also form cluster bound heterodimeric-

complexes with proteins like BolA [52] and Fra2 [53] which seem to function in iron regulation at the cellular level [54, 55].

Another class of proteins involved in cluster transfer are A-type proteins like IscA, SufA and NfuA. IscA can accept clusters from IscU [56] and reductively couple two [2Fe-2S] clusters to generate a [4Fe-4S] clusters [57]. IscA is also capable of transferring [2Fe-2S] and [4Fe-4S] clusters to several cluster targets [58]. Although mechanistic details are poorly understood, knockout studies of IscA show impaired levels of [4Fe-4S] proteins [59] pointing towards a role of IscA in assembly of [4Fe-4S] proteins. Glutaredoxins can transfer clusters to IscA [60] suggesting their involvement in transfer of [4Fe-4S] clusters to targets as well.

Chaperones accelerate cluster transfer from IscU to apo-acceptors in an ATP-dependent fashion [38]. HscB is the co-chaperone generally accepted to be responsible for recruiting IscU to HscA by forming a complex with IscU [39]. However, recent *in vivo* findings suggested that HscB is only required for cluster transfer to targets with a semi-conserved LYR amino acid motif [61]. Recently, HscB has been shown to reduce the rate of cluster assembly on IscU under some conditions [62] which has been suggested to support a CD-silent slow transferring holo-IscU:HscB complex. Yeast studies showed that IscS and HscB compete for binding IscU [63] whereas studies performed in *E. coli* demonstrate simultaneous binding of HscB and IscS to IscU [64]. HscA is an ATPase which selectively binds IscU via a LPPVK recognition motif in a nucleotide-dependent manner. The ATP-bound T-state has low affinity for IscU whereas after hydrolysis, the ADP-bound D-state binds IscU with stronger affinity. Though IscU is the only known

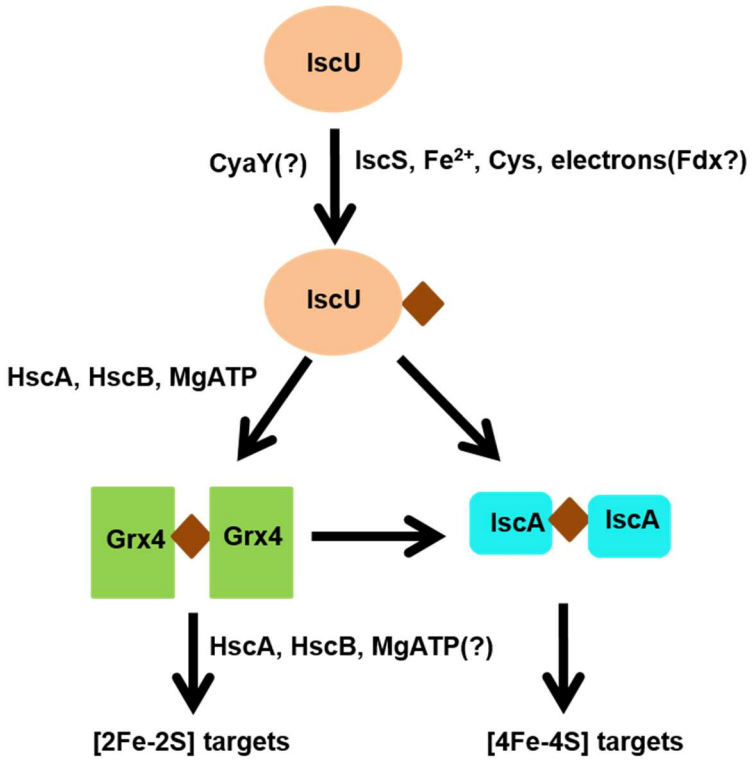

Figure 1.4. Model for the ISC cluster assembly and transfer pathway. A [2Fe-2S] cluster is synthesized on IscU in the presence of IscS, cysteine, ferrous iron, and reducing equivalents. The [2Fe-2S] cluster is then transferred to the intermediate cluster carrier protein, Grx4, in a reaction accelerated by chaperones (HscA-HscB) and dependent on in MgATP. [2Fe-2S]-Grx4 can then transfer the cluster to terminal apo-acceptor targets like ferredoxin in a reaction that may also be chaperone dependent. Grx4 can also transfer clusters to IscA, which apparently matures and delivers [4Fe-4S] clusters to appropriate targets.

client protein known for HscA, many studies have reported interaction of HscA with apo-acceptors like glutaredoxin and apo-BioB [65, 66].

In Vitro Study of Cluster Biosynthesis: Challenges and Strategies

The study of cluster biosynthesis poses many challenges at a technical level. For example, most *in vitro* studies have traditionally used reductants like DTT as a source of electrons in cluster assembly assays. Unfortunately, we now know these reagents initiate thiol-mediated cluster redistribution [67]. Another challenge is the study of cluster transfer from one protein to another using UV spectra as the different holo-proteins exhibit virtually identical spectra. Using CD spectroscopy is an effective alternative but has limitations, including low sensitivity and a high sample requirement and a requirement of data deconvolution gets very complicated for experiments with multi-component cluster-binding species. A novel fluorescence quenching assay developed in our lab addresses some of these issues. Proteins can be labeled with fluorophores, which report on cluster content even in the presence of other cluster binding proteins [59]. While the roles of many proteins remain unknown or controversial, along with the mechanistic details involved, a stepwise analysis of their effect on individual step(s) of cluster biosynthesis process is needed. For this, the entire process of biosynthesis is sub-divided into different steps like cysteine desulfurase activity, sulfur transfer, cluster synthesis and cluster transfer (Fig. 1.5).

Current Work and Future Directions

Many studies have been carried out to better understand the process of cluster transfer and the roles of different components therein but we are still faced with many

unanswered questions and need to re-evaluate some of the previous results in light of recent discoveries.

Glutaredoxin. Although, holo-Grx4 has been shown to transfer iron-sulfur cluster to apo-Fdx, the reaction was carried out in presence of DTT, a reductant that has been shown to mediate non-physiological thiol-mediated redistribution of clusters [67], strongly suggesting a need for a re-evaluation of this effect. Additionally, the intermediacy of glutaredoxin in the cluster transfer from scaffold protein to apo-acceptors like ferredoxin in a one-pot reaction has not been demonstrated. Moreover, the ability of monothiol glutaredoxin to transfer clusters to other apo-targets like HcaC has not yet been explored.

Chaperones. At this point, the mechanistic details of chaperone-assisted cluster transfer from IscU to downstream acceptors have more questions than answers. For example, HscA-HscB have been found to be disposable under certain growth conditions [68], raising the possibility of operation of an alternate cluster transfer pathway not utilizing chaperones *in vivo*. Cluster transfer from IscU to glutaredoxin is accelerated in the presence of chaperones in DTT-independent manner [50]. However, all the studies that have been carried out demonstrating chaperone-dependent acceleration of direct cluster transfer from IscU to ferredoxin have been done in presence of DTT which necessitates re-evaluation of the results. Further investigation is required to test if there are two alternate pathways operative in the process of cluster transfer with one being glutaredoxin-mediated transfer from IscU to apo-Fdx and the other being chaperone-dependent direct transfer from IscU to apo-Fdx. Moreover, the requirement of the LYR motif on-apo acceptors for targeting by HscB is inconsistent with *in vitro* observations where

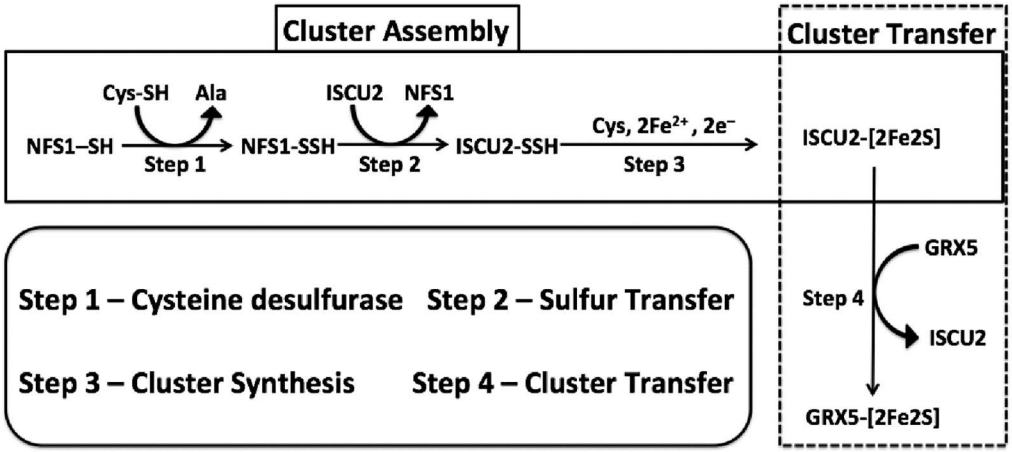

Figure 1.5. Different steps in eukaryotic ISC cluster biosynthesis pathway. The overall process of cluster biosynthesis in humans was divided into four broad steps.

chaperones accelerate the rate of cluster transfer to glutaredoxin and apo-ferredoxin, as neither of the protein contains the LYR motif. The mechanism of partitioning between the process of cluster assembly and transfer is poorly understood. The competition between IscS and HscB for IscU binding in yeast and the contrasting formation of a three-protein complex in bacteria further raises the possibility that the mechanisms are different in bacteria and eukaryotes. Chaperones have been shown to accelerate cluster transfer from IscU to glutaredoxin and apo-Fdx but the effect of chaperones on cluster transfer from glutaredoxin to apo-acceptors, such as ferredoxin, have not been studied. Moreover, the mechanistic details of how HscA binding to holo-IscU facilitate cluster transfer to apo-protein are poorly understood. It has also not been tested whether there is a functional relevance of the interaction between HscA and apo-acceptors like glutatredoxin and apo-BioB with the possibility that HscA has functions in addition to binding IscU.

In this work, we focused on optimizing and developing assays that assist a step-wise analysis of iron-sulfur cluster biogenesis (Chapter II and IV), and permit the study of cluster delivery to terminal apo-targets. We investigate the role of CyaY (bacterial homolog of FXN, chapter III) frataxin (Chapter IV), glutaredoxin (chapter V) and chaperones (chapter VI) in cluster assembly and transfer. This work has helped us to gain some important insights on mechanism of cluster transfer from holo-IscU to apo-acceptors and the glutaredoxin and chaperone-dependence therein.

CHAPTER II

FRATAXIN ACCELERATES [2FE-2S] CLUSTER FORMATION ON THE HUMAN FE-S COMPLEX[1]

Introduction

Proteins containing iron−sulfur (Fe−S) clusters are involved in many critical functions in cells, including oxidative respiration, DNA replication and repair, and cofactor biosynthesis [2]. Sophisticated Fe−S assembly pathways synthesize and deliver Fe−S clusters to apo-target proteins [9, 22, 69-71]. These O_2-sensitive pathways involve more than a dozen proteins and require six substrates to generate the simplest (i.e., [2Fe-2S]) cluster. Numerous protein complexes are assembled and disassembled during cluster formation and transfer reactions. Because of this complexity, assays for investigating the mechanistic enzymology of these pathways have had to simplify this process by including non-physiological reagents and by monitoring partial reactions. An additional challenge is that iron and sulfide can undergo competing non-enzymatic Fe−S cluster self-assembly (spontaneous formation of discrete species similar to biological Fe−S clusters) [72] and Fe−S mineralization chemistry. The resulting Fe−S material can also undergo ligand exchange and cluster conversion reactions [73]. It is important to elucidate the factors that partition between biosynthetic and competing side reactions and to understand the types

---

[1] Reprinted with permission from "Frataxin Accelerates [2Fe-2S] Cluster Formation on the Human Fe−S Assembly Complex" by Nicholas G. Fox, Deepika Das, Mrinmoy Chakrabarti, Paul A. Lindahl, David P. Barondeau, 2015. *Biochemistry*, 54, 3880-3889. Copyright 2015 American Chemical Society.

and properties of Fe−S species that are being generated. The mitochondrial eukaryotic Fe−S biosynthetic pathway builds Fe−S clusters from the substrates L-cysteine, iron, and reducing equivalents, homologous to the chemistry of the prokaryotic ISC pathway. Cysteine desulfurase (human NFS1 or bacterial IscS) catalyzes the PLP-dependent conversion of L-cysteine to L-alanine, while generating a persulfide species on a mobile loop cysteine residue that delivers a sulfane sulfur to the Fe−S catalytic protein (human ISCU2 or bacterial IscU) [74, 75]. Cysteine desulfurase activity is often measured by intercepting this persulfide species using reductive thiol-cleaving reagents and quantitating the generated sulfide [74-76]. Human NFS1 forms a tight complex with ISD11 (the SD complex) that includes two NFS1 and possibly four ISD11 subunits [77]. ISD11 is a eukaryotic protein that stabilizes cysteine desulfurase and may help position the mobile loop cysteine for attack of the substrate [47, 78]. Possible electron donors for *in vivo* Fe−S cluster formation and/or transfer include glutathione (GSH) and NADPH with the ferredoxin/ferredoxin reductase system [79-81]. Notably, *in vitro* Fe−S cluster assembly reactions often use a surrogate electron donor such as dithiothreitol (DTT). Once the Fe−S clusters are assembled, chaperone and Fe−S carrier proteins facilitate the transfer of the intact Fe−S clusters from the Fe−S assembly complex to target proteins [65, 82, 83].

Depletion of human frataxin (FXN) is associated with the loss of Fe−S cluster enzyme activities and the development of the neurodegenerative disease Friedreich's ataxia (FRDA) [84]. FXN binds to an ~160 kDa complex consisting of NFS1, ISD11, and ISCU2 proteins (named SDU) to form the SDUF complex [31, 77]. FXN was initially

proposed to function as an iron donor for Fe−S cluster biosynthesis largely because of its ability to weakly bind iron [43, 85, 86]. Subsequently, FXN was shown to stimulate the activity of the cysteine desulfurase component of the SDUF complex (k_{cat} is ∼10-fold higher for SDUF than for SDU), suggesting a role as an allosteric effector [31, 33, 87].

Notably, FXN variants encoded by FRDA missense mutations have compromised abilities to bind and stimulate the activities of the Fe−S assembly complex [88]. Recent Mössbauer studies suggest that the mouse SDU complex assembles [2Fe-2S] clusters and that the SDUF complex synthesizes [4Fe-4S] clusters [89]. This result is puzzling because an IscU molecule in the SDUF complex would not be expected to dimerize (a requirement for the reductive coupling model of [4Fe-4S] cluster formation) [23] without a significant conformational change compared to the prokaryotic IscS−IscU structure. In addition, proteins previously implicated in [4Fe-4S] cluster formation [59] were not added during the reaction, and the putative [4Fe-4S] cluster was EPR silent under both oxidized and reduced conditions.

The objectives of this study were to elucidate the formation kinetics and types of Fe−S clusters synthesized by the human Fe−S assembly complex under different experimental conditions. Previous kinetic assays for Fe−S cluster formation used the surrogate electron donor DTT and followed the increase in absorbance at 456 nm due to S → Fe charge transfer bands [31, 90-92]. This wavelength is characteristic of an absorbance peak for [2Fe-2S] clusters, but other Fe−S species, including [4Fe-4S] clusters, also absorb at that wavelength. Under these assay conditions, the SDUF complex exhibits activity ∼25-fold higher than that of the SDU complex [31]. However, the nature

of the Fe−S species produced during these assembly reactions were not determined. In this work, different electron donation systems were used for Fe−S cluster assembly reactions and the products of these reactions were established using electronic absorbance, circular dichroism, and Mössbauer spectroscopies [73]. Together, they reveal new details of the Fe−S cluster assembly reaction on the SDUF complex and of competing Fe−S cluster conversion and mineralization chemistry that have implications for the mechanism and study of Fe−S cluster biosynthesis.

Results

Fe−S cluster assembly reaction components were prepared anaerobically in a glovebox and combined in an anaerobic cuvette that was sealed with a rubber septum and removed from the glovebox for activity measurements. Activity assays were initiated by injecting L-cysteine into the sealed cuvette using a gastight syringe. We employed two types of Fe−S assembly assay conditions, called standard and DTT-free (see Materials and Methods), that differed in their electron donation systems. We first investigated the Fe−S cluster assembly reaction for the SDUF complex (with an SD: ISCU2: FXN molar ratio of 1:3:3) under standard assay conditions, which included substrates Fe^{2+} and L-cysteine, and electron donor DTT. After 1 h, the reaction mixture exhibited a broad peak with a maximum at 400 nm that is characteristic of [4Fe-4S] clusters [93] (Fig. 2.1A). In addition, the absorbance for the entire visible region increased with time. The origin of the general absorbance increase at all wavelengths was unclear, but was consistent with an increase in light scattering The absorbance at 400 nm increased rapidly and then more slowly in a second linear phase of the reaction (Fig. 2.1B). The rate and magnitude of the absorbance

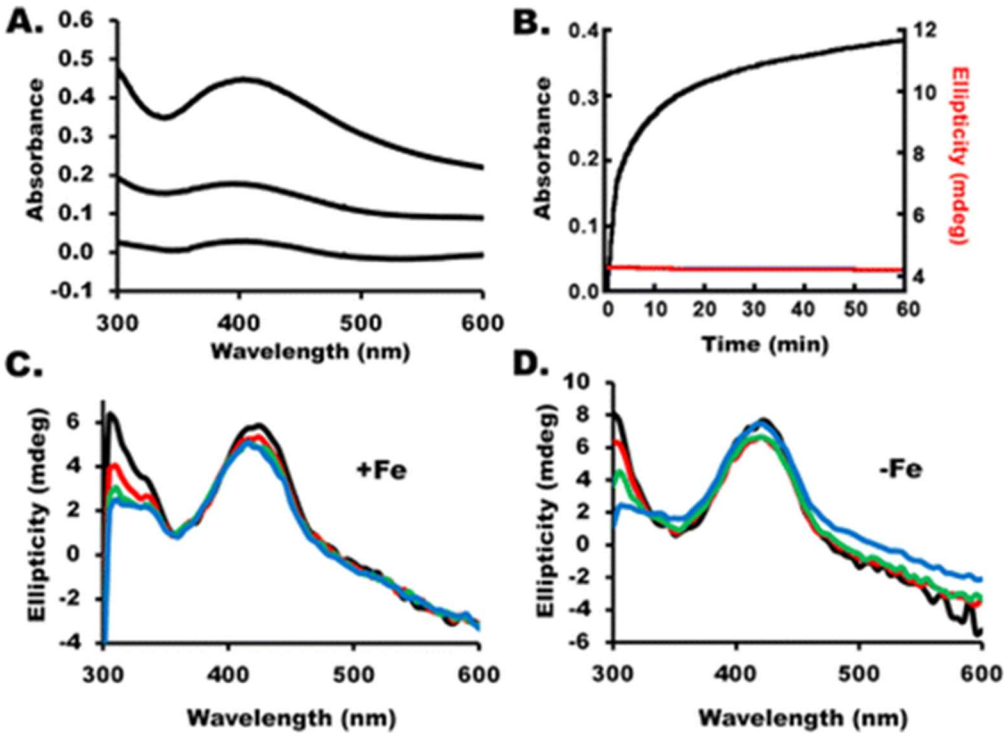

Figure 2.1. SDUF complex generates Fe−S species under standard conditions with spectroscopic properties similar to those of [4Fe-4S] clusters. (A) Absorbance spectrum of the SDUF reaction mixture 45 s (bottom), 2.8 min, and 1 h (top) after the reaction was initiated. (B) Kinetics of the assembly assay reaction monitored by absorbance at 400 nm (black) and CD ellipticity at 430 nm (red). The absorbance was adjusted to zero at 0 min. (C) CD spectra of the reaction mixture recorded at 0 (black), 20 (red), 40 (green), and 90 (blue) min. (D) CD spectra of an equivalent reaction mixture as in C except that it included 10 mM EDTA and excluded Fe^{2+}. Spectra were recorded at 0 (black), 10 (red), 20 (green), and 40 (blue) min.

changes depended on the concentration of Fe^{2+} (data not shown) The lack of a plateau region indicates that more than one reaction occurred and/or that more than one species formed. None of the spectra recorded, even at the earlier reaction times, showed absorbance features typical of a [2Fe-2S] cluster. The corresponding CD spectra exhibited a feature at 420 nm that was largely invariant with time (Fig. 2.1C). This feature was assigned to the PLP cofactor, as a similar peak was observed for the human SD complex and *E. coli* IscS that lack iron−sulfur clusters. The intensity of a second CD peak at 300 nm decreased with time.

The iron independence of this second feature (Fig. 2.1D) suggested that it was also due to the PLP cofactor and not due to an Fe−S cluster. Moreover, these features were inconsistent with the strong [2Fe-2S] cluster-dependent CD signals observed at 330 and 430 nm exhibited by bacterial IscU [34, 83, 94] and human ISCU2 [33]. Rather, they suggested the formation of [4Fe-4S] clusters, which have negligible UV−visible CD intensity compared to that of [2Fe-2S] clusters [56, 95]. These features could also be due to other Fe−S species (such as an Fe−S mineral) that exhibit similar absorbance and CD spectroscopic properties.

We repeated the Fe−S cluster assembly reaction under standard conditions in the absence of FXN (SDU complex with an SD:ISCU2 molar ratio of 1:3). As previously reported [31], the absorbance increase at 456 nm for the SDU complex was significantly slower than that of the SDUF complex. The plot was linear and was not maximized during the time frame of the experiment (Fig. 2.2A, black line). Early time points for the SDU reaction revealed spectral absorption features typical of a [2Fe-2S] cluster Fig. 2.2B).

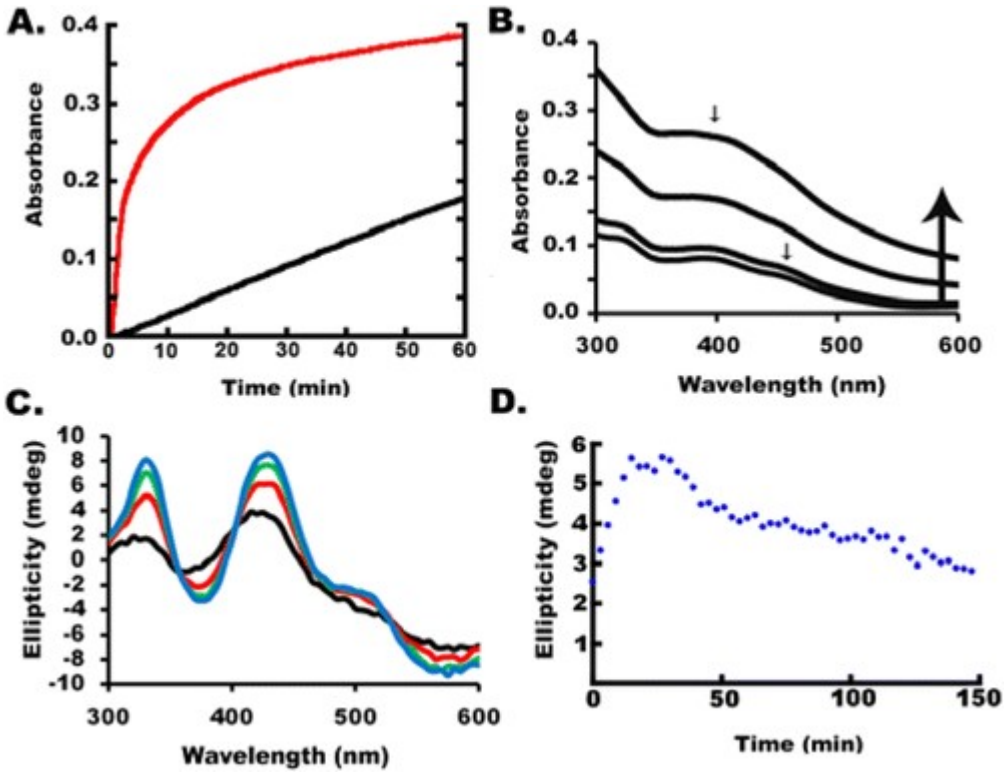

Figure 2.2. SDU complex generates [2Fe-2S] clusters under standard conditions. (A) Comparison of the change in absorbance at 456 nm for the SDU (black) and SDUF (red) complexes. (B) Absorbance spectrum for the SDU reaction mixture recorded at 5, 10, 30, and 60 min. The small arrow at 456 nm highlights the formation of [2Fe-2S] clusters at early times, while the arrow at 400 nm highlights features similar to those of the SDUF reaction (Figure 2.1A) at later times. (C) CD spectra recorded for the SDU reaction at 0 (black), 20 (red), 40 (green), and 90 (blue) min. The features at 330 and 430 nm are assigned to [2Fe-2S]-ISCU2. (D) Time-dependent changes in 330 nm ellipticity for a separate SDU reaction under standard conditions.

The formation of a [2Fe-2S] cluster was further supported by the development of a strong CD signal with peaks at 330 and 430 nm that are characteristic of [2Fe-2S]-IscU (Fig. 2.2C). Absorbance features centered at 400 nm and an overall increase at all wavelengths (Fig. 2.2B) developed at later times, similar to those produced by SDUF reactions. Time-dependent changes in the 330 nm CD signal of a separate SDU sample under standard conditions were monitored. The signal plateaued after ∼30 min and then decreased back to the initial ellipticity value (Fig. 2.2D). This is consistent with the SDU complex generating a [2Fe-2S] cluster that converts into a different species lacking a significant CD signature. The cluster conversion chemistry appears to vary with cysteine desulfurase activity and the amount of sulfide produced (see below). Overall, these results suggest that multiple species are generated in Fe−S assembly reactions under standard conditions.

Fe−S cluster assembly reactions under standard conditions generate high-molecular weight species (HMWS). Human SDU and SDUF complexes were isolated and characterized from similar assembly reactions. Standard reaction conditions were used (except for higher protein concentrations), and products were analyzed by anaerobic analytical size-exclusion chromatography. A brown species eluted in the column void volume (at ∼9 mL) when either SDU (Fig. 2.3A) or SDUF (Fig. 2.3B) complexes were used. SD, SDU, and SDUF complexes eluted at ∼12 mL, and uncomplexed ISCU2 and FXN eluted at ∼16 mL. Forming this HMWS required Fe^{2+}, L-cysteine, and the assembly complex. The reaction was accelerated by DTT (data not shown). Sodium dodecyl sulfate

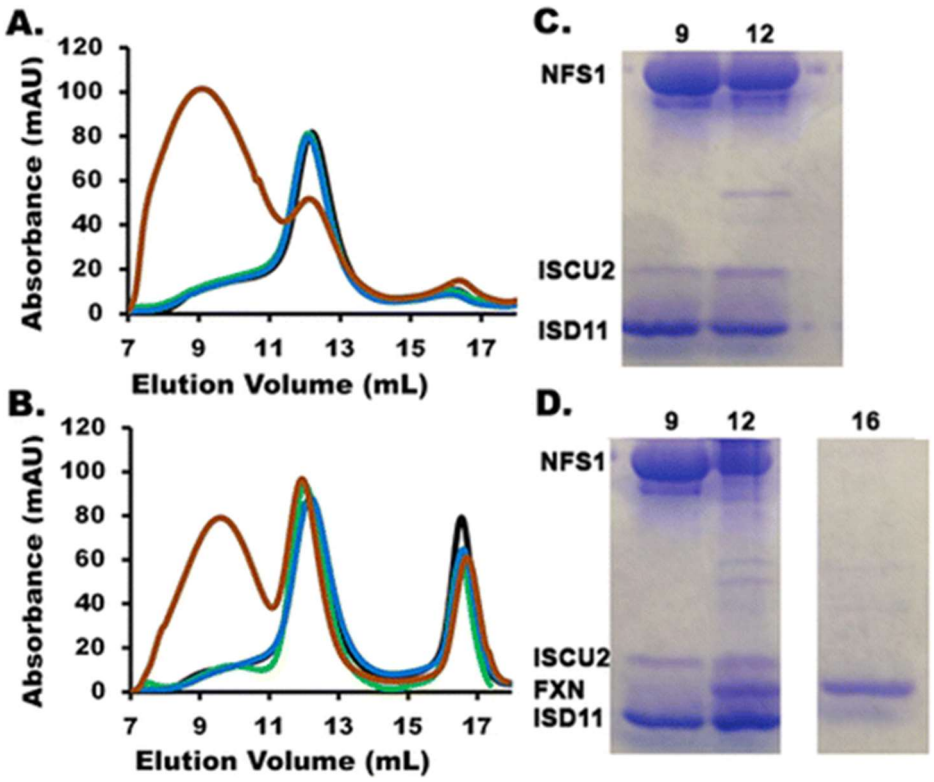

Figure 2.3. HMWS formation during Fe−S cluster assembly reactions under standard conditions. Size-exclusion chromatogram, monitored at A_{280}, of reaction mixtures involving (A) SDU and (B) SDUF under complete standard conditions (brown) but lacking cysteine (green), Fe^{2+} (blue), or both cysteine and Fe^{2+} (black). SDS−PAGE of fractions from Fe−S cluster assembly reactions involving (C) SDU and (D) SDUF. Fractions 9 (void), 12 (native SD, SDU, and SDUF), and 16 mL (uncomplexed ISCU2 and FXN) from anaerobic S-200 columns were analyzed by SDS−PAGE. The gel was stained with Coomassie Blue. Migration positions of NSF1, ISCU2, FXN, and ISD11 are shown.

−polyacrylamide gel electrophoresis (SDS−PAGE) analysis of fractions containing SDU (Fig. 2.3C) and SDUF (Fig. 2.3D) indicated that the HMWS (fraction 9 in each case) contained SD and ISCU2. Most of the iron and sulfide added in the reaction mixture eluted with the HMWS. More iron and sulfide (9 Fe^{2+} and 10 S^{2-} atoms per SDU assuming a 1:2:1 stoichiometry [77]) were found in the HMWS fraction for the SDUF reaction than expected for a standard biological Fe−S cluster. A similar Fe−S cluster associated HMWS could be generated in control reactions (Fig. 2.4) using either the SD complex or *E. coli* IscS in the absence of the scaffold protein (human ISCU2 or E. coli IscU). As the ISCU2/IscU protein is required for biological Fe−S cluster assembly, this suggests that HMWS formation is an off-pathway process that competes with the physiological Fe−S cluster assembly pathway under these assay conditions.

HMWS are solubilized Fe−S mineral species. We generated ^{57}Fe-labeled HMWS to investigate it by Mössbauer spectroscopy. The 5 K spectrum was composed of unresolved magnetic material and a quadrupole doublet (Fig. 2.5A). At 100 K, the magnetic material collapsed into a doublet with δ =0.37 mm/s, ΔE_Q = 0.67 mm/s, and Γ = 0.55 mm/s (Fig. 2.5B). HMWS prepared from similar SDUF or other SD reactions displayed some spectral variability, suggesting multiple species. The Mössbauer magnetic properties and parameters along with the absence of an EPR signal (with or without added dithionite) for the HMWS are inconsistent with [2Fe-2S] or [4Fe-4S] clusters. Instead, they indicate an Fe−S mineral (see Discussion).

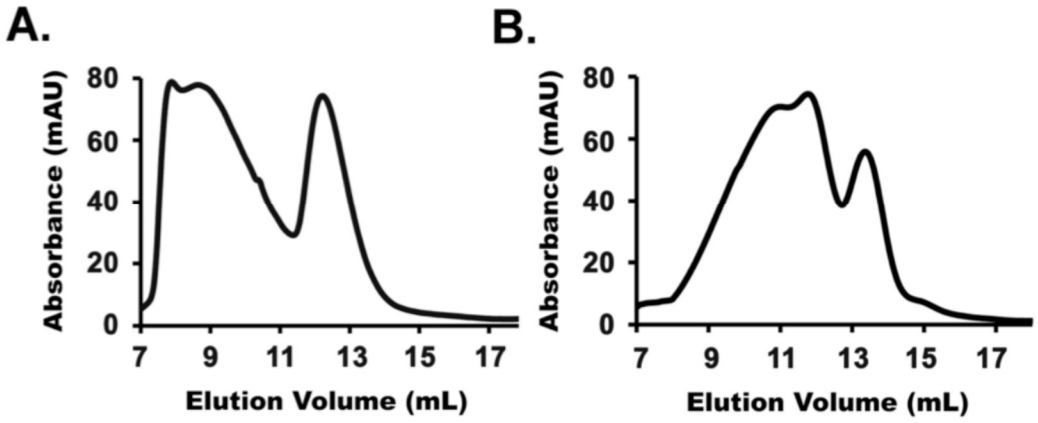

F**igure 2.4. Elution profile of Fe-S assembly reaction**. The solutions show that cysteine desulfurase generates HMWS during Fe-S assembly reactions under scaled up Standard conditions. Reaction mixtures including (A) human SD or (B) *E. coli* IscS and DTT, Fe^{2+}, and L-cysteine were incubated for 45 min at 12 ° C. The samples were then separately applied to an anaerobic S-200 column and monitored by absorbance at 280 nm. The HMWS and cysteine desulfurase elute in fractions 8-12, and 12-14, respectively.

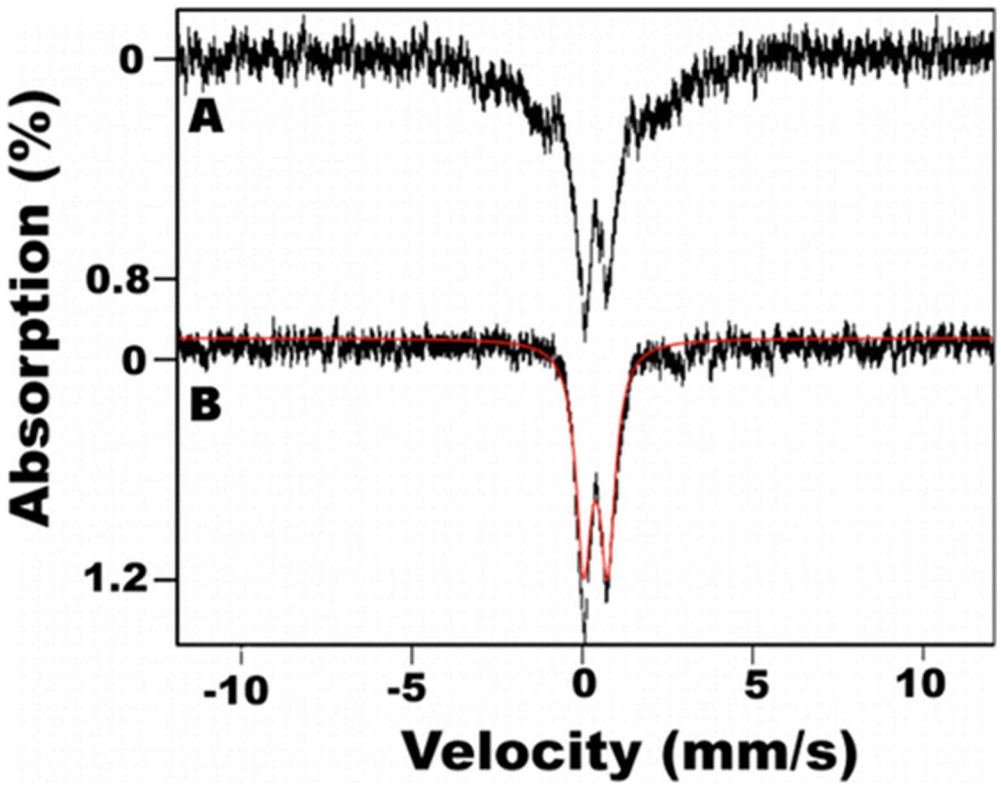

Figure 2.5. Mössbauer spectra of the HMWS mineral. The HMWS was generated with the SD complex under standard conditions and isolated from the void volume fractions of the S-200 column. Low-field (0.05 T) Mössbauer spectra were recorded at (A) 5 and (B) 100 K. The solid red line overlaying the data is a simulation of the quadrupole doublet due to the HMWS.

Formation and reaction properties of HMWS. Next, we attempted to minimize formation of the HMWS material. We considered whether cysteine desulfurase catalyzed L-cysteine turnover and generated sulfide during HMWS formation. That sulfide could then be used in Fe−S cluster self-assembly or Fe−S mineralization. Consistent with this role, sulfide could be substituted for L-cysteine (Fig. 2.6A, red line). However, alkylation of the cysteine residues of NFS1 eliminated HMWS formation even in the presence of sulfide and ferrous ions (Fig. 2.6A, green line). This suggests that NFS1 plays an additional role in HMWS formation, e.g., as a scaffold for assembling or solubilizing an Fe−S species. We then explored what reagent limits product formation for Fe−S cluster assembly reactions using SDUF under standard conditions (Fig. 2.6B). The Fe−S mineral is likely responsible for the increase in both the 400 nm absorbance and the apparent light scattering. The reaction started to plateau at ∼15 min, but adding L-cysteine at that point caused an abrupt rise in absorbance. This suggested that Fe−S mineral formation was limited due to depleted cysteine/sulfide, and that more of this material formed once extra cysteine was added. We wondered whether HMWS could function as a substrate for the chemical reconstitution of apo-target proteins. To test this, the SDUF reaction under standard conditions was repeated with a molar excess of the [2Fe-2S] cluster acceptor protein apo-FDX1. The reaction was analyzed by size-exclusion chromatography. An Fe−S cluster was incorporated into apo-FDX1 while less HMWS formed (Fig. 2.6C). Incorporation of mixtures under DTT-free conditions had features characteristic of a [2Fe-2S] cluster, rather than the broad absorption at 400 nm that was due primarily to HMWS in reaction mixtures that contained DTT (Fig. 2.1A). In addition, the general increase in

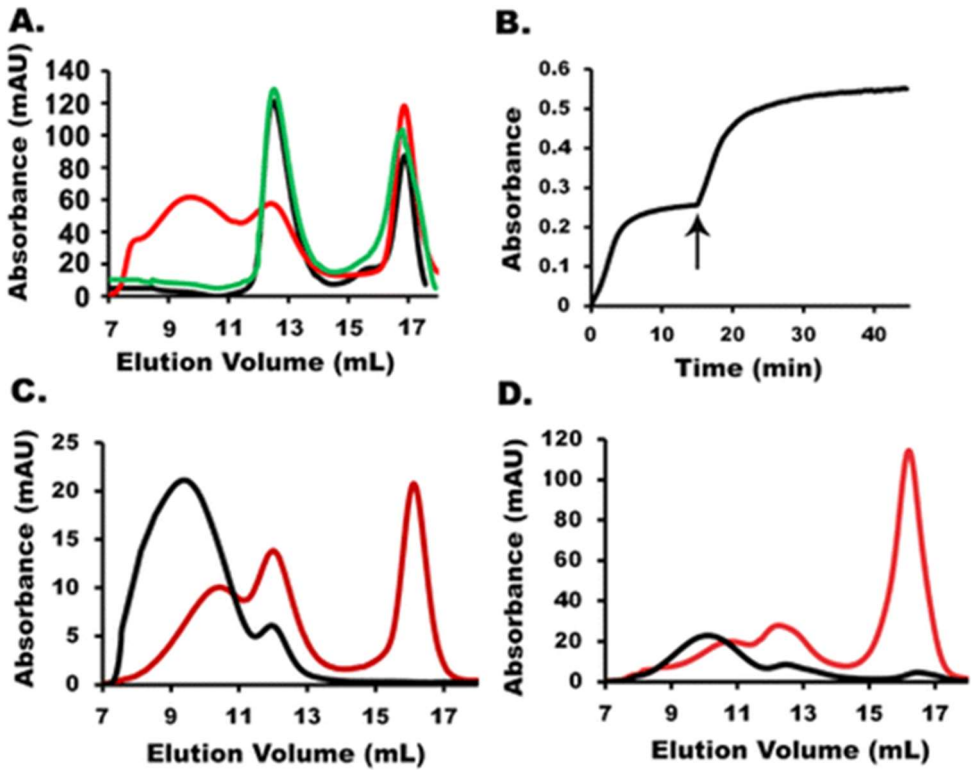

Figure 2.6. Formation conditions and reaction properties of HMWS. (A) Size-exclusion chromatogram, monitored at A_{280}, of the SDUF complex incubated with DTT and S^{2-} (black), Fe^{2+} and S^{2-} (red), or Fe^{2+} and S^{2-} using an SDUF complex in which NSF1 had been alkylated (green). (B) Kinetics of SDUF Fe−S cluster assembly reaction under standard conditions spiked (arrow) with 100 μM L-cysteine show that the plateau in 400 nm absorbance is due to depletion of cysteine/sulfide. (C) Size-exclusion chromatogram, monitored at A_{405}, of the reaction mixture involving the SDUF complex in the absence (black) or presence (red) of apo-FDX1. (D) Size-exclusion chromatogram, monitored by absorbance at A_{405}, of the isolated HMWS with (red) or without (black) added apo-FDX1.

absorption at all wavelengths that was attributed to light scattering from Fe−S mineral formation was diminished. To evaluate whether HMWS were also formed, a separate SDUF Fe−S cluster assembly reaction was analyzed after incubation for 1.5 h by size-exclusion chromatography. Peaks that absorb at 405 nm for SDUF complex and the uncomplexed ISCU2 were detected (Fig. 2.7C), but not for HMWS or low molecular weight species (LMWS). At longer (>2h) time points, an absorbance peak near 400 nm developed along with general increase in absorbance at all wavelengths (Fig. 2.7D) that was consistent with Fe−S cluster-associated HMWS formation. Initial formation of HMWS (Figure 2.7C, shoulder at 10−11 mL) was confirmed for the 3.5 h sample. Thus, the DTT-free reactions delayed and suppressed the rate of HMWS formation compared to standard reactions. This can be rationalized by differences in the ability of cysteine and DTT to release the sulfide from a persulfide intermediate on the assembly complex. Generation of sulfide by cysteine (DTT-free assays) occurs through an intermolecular reaction, whereas the sulfide released by DTT (standard assays) involves an entropically favored intramolecular reaction that forms a disulfide-bonded six-membered ring.

Sulfide converts [2Fe-2S] clusters to HMWS. Under standard conditions, the assembly reaction with SDUF failed to generate [2Fe-2S] CD signals (Fig. 2.1C), whereas with SDU, a [2Fe-2S] CD signal developed and then slowly decayed (Fig. 2.2D). We hypothesized that sulfide, which was generated rapidly for SDUF reactions and slowly for SDU reactions [31], reacted with synthesized [2Fe-2S] clusters to form HMWS. To test this, an assembly reaction involving SDU and DTT-free conditions was used to generate

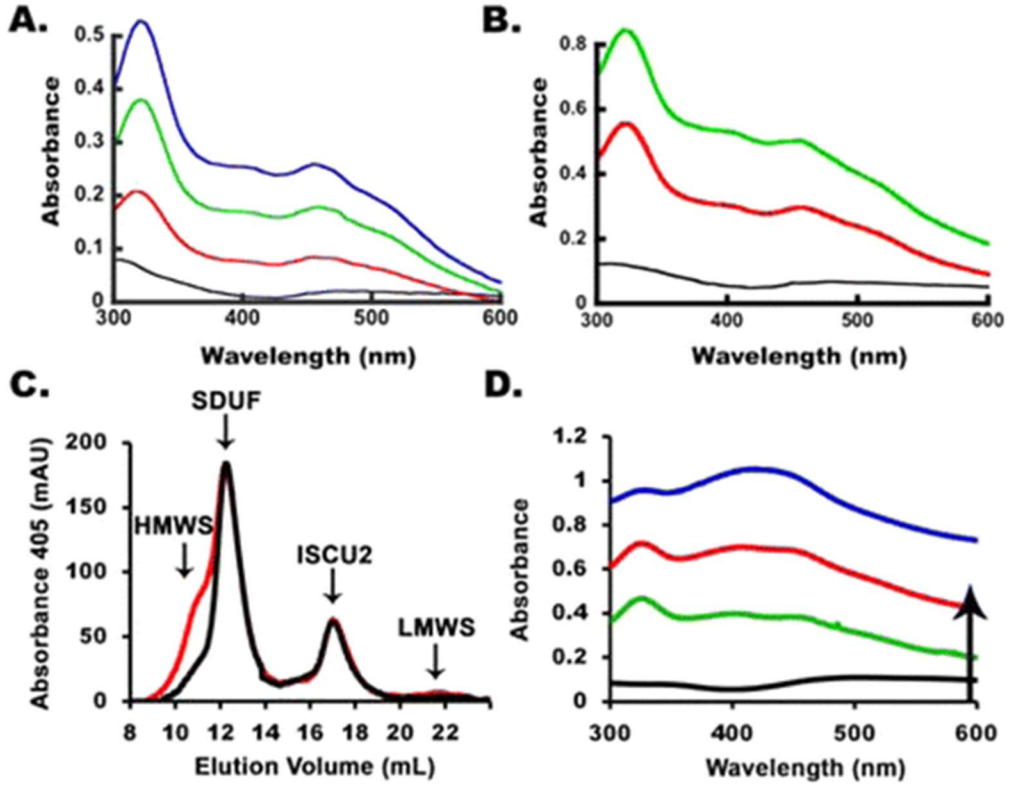

Figure 2.7. Fe−S cluster assembly reactions under DTT-free conditions generate [2Fe-2S] clusters and delay HMWS formation. (A) Absorbance spectra for SDU-catalyzed Fe−S assembly reaction after 0 (black), 30 (red), 60 (green), and 90 (blue) min. (B) Same for the SDUF-catalyzed reaction (same color coding, no 90 min spectrum). (C) Size-exclusion chromatogram, monitored at A_{405}, of the SDUF Fe−S cluster assembly reaction after 1.5 (black) and 3.5 h (red). (D) Absorbance spectra for the reaction in panel C after 0 (black), 2 (green), 3.5 (red), and 5 (blue) h.

[2Fe-2S] clusters (Fig. 2.8A). Addition of Na_2S immediately and dramatically decreased the magnitude of the [2Fe-2S] cluster signal (Fig. 2.8B). Lower concentrations of Na_2S resulted in partial signal loss, whereas higher concentrations completely eliminated the signal (leaving only the PLP CD feature). The addition of sulfide also resulted in an overall increase in absorbance at all wavelengths. The CD and absorbance features are similar to those observed in SDUF reactions under standard conditions and suggest that bisulfide reacts with [2Fe-2S] cluster intermediates to generate HMWS. Thus, Fe–S cluster assembly reactions that generate bisulfide are prone to competing reactions for the synthesis and degradation of [2Fe-2S] clusters (see Discussion).

FXN binding accelerates [2Fe-2S] cluster formation on ISCU2. Using DTT-free conditions that minimize the competing HMWS pathway, we assessed the role of FXN in the kinetics of [2Fe-2S] cluster formation. SDU- and SDUF catalyzed reactions were monitored by both absorption (panels A and B of Fig. 2.7, respectively) and CD (panels A and B of 2.9, respectively) spectroscopies. Strong absorbance and CD signals due to [2Fe-2S]-ISCU2 developed in both reactions, but the rates of formation were significantly more rapid in the SDUF-catalyzed reactions. Fitting the linear regions of the absorbance and CD kinetic traces (panels C and D of Fig. 2.9, respectively) revealed that FXN enhanced the rate of [2Fe-2S]-ISCU2 cluster formation by a factor of nearly 3. The addition of FXN increased the rate of absorbance change from 4.7×10^{-4} mM/min (R^2 = 0.99) to 13.4×10^{-4} mM/min ($R^2 = 0.99$) (assuming an extinction coefficient of 4.58 mM^{-1} cm^{-1} at 456 nm [23]). Notably, the absorbance increase did not plateau for either reaction,

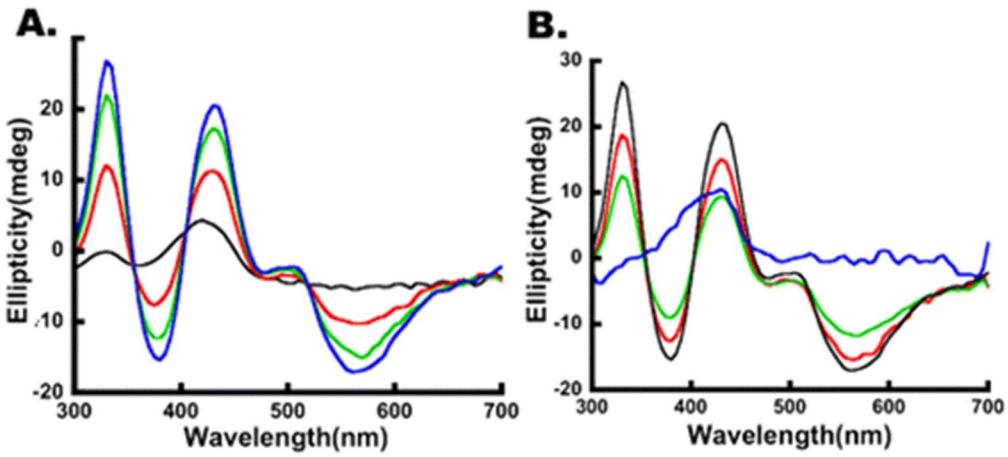

Figure 2.8. Sulfide degrades [2Fe-2S] clusters bound to ISCU2. (A) Development of the [2Fe-2S] cluster CD signal after 0 (black), 30 (red), 60 (green), and 90 (blue) min for the SDU complex under DTT-free conditions. (B) Addition of 0 μM (black), 250 μM (red), 500 μM (green), and 1 mM (blue) Na_2S to the mixture for the completed reaction (90 min) from panel A.

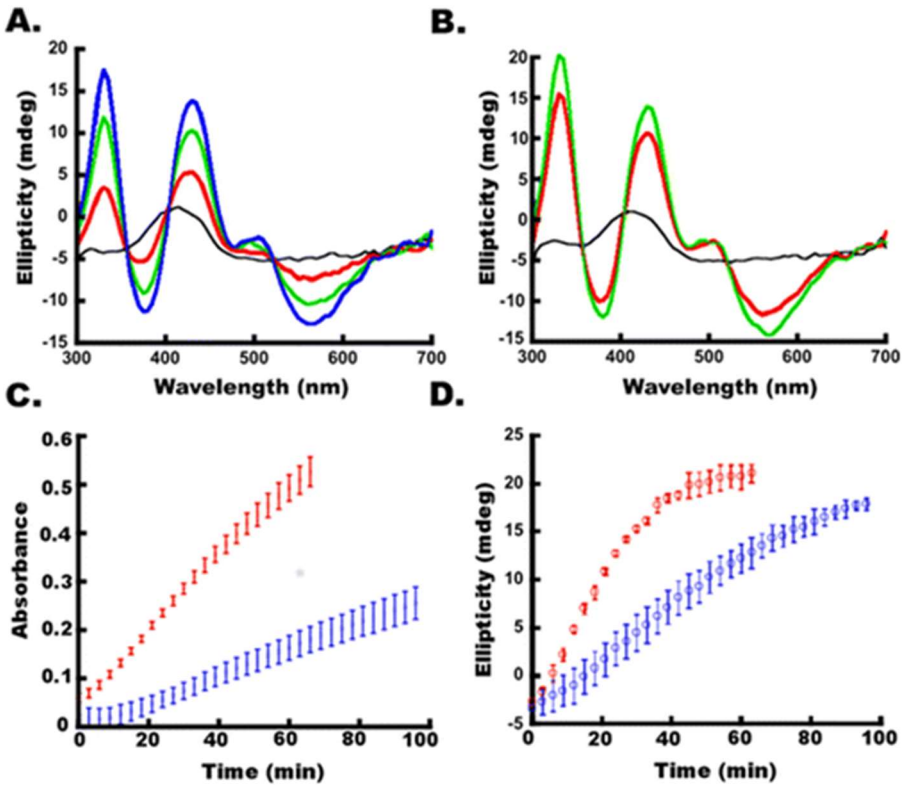

Figure 2.9. FXN accelerates [2Fe-2S] cluster formation. (A) CD spectra of an SDU-catalyzed Fe−S cluster assembly reaction mixture after 0 (black), 30 (red), 60 (green), and 90 (blue) min. (B) CD spectra of an SDUF-catalyzed Fe−S assembly reaction mixture after 0 (black), 30 (red), and 60 (green) min. (C) Absorbance at 456 nm vs time of reaction for SDU-catalyzed (blue) and SDUF catalyzed (red) reactions (shown in Figure 2.6A, B). (D) CD intensity at 330 nm vs time of reaction for SDU-catalyzed (blue) and SDUF-catalyzed (red) reactions. Bars are replicate errors from three experiments.

consistent with the initial formation of [2Fe-2S] clusters and the generation of HMWS at later times (Fig.2.7C, D). In contrast, the CD intensity is more specific for protein-bound $[2Fe\text{-}2S]^{2+}$ clusters. Addition of FXN increased the rate of CD signal growth from 0.40×10^{-4} mM/min (R^2 =0.99) to 0.97×10^{-4} mM/min (R^2 = 0.99). The CD ellipticity at 330 nm plateaued at ∼20 mdeg after ∼30 min for the SDUF reaction and after ∼100 min for the SDU reaction (Fig. 2.9D). The ∼20 mdeg value corresponds to a [2Fe-2S] cluster concentration of ∼30 μM [83], the concentration of ISCU2 used in these experiments. Thus, the plateau in the CD intensity is consistent with the reaction halting after all of the ISCU2 in the solution became bound with [2Fe-2S] clusters. These data also indicate that these [2Fe-2S] clusters are not converted to another Fe−S species. Notably, alternate species such as Fe−S minerals [4Fe-4S] clusters [56, 95] and [2Fe-2S] clusters associated with small molecules rather than proteins [96] do not significantly contribute to this region of the CD spectrum. Overall, these data demonstrate that adding FXN to the SDU complex increases the rate at which the complex synthesizes [2Fe-2S] clusters on ISCU2.

Discussion

Experiments to identify reaction intermediates and elucidate mechanistic details of biosynthetic pathways often rely on monitoring reaction progress with kinetic measurements. This is challenging for Fe−S cluster biosynthesis researchers because the substrates (iron, cysteine, and reducing equivalents) and byproducts (sulfide) also undergo competing non-enzymatic Fe−S cluster self-assembly [72] and mineralization chemistry. Additionally, the synthesized Fe−S clusters are capable of undergoing ligand exchange and cluster conversion reactions [73]. These competing reactions complicate the

interpretation of results and limit mechanistic insight. It is therefore important to elucidate factors that partition reaction intermediates between these competing pathways and to understand the types and properties of Fe−S species that are being generated. Here we have identified conditions that favor pathways that intercept intermediates in Fe−S cluster biosynthesis. We have shown how to minimize this competing pathway by limiting sulfide generation and have provided insight into the reaction chemistry associated with human Fe−S cluster biosynthesis. Fe−S cluster assembly reactions under standard conditions generated products with absorbance and CD properties consistent with [4Fe-4S] clusters. The generation of [4Fe-4S] clusters is consistent with a recent proposal for the murine Fe−S biosynthetic system in which FXN was proposed to have a role in generating [4Fe-4S] cluster intermediates on the assembly complex [89]. However, Mössbauer and biochemical studies revealed that reactions for the human assembly complex under similar conditions generate Fe−S mineral or high molecular weight species (HMWS) and not [4Fe-4S] clusters. The HMWS are an iron-, sulfide-, and protein-containing material that exhibits Mössbauer spectra with a quadrupole doublet that is similar to those of Fe−S minerals such as pyrite ($\delta = 0.25-0.43$ mm/s, and $\Delta E_Q = 0.61-0.66$ mm/s). The Mössbauer parameters of the HMWS doublet are also similar to those assigned to [2Fe-2S]-GSH ($\delta = 0.393$ mm/s, and $\Delta E_Q = 0.676$ mm/s) [96]. However, the spectroscopic properties of HMWS are not consistent with well-characterized $[2Fe\text{-}2S]^{2+}$ or $[4Fe\text{-}4S]^{2+}$ clusters. The former clusters generally have $\delta = 0.25-0.30$ mm/s and $\Delta E_Q = 0.7-0.8$ mm/s. $[4Fe\text{-}4S]^{2+}$ clusters have $\delta = 0.44-0.46$ mm/s and $\Delta E_Q = 0.6-1.5$ mm/ s. Another important difference is that the HMWS exhibit magnetic hyperfine interactions (rather than a doublet) at low

temperatures. This spectral feature collapses into the doublet at higher temperatures. This behavior is distinctly different from those of S = 0 $[2Fe\text{-}2S]^{2+}$ or $[4Fe\text{-}4S]^{2+}$ clusters that exhibit doublets at both low and high temperatures. Also, the HMWS lack an S = 1/2 EPR signal (with or without added dithionite). Fe−S cluster-associated HMWS have been generated during chemical reconstitution of [4Fe-4S] cluster-containing radical SAM enzymes [97]. Standard in vitro Fe−S assembly reactions generate HMWS by intercepting persulfide and [2Fe-2S] cluster intermediates. In humans, a persulfide intermediate on the NFS1 component of the assembly complex is generated (Fig. 2.10, reaction A) and transferred to ISCU2 (Fig. 2.10, reaction B) as an initiating step in Fe−S cluster biosynthesis [33]. Addition of iron and reducing equivalents converts the terminal sulfur of this persulfide species into the bridging sulfur of a [2Fe-2S] cluster (Fig. 2.10, reaction C) [33]. Transfer of the [2Fe-2S] cluster intermediate to a target protein completes the catalytic cycle for the assembly complex (Fig. 2.10, reaction D). Nucleophilic reagents such as surrogate electron donor DTT and the substrate cysteine can attack or intercept protein-bound persulfide intermediates to produce sulfide ions (Figure 2.10, reaction E). Subsequent reaction of sulfide (or bisulfide) with iron and the assembly complex generates HMWS (Figure 2.10, reaction F). Sulfide also appears to be capable of reacting with [2Fe-2S] intermediates and forming HMWS (Fig. 2.10, reaction G), a process that may be accelerated by the addition of FXN. Similar thiol-based extrusion of [2Fe-2S] clusters from proteins has been reported [67, 98]. The two separate paths for forming HMWS are

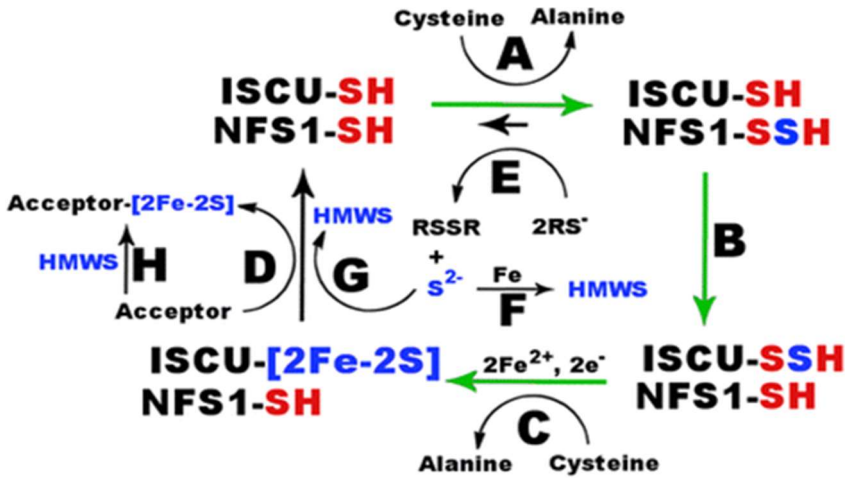

Figure 2.10. Model for competing Fe−S cluster biosynthesis and mineralization pathways. (A) Generation of a persulfide intermediate on NFS1. (B) Transfer of sulfur from NFS1 to ISCU2. (C) Catalytic synthesis of a [2Fe-2S] cluster intermediate. (D) Transfer of the [2Fe-2S] cluster to apo target proteins. (E) Interception of the persulfide intermediate with reductive thiol reagents to produce sulfide. (F) Combination of sulfide, iron, and the assembly complex (not shown) to form HMWS. (G) Degradation of [2Fe-2S] intermediates by sulfide to form HMWS. (H) Chemical reconstitution of apo target protein by HMWS. FXN accelerates [2Fe-2S] cluster formation (green arrows) by the human Fe−S assembly complex.

supported by recent kinetic studies of $SDU^{C35A}F$ and $SDU^{C61A}F$ complexes that exhibit nativelike cysteine desulfurase activities but compromised Fe−S assembly activities under standard conditions [33]. The slow increase in absorbance for $SDU^{C35A}F$ and $SDU^{C61A}F$ complexes compared to that of native SDUF is likely due to a functional persulfide cleavage pathway (Fig. 2.10, reactions E and F) but compromised biosynthetic route (Fig.2.10, reactions A−C and G) to HMWS. The ISCU2 variants for the $SDU^{C35A}F$ and $SDU^{C61A}F$ complexes have mutations in the conserved cysteines used for cluster biosynthesis. These different routes to HMWS may correspond to the initial rapid (biosynthetic route) and secondary slow linear (persulfide cleavage route) changes in absorbance under standard conditions. Overall, these results indicate that Fe−S cluster assembly assays under standard (DTT-containing) conditions may be qualitatively informative (representing primarily the enzymatic [2Fe-2S] biosynthesis and degradation pathway) but are not quantitatively meaningful for measuring the rate of [2Fe-2S] cluster synthesis by the assembly complex.

We elucidated details of the human Fe−S cluster biosynthetic process by identifying reaction conditions that minimize the competing non-enzymatic pathways and by monitoring reaction progress with spectroscopic methods that are uniquely sensitive to [2Fe-2S] clusters bound to proteins. Previously, human FXN was shown to stimulate the cysteine desulfurase activity (10-fold higher k_{cat} for sulfide production) [31] and facilitate the accumulation of persulfide species on ISCU2 [33]. Here, we explored the kinetics of [2Fe-2S] cluster formation under DTT-free conditions. Addition of FXN accelerated the rate of development for [2Fe-2S] CD features and resulted in approximately one [2Fe-2S]

cluster per ISCU2 molecule. We show by Mössbauer spectroscopy and liquid chromatography that, under similar conditions, [2Fe-2S] clusters are present on uncomplexed ISCU2. Together, these results support a model in which FXN accelerates [2Fe-2S] cluster formation on the SDUF complex (green arrows in Fig. 2.10, presumably using cysteine as the electron donor) [73]. This conclusion is supported by recent *in vitro* studies of a primarily *Saccharomyces cerevisiae* system in which the rate of formation for a [2Fe-2S]-Isu1 CD signal was dependent on the addition of Yfh1 (FXN homologue) [81]. Interestingly, the addition of the presumed physiological electron donation system (FDX2, ferredoxin reductase, and NADPH) or non-physiological electron donor DTT resulted in similar rates for the development of the [2Fe-2S]-Isu1 CD signal in the yeast system. This is in contrast to the human system in which the addition of DTT eliminates the [2Fe-2S]-ISCU2 CD signal. Thus, there are fundamental differences in the response of the human and yeast *in vitro* systems to surrogate electron donor DTT. In the future, these *in vitro* studies need to be expanded to evaluate complete cluster synthesis and transfer reactions that include chaperones, intermediate carrier proteins, and different Fe−S target proteins.

In summary, we have provided new details of competing pathways for Fe−S cluster biosynthesis and Fe−S mineralization. The partitioning of reaction intermediates complicates the interpretation of *in vitro* Fe−S assembly results. Deconvoluting the enzymatic and mineralization processes is challenging as there appears to be multiple partitioning branch points, comparable formation kinetics (both ultimately depend on cysteine turnover by NFS1), overlapping absorbance properties, products that co-elute on desalting columns, and similar abilities to transfer (Fig. 2.10, reaction D) or chemically

reconstitute (Fig. 2.10, reaction H) Fe−S clusters on target proteins. In these cases, performing reactions under conditions that minimize off-pathway reactions and monitoring the kinetics with multiple interrelated spectroscopic methods may be required to elucidate mechanistic details for the assembly and/or transfer of Fe−S clusters. Together, our current and previous [31, 33] results are consistent with yeast studies [81, 99] and indicate that FXN accelerates a rate-limiting sulfur transfer step in [2Fe-2S] cluster synthesis for the human Fe−S assembly complex. Our study also tells a cautionary tale of the complexities of Fe−S chemistry that could easily mislead unsuspecting researchers who study Fe−S cluster assembly or chemically reconstitute recombinant Fe−S proteins.

Materials and Methods

Protein expression and purification. NFS1-ISD11 (named SD), ISCU2, and FXN were purified as described previously [31]. The SDUF complex exhibited a cysteine desulfurase activity of 11 mol of sulfide (mol of PLP)$^{-1}$min^{-1}, which is similar to reported values [31, 46]. Briefly, plasmids that contain the genes for human SD, ISCU2, and FXN were individually transformed into BL21(DE3) cells. Cells were grown at 37 °C until an OD_{600} of 0.6 was achieved. Protein expression was induced with either 0.5 mM (ISCU2 and FXN) or 0.1 mM (SD) IPTG; the temperature was reduced to 16 °C, and the cells were harvested 16 h later. Plasmid PET9 encoding human ferredoxin (FDX1, gift of J. Markley) was transformed into Escherichia coli BL21(DE3) cells and grown at 37 °C until an OD_{600} of 0.6 was reached. Expression was induced with 0.4 mM IPTG, 1 mM cysteine, and 0.1 mg/mL ferric ammonium citrate, and the cells were harvested 16 h later. Buffer A [50 mM

HEPES (pH 7.8) and 250 mM NaCl] was used for all experiments unless otherwise stated. The cells were lysed by sonication, and the soluble proteins were loaded onto an anion exchange column (26/20 POROS 50HQ, Applied Biosystems) and eluted with a linear gradient from 0 to 1000 mM NaCl in 50 mM Tris (pH 7.5). Fractions containing FDX1 were further purified on a Sephacryl S100 (26/60, GE Healthcare) size-exclusion column equilibrated in 50 mM Tris (pH 7.4) and 50 mM NaCl. Apo-FDX1 was prepared by incubating purified FDX1 with 10 mM DTT, adding 10% trichloroacetic acid on ice for 10 min, pelleting the sample, rinsing the pellet twice with water, and resuspending the pellet anaerobically in 50 mM Tris (pH 8.0) and 250 mM NaCl. Anaerobic experiments were performed in an Mbraun glovebox at ∼12 °C with an argon atmosphere and <1 ppm O_2 as monitored by a Teledyne model 310 analyzer.

Fe−S cluster formation assays. The Fe−S cluster assembly assay mixtures under two experimental conditions (standard and DTT-free) were prepared anaerobically and transferred to a 1 cm path length anaerobic cuvette for UV−visible (Agilent UV−visible 8453) and circular dichroism (CD) (Chirascan) data collection at 20 °C. Standard assay conditions include 10 μM SD, 30 μM ISCU2, 30 μM FXN with 4 mM D, L-DTT, 100 μM L-cysteine, and either 250 or 400 μM $Fe(NH_4)_2(SO_4)_2$. Final volumes were 250 μL for UV−visible based and 200 or 400 μL for CD-based assays. DTT-free conditions were the same as standard conditions except that (a) the L-cysteine concentration was increased to 1 mM, (b) samples lacked DTT, and (c) the $Fe(NH_4)_2(SO_4)_2$ concentration was decreased from 400 to 250 μM. The initial linear regions for the SDU and SDUF reactions under DTT-free conditions were fit using KaleidaGraph (Synergy Software). For the sulfide

addition experiments, the development of the [2Fe-2S] cluster using 50 μM ISCU2 was monitored with anaerobic CD spectroscopy under DTT-free conditions. Once the CD signal at 330 nm had been maximized (indicating the development of the [2Fe-2S] species), aliquots of a Na_2S stock solution were added to final Na_2S concentrations of 250, 500, and 1000 μM and the CD spectra were immediately measured.

Protein assembly state analysis. Sample mixtures of 50 μM SD and 150 μM ISCU2 with (SDUF) or without (SDU) 150 μM FXN were incubated anaerobically for 20 min at 10 °C with 1.5 mM DTT, 500 μM $Fe(NH_4)_2(SO_4)_2$, and 500 μM L-cysteine (complete reaction conditions). Additional reactions lacking DTT, $Fe(NH_4)_2(SO_4)_2$ and/or L-cysteine were also prepared. Samples were applied to an anaerobic S-200 column (Superdex 200 10/300 GL, GE Healthcare) equilibrated with buffer A. In a second set of experiments, NFS1 was alkylated by incubating 50 μM SD with 1 mM iodoacetamide for 1 h at 12 °C and quenched with 10 mM L-cysteine. Modification of NFS1 residue C381 was confirmed by mass spectrometry. Alkylated or nonalkylated SD was reacted for 15 min at 12 °C with 50 μM ISCU2, 50 μM FXN, 200 μM $Fe(NH_4)_2(SO_4)_2$, 1.5 mM DTT, and 200 μM Na_2S (final concentrations, 0.2−0.5 mL reaction volume) and applied to the S-200 column. In a third set of experiments, 100 μM SDUF (final concentration) was prepared by mixing 100 μM SD, 300 μM ISCU2, 300 μM FXN, 1 mM $Fe(NH_4)_2(SO_4)_2$, and 3 mM DTT in the presence and absence of 500 μM apo-FDX1. The reaction was initiated with 1 mM L-cysteine (final concentration, 0.2−0.5 mL reaction volume). After reacting for 45 min at 12 °C, the solution was applied to an S-200 column. The reaction without apo-FDX1 was repeated, and the high-molecular weight species (HMWS) was isolated from fractions of

the S-200 column. The HMWS sample was split, and half was incubated for 10 min with 4 mM DTT. The other half was incubated for 40 min with 500 μM apo-FDX1 and 4 mM DTT. Samples were then reapplied to an S-200 column. Calibration with molecular weight standards confirmed that the protein samples eluted at volumes corresponding to their known molecular masses. Sulfide production was measured using a methylene blue assay [31, 100, 101]. Iron was quantified by the ferrozine assay [102-104].

Mössbauer analysis of HMWS. Mössbauer samples of HMWS were prepared by reacting 600 μM SD or SDUF with 6 mM L-cysteine, 6 mM ^{57}ferric citrate, and 1.8 mM DTT for 45 min at 12 °C, and isolating the HMWS using an S-200 column equilibrated in buffer A. Mössbauer spectra were recorded using a model MS4 WRC spectrometer (See Co., Edina, MN) at 0.05 T applied parallel to the γ radiation. Spectra were analyzed using WMOSS software (SEE Co.). Parameters are quoted relative to α-Fe foil at 298 K.

CHAPTER III

CYAY INHIBITS CLUSTER FORMATION ON ISCU BY SLOWING DOWN SULFUR TRANSFER FROM ISCS TO ISCU

Introduction

Iron sulfur clusters are essential protein cofactors for most living organisms in all three domains of life [69]. They play crucial roles in electron transport, catalysis, regulation of gene expression, iron homeostasis etc. [6, 105]. Hence, iron sulfur cluster biosynthesis needs to be very tightly regulated. In prokaryotes, three iron sulfur cluster biosynthesis pathways are known – 1) Nitrogen fixation (NIF) [106, 107], 2) Iron sulfur cluster assembly (ISC) [108-110] and 3) Sulfur Formation pathway (SUF) [111]. Among these, ISC pathway is the housekeeping pathway and operates under 'normal' growth conditions. On the other hand, NIF and SUF are more specialized systems. NIF is used exclusively to synthesize iron sulfur clusters on nitrogenase whereas SUF is employed to make iron sulfur cluster under oxidative stress and limited iron conditions [112]. ISC pathway is also the only pathway that is shared between prokaryotes and eukaryotes. Therefore, the proteins involved in ISC pathway are highly conserved. In *E. coli*, ISC operon encodes genes for IscR (iron sulfur cluster containing transcriptional regulator), IscS (cysteine desulfurase) [113], IscU (scaffold protein) [23, 114], IscA (alternate scaffold/iron donor) [115-117], HscB (co-chaperone) [83, 118], HscA (chaperone) [83, 119], Fdx (putative electron donor) [120, 121] and IscX (effector) [28, 122].

The mechanism of iron sulfur cluster biosynthesis is also very well conserved across prokaryotes and eukaryotes. IscU is the scaffold protein on which the cluster is

assembled. IscS is a PLP dependent cysteine desulfurase that provides the sulfur to scaffold protein IscU in the form of a persulfide via an absolutely conserved mobile loop cysteine assisted conversion of cysteine to alanine. That sulfane sulfur then reacts with ferrous iron and electrons provided most likely from reduced Fdx to form a $[2Fe2S]^{2+}$ on IscU in a process that is still very poorly understood. The scaffold protein then transfers the cluster to Grx4 in a reaction accelerated by HscA-HscB pair in an ATP dependent manner. Grx4 then transfers the clusters downstream to terminal acceptors like Fdx, Rieske etc.

Frataxin (FXN), a eukaryotic protein, has been shown to act as an allosteric activator of the eukaryotic cysteine desulfurase [31]. It activates iron sulfur cluster biosynthesis in eukaryotes by accelerating quinonoid decay and sulfur transfer from cysteine desulfurase (NFS1) to scaffold protein (ISCU2) (Chapter IV). Absence of this activation without FXN such as in neurodegenerative disease Friedreich's Ataxia (FRDA) [123, 124] leads to impairment of iron sulfur cluster biosynthesis, severe iron overload in mitochondria and subsequent elevated oxidative stress that cause severe damage to the cell leading to cell death [125-127]. It may also cause neurodegenerative disease Friedreich's Ataxia. In stark contrast to eukaryotic system, CyaY (bacterial homolog of FXN) has been shown to inhibit iron sulfur cluster assembly on scaffold protein *in vitro* [128]. It was later shown that FXN also inhibits iron sulfur cluster biosynthesis on *E. coli* IscU and that the inhibitory effect of CyaY/FXN is dependent on cysteine desulfurase (prokaryotic vs. eukaryotic) [46]. However, the exact mechanism of how CyaY inhibits iron sulfur cluster biosynthesis on IscU is still unknown. Deletion of CyaY did not produce

any of the phenotypes associated with FXN deletion most likely because under normal growth conditions, iron sulfur cluster biosynthesis is not required to be slowed down/inhibited [128]. However, it was recently shown that CyaY is required for cellular fitness under oxidative stress and limited iron conditions and has an overall positive role [122, 129, 130]. Along the same line, a single mutation (I108M) on IscU was shown to make the cell dependent on CyaY by somehow slowing down iron sulfur cluster biosynthesis creating condition of oxidative stress [131].

In this study, we aimed to determine how CyaY inhibits iron sulfur cluster biosynthesis on IscU and whether the inhibition translates to a slower rate of cluster delivery to terminal targets. Furthermore, we tested if CyaY has any effect on the process of iorn-sulfur cluster transfer from holo-IscU to apo-Grx4. We also investigated in detail the effect of I108M mutation on *E. coli* IscU on the rate of cluster assembly on IscU in presence and absence of CyaY. Using a combination of stopped flow experiments, a novel persulfide formation assay and CD spectroscopy, we determined that CyaY slows down iron sulfur cluster formation on IscU by inhibiting sulfur transfer from IscS to IscU and that the inhibitory effect is indeed translated to slower rate of cluster delivery to Grx4 which functions as an intermediate cluster carrier. Moreover, we did not see any effect of $IscU^{I108M}$ mutation in presence or absence of CyaY.

Results

Both CyaY and IscU^{I108M} do not affect quinonoid decay[2]. It has been shown that FXN as well as CyaY accelerate quinonoid decay for eukaryotic cysteine desulfurase resulting in facilitated production of persulfide on mobile loop cysteine of NFS1 (Chapter IV). This is in accordance with previously published result that both FXN and CyaY act as allosteric activators of eukaryotic cysteine desulfurase. To determine whether or not CyaY slows down quinonoid decay for prokaryotic cysteine desulfurase IscS, we decided to monitor the formation and decay kinetics of quinonoid intermediate using stopped-flow spectroscopy. For this, we determined the λ_{max} (wavelength of maximal absorbance) for the quinonoid, aldimine and ketimine intermediates by scanning a 100 nm window in the range of 300 nm to 700 nm every 2 ms for 2 s (see methods). This gave us λ_{max} of quinonoid and aldimine intermediate as 508 nm and 410 nm respectively. Unfortunately, we did not see a peak around 340 nm for ketimine intermediate in any of our runs. We decided to use 340 nm to monitor the kinetics of ketimine intermediate nevertheless as this wavelength has been previously used to monitor ketamine intermediates [75]. As can be seen in Fig. 3.1A-D, quinonoid decay kinetics looks very similar for all the complexes and the rates of quinonoid decay were found to be very similar when fitted to consecutive B equation (Table 3.1) with no effect of CyaY or IscU^{I108M} on quinonoid decay. We also followed aldimine and ketimine formation kinetics by monitoring 410 nm and 340 nm

[2] The experiments in this section are performed and analyzed by Shachin Patra from Barondeau group at Texas A&M University.

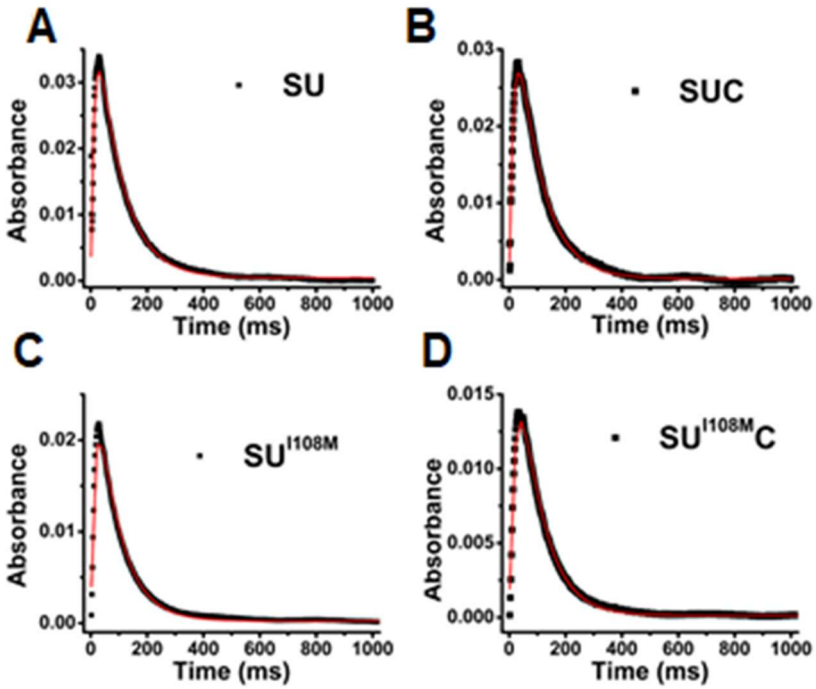

Figure 3.1. Both CyaY and IscU^{I108M} do not affect the rate of quinonoid formation and decay. The formation and decay of quinonoid intermediate were monitored by stopped flow at 508 nm wavelength. Reaction contained 50 μM of all the proteins (IscS, IscU/IscU^{I108M}, CyaY) and 5 mM cysteine (final concentrations). Reactions were carried out in absence (A, C), and presence (B, D) of CyaY for WT IscU and IscU^{I108M} respectively. The rates were obtained by fitting the data to the equation [y=y0 + A*(m1/(m3-m2))(exp(-m2*x)-exp(-m3*x))], where m2 and m3 values give the apparent rate of formation and decay of the quinoid intermediate respectively.

Table 3.1. Effect of CyaY and ISCU^{I108M} on kinetic parameters on all the steps in iron sulfur cluster biosynthetic pathway.

	Rate of Quinonoid Decay (x1000) (mAU.ms-1)	Kcat (min-1)	KM (μM)	Cluster Assembly Rate on IscU (mdegmin^{-1})	Cluster transfer Rate (mdegmin^{-1})	Cluster Assembly Rate on Grx4 (mdegmin^{-1})
IscS	11.05 ± 0.09	nd	nd	nd	nd	nd
IscS^{C328A}	0.082 ± 0.003	nd	nd	nd	nd	nd
SU	11.21 ± 0.1	5.35±0.17	14±2	4.6 ± 0.1	0.067 ± 0.006	0.164 ± 0.002
SUC	11.48 ± 0.07	3.96±0.03	14±1	0.26 ± 0.01	0.068 ± 0.007	0.046 ± 0.003
SU^{I108M}	12.36 ± 0.10	4.79±0.10	12±1	4.2 ± 0.2		0.177 ± 0.004
SU^{I108M}C	12.34 ± 0.11	4.23±0.09	19±2	0.54 ± 0.01		0.020 ± 0.004

respectively for SU and SUC complex. The kinetics were found to be similar in presence and absence of CyaY.

CyaY inhibits sulfur transfer from IscS to IscU but does not affect persulfide formation on IscS[3]. Next, we wanted to see if CyaY has any effect on persulfide formation on IscS and IscU which is the next downstream step after PLP chemistry. We incubated IscS and IscU in presence and absence of CyaY with cysteine that contains trace amount of radioactive ^{35}S-cysteine. We then quenched the reaction at different time points, separated proteins using HPLC (Fig. 3.2A) and quantified the amount of radioactivity via scintillation counting. The amount of radioactivity associated was then converted to the amount of persulfide on each protein using a standard curve. As can be seen in Fig. 3.2B, overall kinetics of persulfide formation on IscS in presence and absence of CyaY looked very similar but the extent of reaction completed were different. This corresponds well with our previous observation that CyaY does not affect PLP chemistry, which directly results in persulfide formation on IscS. Contrary to this, CyaY significantly slowed down sulfur transfer from IscS to IscU (Fig. 3.2C). Interestingly, this contrasts with the effect of FXN on human system where FXN accelerates sulfur transfer from NFS1 to ISCU2.

[3] The experiments in this section are performed and analyzed by Shachin Patra from Barondeau group at Texas A&M University.

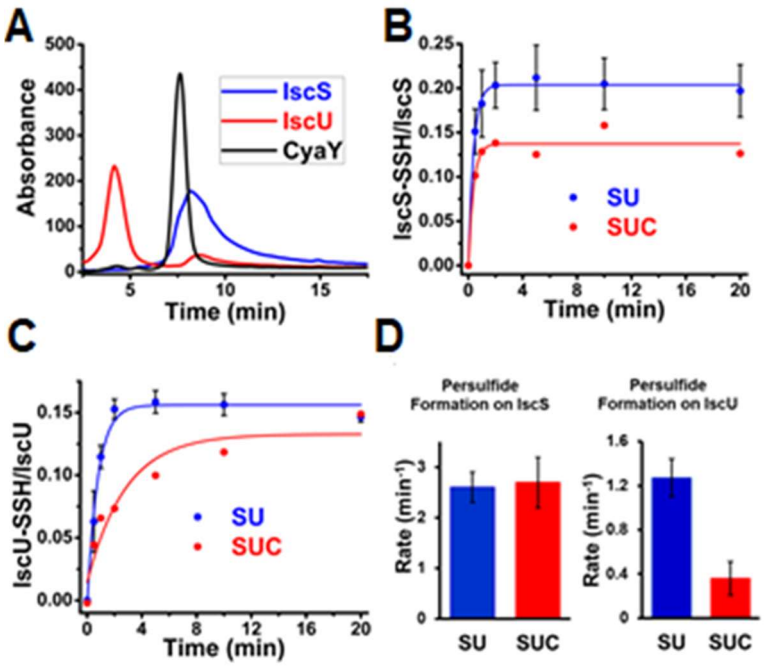

Figure 3.2. CyaY does not affect the rate of persulfide formation on IscS but slows down persulfide formation on IscU. (A) Separation of proteins by HPLC. 50 µM IscS, 150 µM IscU and 50 µM CyaY were loaded onto Deltapack C4 column after diluting with quenching solution in 1:3 ratios to a final volume of 200 µL (see methods). Chromatogram shows that IscS and IscU are well separated. Although CyaY co-elutes with IscS, that does not affect our analysis. (B), (C) Persulfide formation on IscS and IscU in presence and absence of CyaY was monitored by reacting 30 uM of IscS, IscU, CyaY and Cysteine (containing 0.204% ^{35}S-cysteine) at 37ºC for different time (in 0 - 20 min range). The samples were analyzed with HPLC and scintillation cocktail was added after quenching with 1:4 mixture of conc. HCl and 6M guanidine hydrochloride at given time points. The area under IscS and IscU in scintillation trace were converted into amounts of persulfide using a standard curve made from ^{35}S-cysteine standard. The data were fitted with exponential rise equation [y=m1+m2*(1-exp (-m3*x))] where m3 value gives the apparent rate of formation which is plotted in (D).

CyaY and IscU^{I108M} do not affect cysteine desulfurase activity[4]. Cysteine desulfurase activity for all four complexes (SU, SUC, SU^{I108M}, SU^{I108M}C) were measured according to previously published protocol. Cysteine desulfurase activity was comparable for all four complexes (Fig. 3.3A-D). The absence of an inhibitory effect of CyaY is consistent with the lack of any effect on quinonoid decay and persulfide formation on IscS.

CyaY inhibits iron sulfur cluster formation on scaffold protein while IscU^{I108M} has no effect. Iron sulfur cluster formation rates on scaffold protein (IscU or IscU^{I108M}) in presence and absence of CyaY were determined using CD spectroscopy by monitoring the ellipticity change at 330 nm. Consistent with previously published results, CyaY was observed to strongly inhibit iron sulfur cluster formation on scaffold protein **(**Fig. 3.4). This inhibition can be explained as a direct consequence of inhibited sulfur transfer to scaffold protein. On the other hand, contrary to literature, the rates were comparable for SU and SU^{I108M} in absence of CyaY. Moreover, CyaY did not accelerate iron sulfur cluster synthesis in the case of IscU^{I108M} as had been suggested in literature.

CyaY does not affect iron sulfur cluster transfer from IscU to Grx4. Next, we wanted to explore if CyaY has any other effect(s) on cluster biosynthesis process in addition to inhibition of cluster assembly on scaffold protein IscU. To determine if CyaY has any effect on cluster transfer step, we reconstituted IscU (see methods) followed by addition of apo-Grx4 to initiate the reaction. The cluster transfer reaction was monitored using CD

[4] The experiments in this section are performed and analyzed by Shachin Patra from Barondeau group at Texas A&M University.

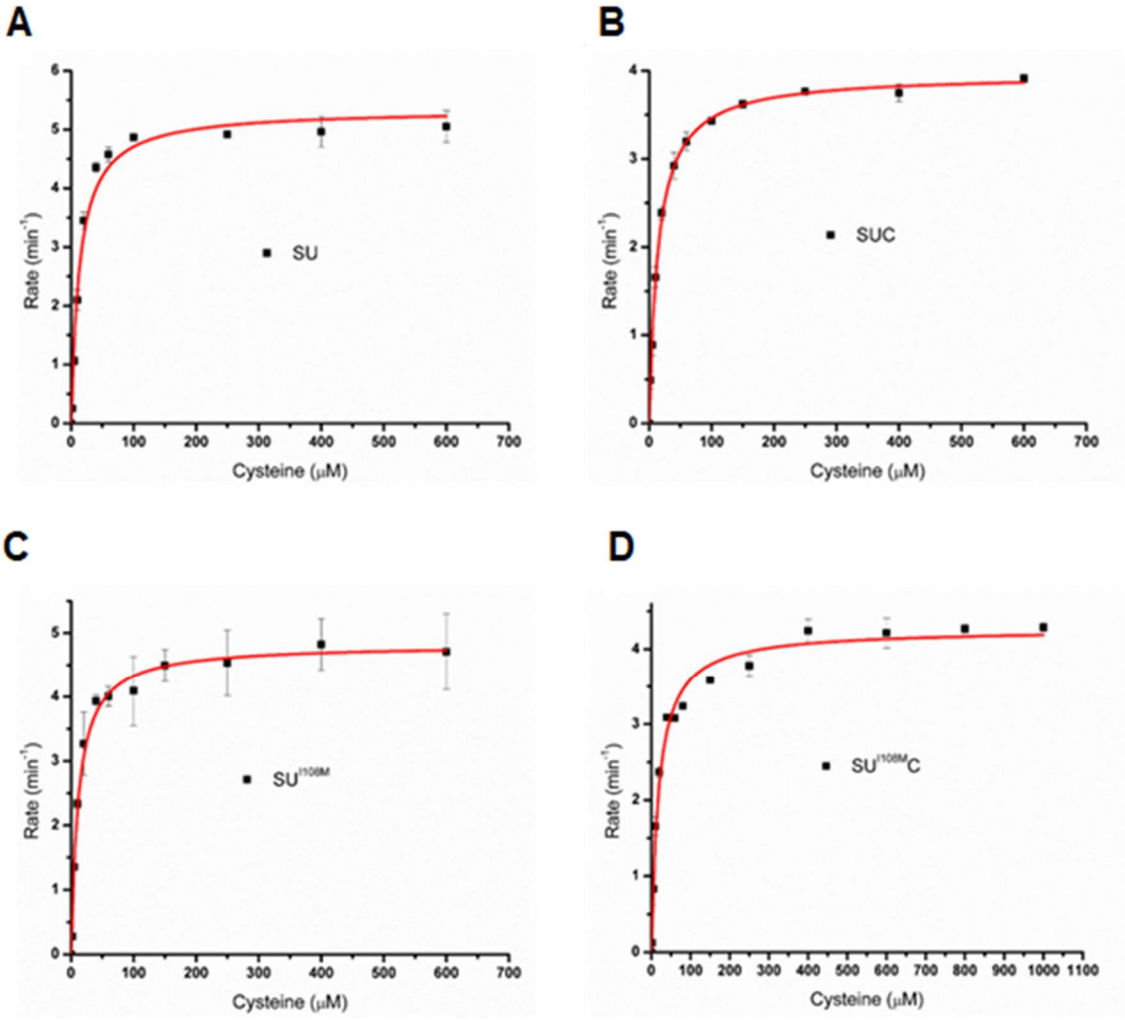

Figure 3.3. Both CyaY and IscU^{I108M} do not affect cysteine desulfurase activity. The reactions contained 0.5 μM IscS, 2.5 μM IscU/IscU^{I108M}, 5 μM CyaY, 4 mM D, L-DTT. Reactions were carried out in absence (A, C), and presence (B, D) of CyaY for WT IscU and IscU^{I108M} respectively. Reactions were initiated by adding cysteine and incubated for 6 min before quenching with DPD and $FeCl_3$ solution. Solutions were further incubated for 20 min. Then the samples were centrifuged and absorbances at 670 nm were measured which were converted to concentration of sulfide using a standard curve generated from known amount of sulfide. The data points were fitted to Michaelis-Menten equation (y = m1*x/(m2 + x)), where m1 and m2 are k_{cat} and K_M respectively.).

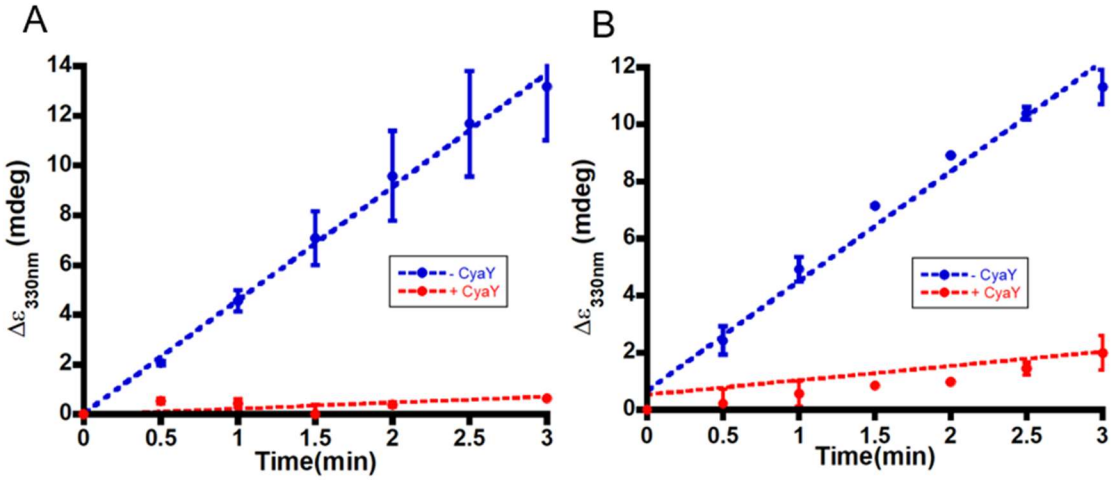

Figure 3.4. CyaY inhibits cluster assembly on IscU/IscU^{I108M}. Reaction consists of 8 µM IscS, 40 µM IscU (A) or IscU^{I108M} (B), 200 µM $Fe_2(NH_4)_2SO_4$ in the presence and absence of 50 µM CyaY and initiated by the addition of 10 mM GSH and 100 µM cysteine.

spectroscopy by monitoring ellipticity change at 450 nm (where Holo-Grx4 has much larger contribution compared to Holo-IscU). The rates were found to be comparable with and without CyaY. This shows that CyaY does not affect cluster transfer from holo-IscU to apo-Grx4.

CyaY inhibits one-pot cluster synthesis on Grx4 while IscU^{I108M} has no effect. We further tested whether or not the inhibitory effect of CyaY on sulfur transfer step and consequently, iron sulfur cluster assembly on scaffold protein results in inhibition of holo-Grx4 synthesis in a one-pot reaction where Holo-IscU is not pre-formed and cluster assembly on Grx4 is monitored by recording ellipticity change at 450 nm. CyaY strongly inhibited cluster synthesis on Grx4 (Fig. 3.5). On the other hand, IscU^{I108M} had no effect. This is in stark contrast to the effect of opposite mutation on human ISCU2^{M106I} which has been shown to accelerate cluster transfer from ISCU2 to GRX5.

Discussion

Although it has been well known for a long time that CyaY inhibits iron sulfur cluster synthesis on scaffold protein IscU [46, 132, 133], the mechanism of inhibition remained unknown. More specifically, it remained to be discovered which upstream step(s) is specifically inhibited by CyaY. Using a step-wise detailed analysis of the effects of CyaY on each and every upstream step and one downstream step, we sought to pinpoint the step(s) affected by CyaY. To accomplish this, we divided the whole pathway into four major steps – 1) persulfide formation, 2) sulfur transfer, 3) cluster synthesis and 4) cluster

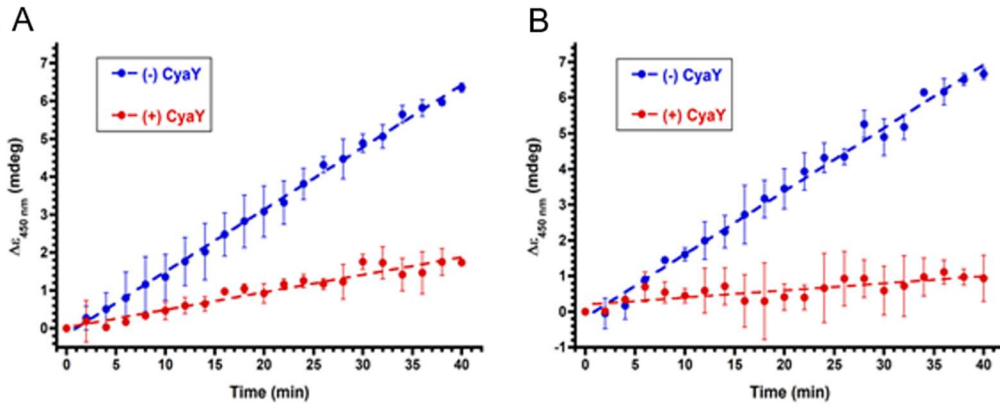

Figure 3.5. CyaY inhibits one pot cluster assembly on Grx4 while IscU^{I108M} has no effect. Reactions included 0.5 µM IscS, 20 µM IscU (A) or IscU^{I108M} (B) 200 µM $Fe_2(NH4)_2SO_4$ and 40 µM Grx4 in the presence and absence of 40 µM CyaY. The reaction was initiated with addition of 100 µM cysteine and 10 mM GSH. Cluster assembly on apo-Grx4 was measured by monitoring ellipticity at 450 nm.

transfer (Fig. 3.6). We were aware that FXN activates persulfide formation on NFS1 by accelerating quinonoid decay. Therefore, we first tested if CyaY affects quinonoid decay. Using stopped-flow spectroscopy, we found that CyaY does not affect quinonoid decay. Interestingly, we observed that mobile loop cysteine (C328) of IscS is the proton donor that causes quinonoid decay to ketimine. The same result had been obtained for human system where mobile loop cysteine of NFS1 was the proton donor (chapter II). This strongly suggests that despite the structural and functional differences of prokaryotic and eukaryotic type-I cysteine desulfurases, proton donation to quinonoid via mobile loop cysteine is common mechanistic step for all type-I cysteine desulfurases. Also, similar effect was observed when mobile loop cysteine of SufS of Synechocystis sp. PCC 6803 (a type-II cysteine desulfurase) was mutated to alanine [75]. This further suggests that mobile loop proton donation to quinonoid occurs for all cysteine desulfurases. It will be interesting to understand why mobile loop cysteine became the obligate proton donor for quinonoid decay instead of PLP-binding lysine residue which has been shown to function as proton donor in a number of cases.

Next, we examined if CyaY inhibits persulfide formation on IscS and IscU. Using the persulfide formation assay, we found that CyaY does not affect persulfide formation on IscS. This is consistent with our observation that CyaY does not accelerate quinonoid decay. It is unlike the effect of FXN on human system where FXN was shown to accelerate persulfide formation on NFS1. This suggests that unlike FXN based activation, CyaY does not perturb mobile loop trajectory. Further, we found that CyaY did not affect cysteine desulfurase activity, consistent with previous literature. As persulfide formation on IscS

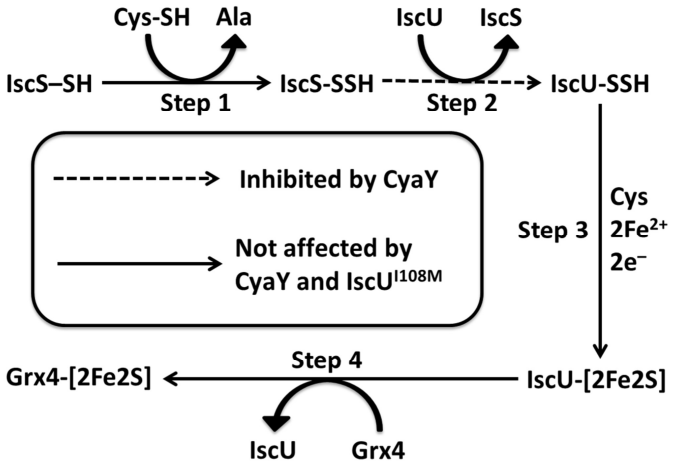

Figure 3.6 Schematic diagram showing the effect of CyaY and IscU^{I108M} on each step. CyaY inhibits only sulfur transfer step and IscU^{I108M} has no effect

remained same in presence of CyaY, persulfide cleavage step must also be similar to result in similar rate of sulfide production in methylene blue assay. From this, we can further deduce that CyaY does not perturb electrophilicity of the mobile loop persulfide which is in a stark contrast to FXN. However, in that same persulfide formation assay, we found that CyaY strongly inhibits persulfide formation on IscU. This is exactly opposite to the effect of FXN which, has been shown to accelerate persulfide formation on ISCU2. The question is how does CyaY inhibits persulfide formation on IscU. As we deduced earlier that CyaY does not perturb either mobile loop trajectory or electrophilicity, we think CyaY may be causing a small conformational change in IscU, which results in misalignment of mobile loop trajectory and the cysteine residue on IscU that accepts sulfane sulfur. In absence of crystal structure of SUC complex, it is extremely difficult to determine if this is the case. It is also possible that CyaY simply sterically prevents mobile loop cysteine from reaching to IscU and prevents sulfur transfer, which has been predicted using an in-silico study [134]. As expected, consistent with previous literature, CyaY was also found to strongly inhibit iron sulfur cluster formation on IscU. This shows that inhibition of sulfur transfer to scaffold protein directly translates into the inhibition of iron sulfur cluster biosynthesis.

After successfully determining sulfur transfer as the step that is primarily inhibited by CyaY resulting in slower iron sulfur cluster formation on IscU, we went further to determine - 1) if CyaY has any further role down-stream and 2) if this inhibitory effect translates to a slower rate of cluster synthesis on downstream acceptors. We found that CyaY does not affect cluster transfer from holo-IscU to apo-Grx4 but inhibits one-pot

cluster synthesis on Grx4. This shows that the inhibitory effect of CyaY on IscU cluster assembly slows down overall cluster biosynthesis process. This leads us to an important question - how does this inhibitory effect affect fitness of an organism? We can predict that in absence of CyaY, an organism will produce iron sulfur cluster at a much faster rate. However, this also means transcriptional regulator IscR will also get iron-sulfur cluster faster and will start repressing protein translation to prevent overproduction of iron sulfur cluster i.e. iron sulfur cluster production will remain normal in absence of CyaY and there would not be any usual phenotypes such as growth defect, unusual activity of iron sulfur cluster containing proteins etc. That is exactly what has been reported for CyaY deleted strain when grown in normal rich media [122, 128]. However, a number of publications also reported that CyaY deletion affects organism's fitness under specific conditions and proposed that CyaY has a positive role in iron sulfur cluster biosynthesis. However, those reports did not discuss the inhibitory effect of CyaY *in vitro* and how this inhibitory effect may make CyaY important under those conditions. It has been shown that when YggX and ApbC genes were deleted together or separately, the presence of CyaY becomes crucial. YggX has been shown to sequester Fe(II) from participating in Fenton chemistry while keeping it available for iron dependent cellular processes and thereby preventing oxidative damage[135, 136]. ApbC is a member of MinD protein family and takes part in iron sulfur cluster metabolism process [137-140]. Understandably, absence of ApbC results in iron sulfur cluster metabolism defect and subsequent oxidative stress. When cells were grown in presence of H_2O_2, NO or paraquat, deletion of CyaY inhibited growth. This inhibition was exacerbated when YggX was also deleted [129]. Considering these results,

CyaY definitely seems to have a positive effect on the fitness of organism under oxidative stress conditions. Interestingly, IscR deletion strain which cannot regulate iron sulfur production through transcriptional inhibition becomes hypersensitive to oxidative stress just like CyaY deletion strain [141]. It seems as if iron sulfur cluster acts as fuel for reactive oxygen species. Taken together, overproduction of iron sulfur cluster seems to be detrimental to the fitness of an organism in the event of oxidative stress and inhibitory effect of CyaY on iron sulfur cluster production can explain the apparent positive effect of CyaY. At present, there is no direct evidence that overproduction of iron sulfur cluster can exacerbate oxidative stress by acting as fuel for it but if that is the case, it will change our understanding significantly.

It had been shown by Dancis group that a single point mutation (M → I) on scaffold protein in yeast can rescue all FXN deletion phenotypes via bypassing FXN i.e. M → I mutation on scaffold protein in eukaryotes can make the organism FXN independent [142, 143]. As deletion of CyaY has no effect under normal growth condition, *E. coli* is CyaY independent. This led to study by Roche *et al.* to determine if the reverse mutation I → M would render *E. coli* CyaY-dependent [131]. They showed that cellular iron sulfur cluster level decreased for I → M mutation in *E. coli* and was even worse in absence of CyaY. Recently we determined that ISCU2^{M106I} bypasses FXN by accelerating cluster transfer to GRX5 in human system. Here, we did a similar step-wise analysis to study the effect of IscU^{I108M} on each step in the presence and absence of CyaY. More specifically, we tested if IscU^{I108M} slows down any step and whether CyaY rescues the rate. We found that IscU^{I108M} variant behaved just like wild type in all the steps and the

effect of CyaY on cluster assembly of scaffold protein was also similar for $IscU^{I108M}$ and wt-IscU i.e. inhibitory rather than accelerating. Therefore, we still don't have a mechanism that explains the effect of I → M mutation on scaffold protein of *E. coli in vivo*.

Materials and Methods

Protein purification. IscS, IscU and CyaY were purified as described previously [46]. The QuikChange method (Stratagene) was used to introduce point mutation (I108M) into plasmid containing wt-IscU [133]. The mutation was confirmed by DNA sequencing (Gene Technology Lab, TAMU). $IscU^{I108M}$ was purified using the same protocol as wt-IscU. Grx4 was purified following literature procedure[144]. Unless otherwise stated, all the reactions were carried out in an anaerobic glove box (O_2 < 1 ppm).

Stopped flow kinetics. Proteins (100 μM final concentration of each protein) were taken in one of the two syringes of the stopped flow apparatus (KinTek Corporation). The other syringe contained 10 mM Cysteine. They were mixed together by pressing both the syringes simultaneously. First λ_{max} of each intermediate were determined by monitoring the change of absorbance every 2 ms in a 100 nm window. λ_{max} for quinonoid and aldimine intermediate were found to be 508 nm and 410 nm respectively, which were later used to monitor the kinetics of the intermediate. We could not detect a sharp peak around 340 nm for ketimine intermediate. We therefore used 340 nm as this wavelength has been used previously [75]. Next, formation of aldimine, quinonoid and ketimine intermediate were followed by monitoring absorbance at 410, 508 and 340 nm respectively. For quinonoid kinetics, traces of 508 nm with time were fitted with Origin software (OriginLab) to Consecutive B equation [$y = y0 + (k_1*[A]_0/(k_2-k_1))*(\exp(-k_1*t)-\exp(-k_2*t))$], where k_1

and k_2 are rate constants of the formation and decay of cys-qiononoid intermediate respectively. The rates were compared for IscS, $IscS^{C328A}$, SU, SUC, SU^{I108M} and $SU^{I108M}C$ (Fig. 3.1). [R^2 values: IscS (0.99), $IscS^{C328A}$ (0.83), SU (0.99), SUC (0.99), SU^{I108M} (0.99), $SU^{I108M}C$ (0.99)]. Aldimine and ketimine (410 nm and 340 nm traces respectively) could not be fit using Consecutive B equation as kinetics was more complex.

Separation of proteins for sulfur transfer reaction. All the proteins (IscS, IscU and CyaY) were separated using C4 column (WAT011807, Waters) on HPLC (1260 Infinity, Agilent Technologies) at pH 2.0 (0.1 % TFA in water, Buffer A) by running a gradient of Buffer B (60% CH_3CN, 40% Isopropanol, 0.1% TFA) from 30% to 70% within 40 min with 1mL/min flow rate (Fig. 3.2A).

Measurement and quantification of radioactivity on proteins. The amount of radioactivity and in turn persulfide on IscS and IscU were determined using a similar procedure as described in detail (Chapter IV). Briefly, [^{35}S]-cysteine (PerkinElmer, 10.2 μM, 1.00796 mCi) was diluted 50 times by 1 mM non-radioactive cysteine resulting in a 204 nM final concentration of [^{35}S]-cysteine in the stock solution and the ratio of [^{35}S]-cysteine over cold cysteine became 0.000204. After elution, the protein was passed through a mixer where it was combined with scintillation cocktail (BioCount 111182) and signal was recorded with β-RAM radio-HPLC detector (Model 5C, LabLogic). Data collection and analysis were done with Laura software (LabLogic). Area under the scintillation peak (in CPM) was determined for each protein and converted into [^{35}S] concentration associated with protein by using a standard curve plotted from known amounts [^{35}S]-cysteine (and determining area under the peak corresponding to cysteine).

Total amount of persulfide on protein was obtained via dividing it by the [^{35}S]-cysteine and non-radioactive cysteine ratio.

Persulfide formation assay. Protein complexes (SU and SUC) were reacted with 30 μM cysteine (contains 0.0204% [^{35}S]-cysteine) at 37°C followed by quenching at different time points starting from thirty seconds to one hour. Final protein concentrations were 30 μM IscS, 30 μM IscU and 75 μM CyaY (for SUC) with 50 μL reaction volume. The samples were quenched by mixing 150 μL quenching solution (conc. HCl and 6 M Guanidine hydrochloride (in 1:4 ratio, pH<1) to the 50 μL reaction. 150 μL of the resulting 200 μL was injected into HPLC for analysis. Amount of persulfide associated with IscS and IscU was calculated as described above and plotted against time (Fig. 3.2). The data points were fitted using Origin software (OriginLab) to exponential rise equation [y=m1+m2*(1-exp (-m3*x))] where m3 value gives the apparent rate of formation. [R^2 values; IscS-SSH formation: 0.98 (SU), 0.98 (SUC); IscU-SSH formation: 0.98 (SU), 0.88 (SUC)].

Cysteine desulfurase activity. Cysteine desulfurase activities were measured for each complex (SU, SUC, SU^{I108M} and $SU^{I108M}C$) according to following procedure**.** In short, a heating block was used to bring the temperature to 37°C. The proteins were mixed to a final concentration of 0.5 μM IscS, 2.5 μM IscU (or $IscU^{I108M}$), 5 μM CyaY and 2 mM DTT followed by incubation for 15 minutes on heating block already at 37°C, cysteine was then added and the reaction was then incubated for additional 6 min before quenching the 800 μL reaction mixture with 100 μL of *N, N′*-diphenyl-*p*-phenylenediamine (DPD, in 7.2 M HCl) and 100 μL of $FeCl_3$ (in 1.2 M HCl) with final concentration of DPD and

$FeCl_3$ being 30 μM and 20 μM respectively. The samples were centrifuged after 20 min incubation at 37ºC and absorbance was measured at 670 nm. The amount of sulfide produced was determined for each data point using a standard curve. Rates ($[S^{2-}]$/([SD]*min)) were plotted against the amount of cysteine added and fitted with Origin software (OriginLab) using Michaelis-Menten Equation to obtain k_{cat} and K_M values for each complex (Fig. 3.3). [R^2 values: SU (0.98), SUC (0.998), SU^{I108M} (0.99), $SU^{I108M}C$ (0.99)].

CD spectroscopy. CD spectra were recorded on a Chirascan CD spectrometer (Applied Photophysics) using a 1 cm path length cuvette. Cuvettes were sealed with a rubber septa and electrical tape in a glove box (O_2 < 1 ppm). The assays were run in 50 mM HEPES, 150 mM KCl, and 10mM $MgCl_2$ (pH 7.5) at 22ºC.

Cluster assembly assay on IscU. The assay constituted 8 μM IscS, 40 μM IscU (or $IscU^{I108M}$), 50 μM CyaY, 200 μM $Fe(NH_4)_2(SO_4)_2$ and was initiated with addition of 10 mM GSH and 100 μM cysteine using air tight syringes. The cluster assembly rates were measured for SU, SUC, SU^{I108M}, $SU^{I108M}C$ by monitoring the ellipticity change at 330 nm over time and fitting the initial data points using Kaleidagraph (synergy software) to linear equation ($y=m_1x+m_2$), where m_1 gives the initial rate of cluster synthesis **(**Fig. 3.4**)**. [R^2 values: SU (0.99), SUC (0.96), SU^{I108M} (0.99), $SU^{I108M}C$ (0.99)].

Cluster transfer assay from holo-IscU to apo-Grx4. 20 μM IscU was re-constituted using 1 μM IscS, 40 μM CyaY, 400 μM $Fe(NH_4)_2(SO_4)_2$ and 40 μM cysteine with cysteine being the limiting reagent to inhibit any further cluster-synthesis. 40 μM Grx4 was then injected into the cuvette anaerobically using an air-tight syringe and the cluster transfer to

the latter was followed by monitoring the ellipticity change at 450 nm over time and fitting the initial data using Kaleidagraph (synergy software) to linear equation ($y=m_1x+m_2$), where m_1 gives the initial rate of cluster transfer from Holo-IscU to apo-Grx4. 450 nm was chosen as the wavelength to monitor the transfer due to minimal contribution from holo-IscU at that wavelength. The rates were compared for SU, SUC. [R^2 values: SU (0.93), SUC (0.93)].

One-pot cluster synthesis on apo-target. 0.5 μM IscS, 20 μM IscU (or $IscU^{I108M}$), 40 μM CyaY, 40 μM Grx4, 200 μM $Fe(NH_4)_2(SO_4)_2$ and initiated by the addition of 10 mM GSH and 100 μM cysteine. Cluster formation on Grx4 was then measured for SU, SUC, SU^{I108M}, $SU^{I108M}C$ by monitoring the change of ellipticity at 450 nm over time and fitting the initial time points using Kaleida graph (synergy software) to linear equation ($y=m_1x+m_2$), where m_1 gives the initial rate of cluster formation on Grx4 **(**Fig. 3.5**)**. [R^2 values: SU (0.99), SUC (0.94), SU^{I108M} (0.99), $SU^{I108M}C$ (0.62)].

CHAPTER IV

MECHANISM FOR ACTIVATION AND BYPASS OF FRATAXIN IN HUMAN IRON SULFUR CLUSTER BIOSYNTHESIS

Introduction

Iron sulfur (Fe-S) clusters are ubiquitous protein cofactors that are required for critical cellular processes in most organisms [2, 69]. Fe-S clusters exist in a variety of stoichiometries, most often as $[2Fe\text{-}2S]^{2+/1+}$ and $[4Fe\text{-}4S]^{2+/1+}$ species, and commonly function in substrate activation and as electron transfer conduits. These Fe-S clusters are synthesized and distributed to apo-target proteins by conserved biosynthetic pathways The structural core of this assembly complex consists of cysteine desulfurase (NFS1), eukaryotic-specific LYR protein (ISD11), and acyl carrier protein (ACP) subunits and is referred to as the SDA complex [145, 146]. The ISD11 and ACP subunits are required for function, stabilize NFS1, and favor different quaternary interactions for NFS1 than its prokaryotic homologs [47, 78, 146-148]. Sulfur is then transferred from NFS1 to a cysteine residue on the scaffold protein ISCU2 (Fig. 4.1, step 2). ISCU2 combines sulfane sulfur with Fe^{2+} and electrons to produce $[2Fe\text{-}2S]^{2+}$ clusters (Fig. 4.1, step 3) in a poorly understood process. To complete catalytic turnover, intact [2Fe-2S] cluster intermediates on ISCU2 are transferred to a cluster carrier protein, such as the monothiol glutaredoxin GRX5 (Fig. 4.1, step 4), as a part of the cluster distribution network.

Although eukaryotes clearly also require frataxin (FXN) for the synthesis of Fe-S clusters [149, 150], the precise role of FXN remains controversial. The loss of *FXN* is linked to the fatal neurodegenerative disease Friedreich's ataxia [84], and results in

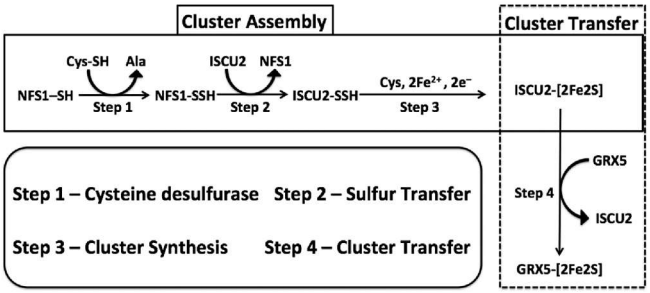

Figure 4.1. Steps involved in cluster biosynthesis pathway. The overall process of cluster biosynthesis in humans was divided into four broad steps and used as a general guideline to evaluate which step(s) FXN and ISCU2^{M106I} are affecting.

decreased activity for Fe-S cluster enzymes, accumulation of iron in the mitochondria, and susceptibility to oxidative stress [42]. Identifying the role of FXN has been complicated by the existence of isoforms of different lengths. The longer form, FXN_{56-210}, can undergo an iron-dependent oligomerization to produce a species reminiscent of ferritin that may function in iron storage [151, 152]. The truncated form, $FXN^{\Delta 1-80}$, is widely considered to be the functional form *in vivo*; truncated FXN is monomeric even in the presence of iron [153], interacts with the NFS1-ISD11-ISCU2 complex [31, 77, 89, 154, 155], and rescues cells challenged with *FXN* depletion [156]. Early studies revealed that $FXN^{\Delta 1-80}$ has a modest binding affinity for iron (3-55 μM) and led to the proposal that FXN accelerates Fe-S cluster synthesis by functioning as a chaperone that donates iron [43, 44, 85, 86, 154, 157-160] More recently, multiple studies provide evidence that FXN functions as an allosteric activator that enhances cysteine desulfurase activity and the subsequent rate of Fe-S cluster assembly on the scaffold protein [31, 33, 89, 161]. FXN has been proposed to affect the sulfur chemistry by enhancing cysteine binding to the PLP cofactor of the cysteine desulfurase [99], and increasing sulfur transfer to the scaffold protein and small molecule thiols [31, 161]. Conflicting results indicate that FXN does [33, 99] or does not [161] affect persulfide formation on NFS1. Interestingly, a suppressor mutant on *Saccharomyces cerevisiae* Isu1 (homolog of human ISCU2; $Isu1^{M107I}$ also known as $Isu1_{Sup}$) was identified that rescues the depletion of *S. cerevisiae* Yfh1 (homolog of human FXN) [142, 162]. Initial studies have suggested that $Isu1^{M107I}$ increases the accumulation of persulfide species on Nfs1 similar to the addition of FXN [33, 99]. Despite these

advances, mechanistic details of how FXN functions in Fe-S cluster biosynthesis are still lacking.

Here, new assays were developed to probe how FXN and human ISCU2^{M106I} (equivalent to Isu1^{M107I}) affect the kinetics of individual steps in Fe-S cluster biosynthesis. We found that the addition of either FXN or substitution of ISCU2 with ISCU2^{M106I} increased the overall rate of cluster synthesis and transfer to GRX5. Further, these studies provide compelling evidence that FXN accelerates reactions involving the NFS1 mobile S-transfer loop that result in an increased rate of [2Fe-2S] cluster assembly on ISCU2. In contrast, ISCU2^{M106I} primarily affects the transfer rate of intact [2Fe-2S] clusters from ISCU2 to GRX5. Overall, our results provide new mechanistic insight into Fe-S cluster biosynthesis and indicate FXN and ISCU2^{M106I} function at distinct stages of this pathway.

Results

Both the ISCU2^{M106I} substitution and FXN accelerate the formation of [2Fe-2S] clusters on GRX5. Our initial objective was to test if substitution of human ISCU2 with the ISCU2^{M106I} variant functions analogously to FXN and stimulates Fe-S cluster biosynthesis. A circular dichroism (CD) assay was developed to monitor an entire Fe-S cluster assembly and transfer reaction (Fig. 4.1, steps 1-4) to better reproduce the *in vivo* biosynthetic pathway than previously reported assays that only monitor partial reactions. This assay takes advantage of the positive ellipticity from [2Fe-2S]-GRX5 and low ellipticity from [2Fe-2S]-ISCU2 at 450 nm. The reaction conditions contained the recombinantly expressed human NFS1-ISD11 complex that co-purified with *Escherichia coli* ACP (SDA_{ec}) [4, 41], with the addition of recombinant human ISCU2 ($SDA_{ec}U$),

ISCU2^{M106I} (SDA_{ec} U^{M106I}), or ISCU2 and FXN (SDA_{ec} UF). Reactions were initiated with the addition of L-cysteine and glutathione, which is required for binding the Fe-S cluster to GRX5. All complexes exhibited final CD spectra consistent with [2Fe-2S]-GRX5. Similar overall rates were observed for the SDA_{ec} UF and $SDA_{ec}U^{M106I}$ complexes (Fig. 4.2A and Table 4.1), which were about 3 times greater than the SDAecU complex. The results from this in vitro Fe-S cluster biosynthetic assay are consistent with both the stimulation of activity by FXN and the bypass of FXN by ISCU2^{M106I}.

FXN and ISCU2^{M106I} operate at different steps in Fe-S cluster biosynthesis. We tested the effect of adding FXN to the $SDA_{ec}U^{M106I}$ complex in complete cluster assembly and transfer reactions (Fig. 4.1, steps 1-4). The $SDA_{ec}U^{M106I}$F complex had a rate that was faster than SDA_{ec}U (nearly 7-fold greater) and was about twice the rate of either the SDA_{ec}UF or $SDA_{ec}U^{M106I}$ complex (Fig. 4.2A and Table 4). This additive result in the Fe-S assembly assay hints that the stimulatory effects of FXN and ISCU2^{M106I} occur at different steps in Fe-S cluster biosynthesis. As FXN was previously shown to increase the rates of partial reactions, including the Fe-S cluster assembly reaction on ISCU2 and the cysteine desulfurase activity of SDA_{ec}U [31, 49, 163], we tested whether ISCU2^{M106I} also affected those steps of Fe-S cluster biosynthesis.

The ISCU2^{M106I} variant was tested for its ability to mimic FXN and increase the rate of [2Fe-2S] cluster formation on ISCU2 (Fig. 4.1, steps 1-3). We used CD to monitor [2Fe-2S] cluster formation on ISCU2 and ISCU2^{M106I} by following changes in ellipticity at 330 nm, similar to a previously reported assay [163]. Here, the addition of FXN to the SDA_{ec}U complex was shown to accelerate Fe-S cluster formation on ISCU2

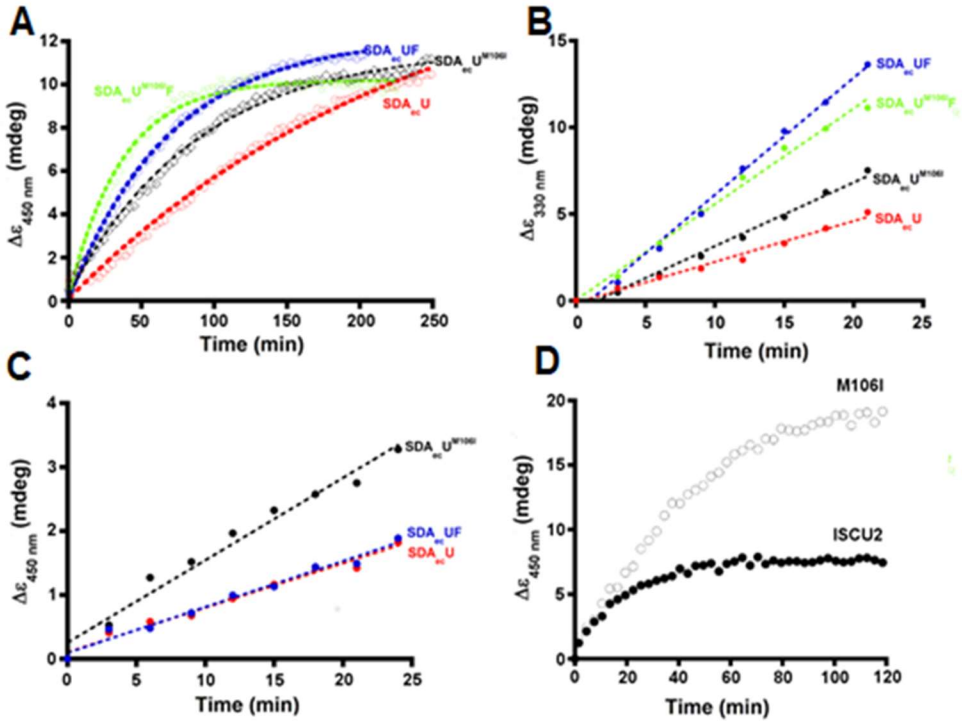

Figure 4.2. FXN and the ISCU2^{M106I} substitution accelerate different steps in Fe-S cluster biosynthesis. A) Kinetics of Fe-S cluster synthesis and transfer to GRX5 were monitored for different assembly complexes by the change in ellipticity at 450 nm. The average change in ellipticity (n = 3; maximum error of 1.8 in ellipticity) is plotted and fit with an exponential rise equation. B) Fe-S cluster assembly reactions on ISCU2 were monitored for assembly complexes by the change in ellipticity at 330 nm. The average change in ellipticity (n = 3; maximum error of 1.8 in ellipticity) is plotted and fit with a linear equation. C) Kinetics of cluster transfer from pre-formed holo-ISCU2 to apo-GRX5 were monitoring by the change in ellipticity at 450 nm. Reactions were initiated (time = 0) by the anaerobic injection of GRX5 (with or without FXN). The average change in ellipticity (n = 3; maximum error of 0.8 in ellipticity) is plotted and fit with a linear equation. D) Chemically reconstituted ISCU2 (or ISCU2^{M106I}) was reacted with GRX5 and the [2Fe-2S] cluster transfer was monitored by the increase in ellipticity at 450 nm. Color scheme: SDA$_{ec}$U (red), SDA$_{ec}$UF (blue), SDA$_{ec}$U^{M106I} (black) and SDA$_{ec}$U^{M106I}F (green).

Table 4.1. Effect of FXN and ISCU2^{M106I} on kinetic parameters in all the steps in iron sulfur cluster biosynthesis pathway

						Relative Rate with respect to $SDA_{ec}U$	
		$SDA_{ec}U$	$SDA_{ec}U^{M106I}$	$SDA_{ec}UF$	$SDA_{ec}U^{M106I}F$	$SDA_{ec}U^{M106I}$	$SDA_{ec}UF$
Cysteine desulfurase activity	k_{cat} (min^{-1})	0.82 ± 0.03[a]	0.90 ± 0.02	10.07 ± 0.15[a]	7.34 ± 0.34	1.1	12.3
	K_M (μM)	0.62 ± 0.11[a]	0.65 ± 0.09	11.61 ± 0.92[a]	8.0 ± 2.0		
Complete reaction	Cluster synthesis & transfer to GRX5 (mdeg/min $X10^{-3}$)	4.1 ± 0.3	11.3 ± 0.2	14.4 ± 0.2	27.2 ± 0.9	2.8	3.5
Cluster transfer	Cluster transfer ISCU2 to GRX5 (mdeg/min X 10^{-3})	70 ± 0.5	130 ± 1	68 ± 5	ND	1.9	1.0
Cluster synthesis	Cluster formation on ISCU2 (mdeg/min X 10^{-2})	24 ± 1	37 ± 2	68 ± 2	55 ± 1	1.5	2.8
Sulfur transfer reactions with [^{35}S]-Cys (min^{-1} X 10^{-2})	Persulfide formation on NFS1 (k_1 and k_3)	0.8 (0.75 – 0.81)[b]	ND	5.2 (5.1 – 5.2)[b]	ND	–	6.5
	Persulfide transfer NFS1 to ISCU2 (k_2)	8.6 (8.5 – 9.6)[b]	ND	266 (252 – 282)[b]	ND	–	30.9
	Persulfide back transfer ISCU2 to NFS1 (k_{-2})	8.4 (8.2 –10.0)[b]	ND	254 (241 – 270)[b]	ND	–	30.2
Pulse-chase experiments (min^{-1} X 10^{-2})	Persulfide decay for NFS1	8 ± 1[c]	ND	42 ± 7[c]	ND	–	5.3
	Persulfide decay for ISCU2	6 ± 2[c]	ND	0.048 ± 0.0015[c,d]	ND	–	0.008
PLP Chemistry	Cys-quinoid formation (s^{-1})	19.5 ± 0.5	9.3 ± 0.1	17.5 ± 0.4	ND	0.5	0.9
	Cys-quinoid decay (s^{-1})	1.19 ± 0.03	1.47 ± 0.01	4.80 ± 0.07	ND	1.2	4.0

[a]Data from reference 4, [b]The values in parentheses denotes the lower and upper limit of the best fit value (rate constant). These were calculated at 99% and 99.7% confidence contours for $SDA_{ec}U$ and $SDA_{ec}UF$ complexes, respectively. [c]Spiked with 1 mM non-radioactive L-cysteine. [d]Determined with linear fit. ND – Not determined.

(2.8 fold greater) under a comparable set of conditions (Fig. 4.2B, Table 4.1). The $SDA_{ec}U^{M106I}$ complex exhibited 1.5 times greater cluster synthesis activity compared to the native $SDA_{ec}U$ complex, but only about half the activity of $SDA_{ec}UF$. Addition of FXN to the $SDA_{ec}U^{M106I}$ complex further enhanced the activity (1.5 fold greater), consistent with FXN stimulation of the native system.

We also tested the effect of substituting the $ISCU2^{M106I}$ variant for ISCU2 in cysteine desulfurase activity assays. SDA_{ec} was previously shown to exhibit a low k_{cat} (0.60 min^{-1}) for the cysteine desulfurase reaction [49], which was not affected by the addition of ISCU2, but showed a stimulation by an order of magnitude upon the addition of both ISCU2 and FXN [31, 49]. The $SDA_{ec}U^{M106I}$ complex exhibited kinetic parameters highly similar to the $SDA_{ec}U$ complex with a k_{cat} 10-fold lower than the $SDA_{ec}UF$ complex (Table 4.1). Moreover, addition of FXN to the $SDA_{ec}U^{M106I}$ complex stimulated k_{cat} in a manner reminiscent of the wild type system. Overall, the additive effect in complete synthesis and transfer assays coupled to the inability of $ISCU2^{M106I}$ to replace FXN in partial Fe-S cluster assembly and cysteine turnover reactions are consistent with FXN and $ISCU2^{M106I}$ affecting different steps of Fe-S cluster biosynthesis.

The $ISCU2^{M106I}$ substitution accelerates cluster transfer to GRX5. Since ISCU2 acts as a scaffold for [2Fe-2S] cluster synthesis and functions as an intermediate to transfer these clusters to target proteins, we evaluated the ability of FXN and $ISCU2^{M106I}$ to affect the transfer of the [2Fe-2S] cluster intermediate from ISCU2 to GRX5 (Fig. 4.1, step 4). The $SDA_{ec}U$ and $SDA_{ec}U^{M106I}$ complexes were incubated with L-cysteine and ferrous iron in the absence of GRX5 and the development of the characteristic [2Fe-2S]-ISCU2 CD

spectrum was observed. After completion of the [2Fe-2S]-ISCU2 formation reaction, apo-GRX5 (with or without FXN) was added under anaerobic conditions, and the cluster transfer reaction from ISCU2 to GRX5 was followed by monitoring the increase in ellipticity at 450 nm (Fig. 4.2C). The rates of cluster transfer for the native complex with and without FXN were the same within error (Table 4.1), establishing that FXN does not have a role in cluster transfer under these conditions. In contrast, Fe-S assembly complexes containing the ISCU2^{M106I} substitution almost doubled the rate of cluster transfer to GRX5 compared to those with wild-type ISCU2.

Next, we tested whether the dissociation of [2Fe-2S]-ISCU2 or [2Fe-2S]-ISCU2^{M106I} from the SDA_{ec} complex, which is thought to be necessary to facilitate cluster transfer, impacts cluster exchange reactions with GRX5. Fe-S clusters were chemically reconstituted on ISCU2 and ISCU2^{M106I} in the absence of the SDA_{ec} complex. After purification, ISCU2 and ISCU2^{M106I} each bound approximately two iron atoms and two sulfide atoms per protein. The [2Fe-2S]-bound proteins were reacted with GRX5 and shown to have similar initial kinetics but different overall extents of transfer (Fig. 4.2D). The ellipticity change for ISCU2^{M106I} was approximately 4 times greater than that for native ISCU2, suggesting that the ISCU2^{M106I} substitution alters the cluster-binding equilibrium compared to native ISCU2 and favors the cluster-bound GRX5 species. One possible explanation for this result is that the [2Fe-2S] cluster bound to ISCU2^{M106I} is less stable leading to enhanced transfer to GRX5. To test this possibility, a DTT extrusion assay was used to examine the susceptibility of ISCU2 and ISCU2^{M106I} to loss of their [2Fe-2S] clusters. [2Fe-2S] clusters were enzymatically generated on ISCU2 (or

ISCU2^{M106I}) and the proteins were combined with DTT. Both samples lost a majority of their cluster-dependent CD signal within 30 min. The similar rates of cluster loss (within 15% of one another; indicates the much greater extent of [2Fe-2S] cluster transfer from the ISCU2^{M106I} sample to GRX5 (Fig. 4.2D) involves more than just a change in cluster stability. Overall, these studies indicate that the ISCU2^{M106I} substitution, but not FXN, affects the Fe-S cluster transfer reaction from ISCU2 to GRX5.

FXN accelerates persulfide formation on NFS1 and ISCU2[5]. Our next objective was to further define how FXN accelerates Fe-S cluster synthesis. To probe the effect of FXN on the rates of sulfur accumulation on NFS1 and ISCU2 (Fig. 4.1, steps 1 and 2), a rapid acid quench assay was developed that couples HPLC separation with radiolabeled sulfur detection. In this assay, various Fe-S assembly complexes are reacted with L-[^{35}S]-cysteine substrate, quenched with acid after different reaction times, and applied to a reverse phase HPLC column for analysis of protein content (absorbance) and persulfide label (radioactivity). The ability to rapidly protonate thiolate nucleophiles, which inhibits sulfur transfer reactions [164], and analyze proteins for ^{35}S incorporation under quench conditions are critical aspects of this assay. Control experiments established conditions to separate proteins in the SDA$_{ec}$UF complex that contain cysteine residues (NFS1 and ISCU2). The effectiveness of acid in quenching sulfur transfer from NFS1 to ISCU2 was established by reactions under normal and quench conditions. Initial studies with excess

[5] The experiments in this section are performed and analyzed by Shachin Patra from Barondeau group at Texas A&M University.

L-[^{35}S]-cysteine substrate resulted in labeling of multiple cysteine residues on NFS1 and ISCU2. Some of these labeled cysteine residues, especially on NFS1 (C158, C163, C353, and C426), are likely due to side-reactions of the $SDA_{ec}U$ complex that occur with excess cysteine substrate, long incubation times, and no additional reductant or iron; these conditions likely permit sulfur transfer reactions from persulfide species to excess cysteine and subsequent scrambling of the radiolabel.

The rates of persulfide formation on NFS1 and ISCU2 were determined using stoichiometric amount of substrate. The $SDA_{ec}U$ and $SDA_{ec}UF$ complexes were combined with L-[^{35}S]-cysteine, quenched after different reaction times, and the proteins were separated under quenching conditions. Plotting the amount of radiolabel as a function of time revealed saturation between 0.20-0.25 labels per NFS1 (Figs. 4.3A and 4.3B) and ISCU2 (Figs. 4.3C and 4.3D) for the $SDA_{ec}U$ and $SDA_{ec}UF$ complexes. Interestingly, the amount of label on NFS1 did not decrease at longer times as one might expect for sequential irreversible reactions using limited substrate (Fig. 4.1, steps 1 and 2). Persulfide formation on NFS1 and ISCU2, which were fit simultaneously, matched well with an equilibrium sulfur transfer model with a second cysteine turnover (Fig. 4.3E). Models that lack the equilibrium step (k_{-2}) or second cysteine turnover (k_3) did not adequately fit the data. The rates of persulfide formation on NFS1 were constrained to be the same for the $SDA_{ec}U$ (or $SDA_{ec}UF$) complex with or without a persulfide-bound ISCU2 ($k_1 = k_3$). Under these conditions, the slow step for both $SDA_{ec}U$ and $SDA_{ec}UF$ complexes was the formation of the persulfide species on NFS1 (Table 4.1 and Fig. 4.3). FXN accelerated both the rate of persulfide formation on NFS1 (6.5 fold greater) and sulfur transfer from

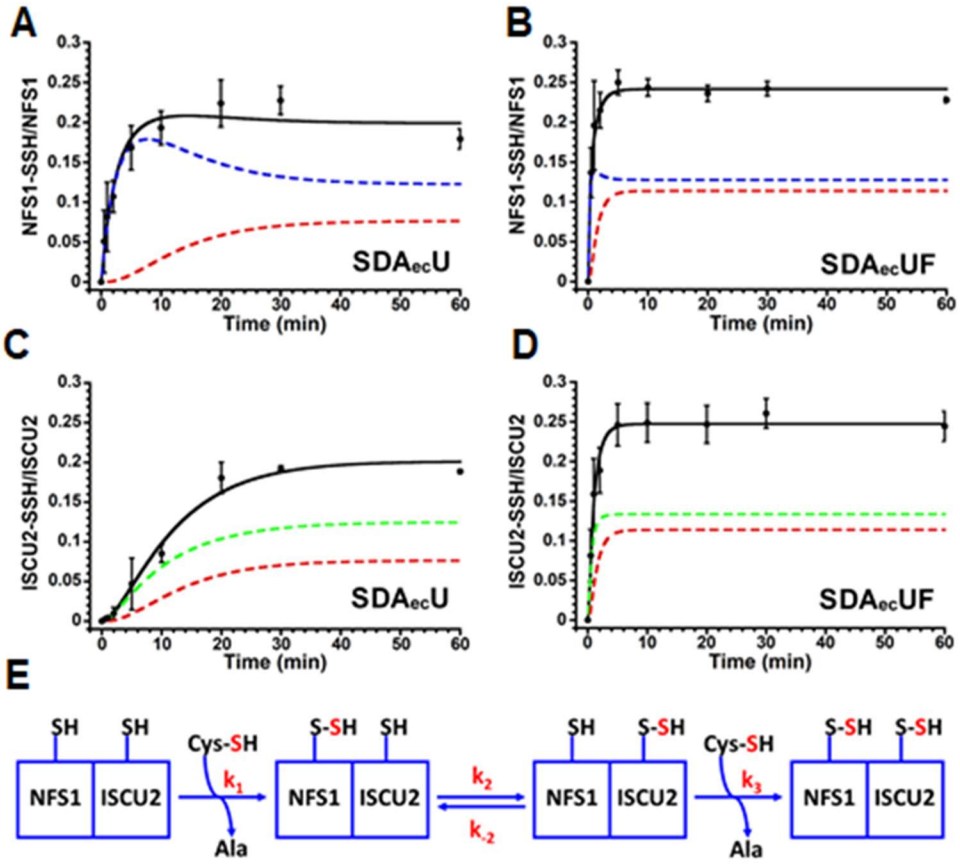

Figure 4.3. FXN accelerates the persulfide formation kinetics on NFS1 and ISCU2. $SDA_{ec}U$ and $SDA_{ec}UF$ complexes were reacted with a stoichiometric amount of L-[^{35}S]-cysteine, quenched with acid, and the proteins were separated using conditions similar to Fig. S9. Formation of [^{35}S]-persulfide was quantitated and plotted for A) NFS1 ($SDA_{ec}U$), B) NFS1 ($SDA_{ec}UF$), C) ISCU2 ($SDA_{ec}U$), and D) ISCU2 ($SDA_{ec}UF$). E) Best-fit kinetic model ($k_1 = k_3$) for persulfide accumulation on cysteine residues of NFS1 and ISCU2. The data for $SDA_{ec}U$ or $SDA_{ec}UF$ were fit simultaneously with KinTek and the fits were validated using FitSpace (Fig. S13). Blue, green, and red dashed lines represent the simulated amounts of persulfide on NFS1, ISCU2, or both NFS1 and ISCU2, respectively. Black lines indicate the total amount of simulated persulfide on NFS1 or ISCU2.

NFS1 to ISCU2 (30 fold greater). This kinetic model suggests the persulfide transfer reaction from NFS1 to ISCU2 is reversible with an equilibrium constant near one for both complexes. These experiments strongly support the proposed role of FXN as an allosteric activator that accelerates sulfur transfer chemistry [31, 33, 161].

FXN affects the rate of persulfide cleavage by free cysteine[6]. Pulse chase experiments were designed to evaluate the ability of FXN to labilize persulfide species and facilitate sulfur transfer chemistry. The cysteine desulfurase substrate, L-cysteine, was tested for its ability to cleave persulfide species associated with the $SDA_{ec}U$ and $SDA_{ec}UF$ complexes. A stoichiometric amount of L-[^{35}S]-cysteine was first incubated with the individual complexes. The labeled complexes were then combined with non-radioactive L-cysteine for various times, quenched with acid, and analyzed as described above. For the $SDA_{ec}U$ complex, spiking the sample with non-radioactive cysteine resulted in the loss of most of the labeled sulfur on both NFS1 and ISCU2, which occurred at similar rates (Fig. 4.4A and 4.4B; Table 4.1). Intriguingly, the addition of FXN resulted in an approximate 5-fold increased rate of sulfur loss from NFS1, but almost no loss of label from ISCU2. To rationalize these results with the above equilibrium kinetic model (Fig. 4.4E), we suggest that cleavage of the [^{35}S]-label occurs primarily from the mobile S-transfer loop of NFS1 and not from ISCU2 (Fig. 4.4C). After NFS1 persulfide cleavage, slow cysteine turnover for the $SDA_{ec}U$ complex results in re-equilibration of the label through inter-protein sulfur

[6] The experiments in this section are performed and analyzed by Shachin Patra from Barondeau group at Texas A&M University.

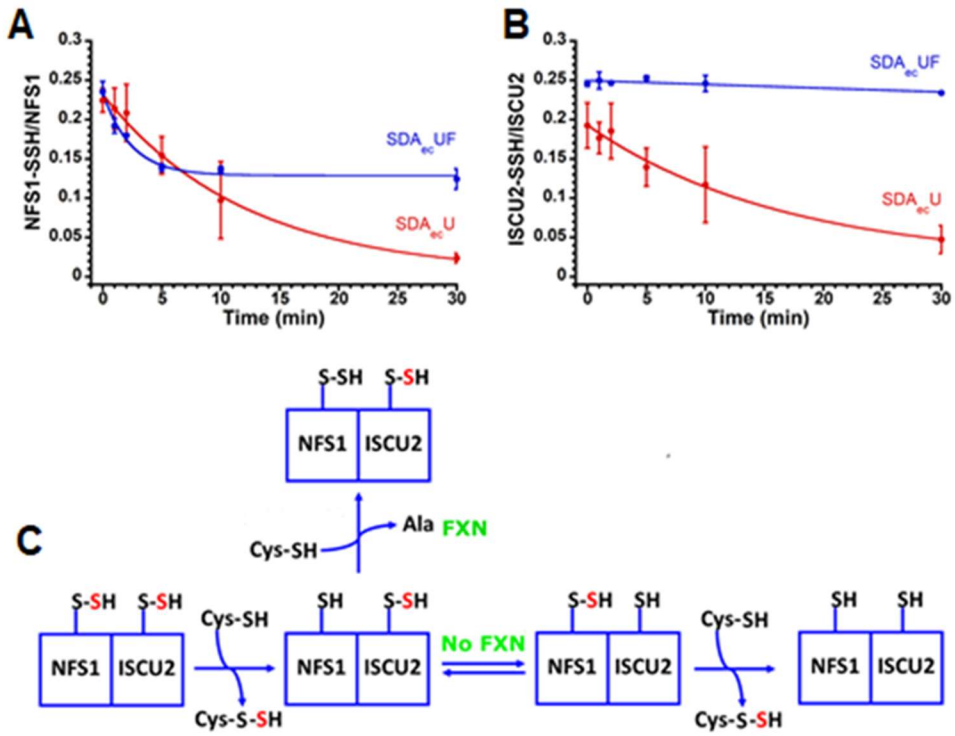

Figure 4.4. FXN accelerates the persulfide decay kinetics from NFS1. $SDA_{ec}U$ (red) and $SDA_{ec}UF$ (blue) complexes were reacted with stoichiometric amounts (30 μM) L-[^{35}S]-cysteine for 40 min and then chased with 1 mM non-radioactive L-cysteine. Samples were then quenched with acid at various times and the amount of remaining [^{35}S]-label on A) NFS1 and B) ISCU2 were determined. The data were fit to an exponential decay or linear (loss of ISCU2 label from $SDA_{ec}UF$ complex) equation. C) Model for the effect of FXN on persulfide decay from the $SDA_{ec}U$ and $SDA_{ec}UF$ complexes. The NFS1 persulfide is proposed to be the primary species cleaved during the chase experiment. In the presence of FXN, the persulfide on NFS1 is rapidly regenerated by turnover with non-radioactive L-cysteine. In the absence of FXN, slower cysteine desulfurase turnover results in re-equilibration (transfer) of the ISCU2 radiolabeled sulfur (atom colored red) to NFS1 and subsequent cleavage.

transfer from ISCU2, explaining the similar persulfide depletion rates for NFS1 and ISCU2 (Table 4.1 and Fig. 4.4). In contrast, the $SDA_{ec}UF$ complex is proposed to repopulate the mobile S-transfer loop of NFS1 through rapid enzymatic cysteine turnover rather than re-equilibration, reconciling the apparent protection by FXN of the [^{35}S]-label on ISCU2. Overall, these radiolabeling studies coupled to previous cysteine desulfurase assay results suggest that FXN accelerates PLP-associated chemistry and sulfur transfer reactions from NFS1 to thiol-containing molecules (ISCU2, DTT, and L-cysteine).

FXN accelerates the decay of the PLP quinonoid intermediate for NFS1. To determine how FXN accelerates persulfide formation on NFS1, the PLP chemistry associated with the cysteine desulfurase reaction was directly probed using stopped-flow kinetics (Fig. 4.1, step 1). The proposed cysteine desulfurase mechanism includes sequential formation of cys-aldimine, cys-quinonoid, and cys-ketimine intermediates (Fig. 4.5A) [74, 75, 165], which have distinct absorbance maxima. The $SDA_{ec}U$ and $SDA_{ec}UF$ complexes were combined with L-cysteine and changes in absorbance were monitored. A high substrate concentration (10 mM) was used to increase the accumulation of PLP-based intermediates in the reaction. The first observed event is a rapid increase in absorbance at 410 nm, which was assigned to the cys-aldimine intermediate [75]. The $SDA_{ec}UF$ sample developed this signal more rapidly (the formation occurred during the dead time of the instrument) compared to the $SDA_{ec}U$ sample and accumulated approximately 8-fold more of this intermediate. Decay of this 410 nm species occurred at similar rates for the two complexes. The next intermediate, which absorbed maximally at 508 nm and was assigned to the cys-quinonoid species [75], developed at similar rates in the presence and absence of FXN

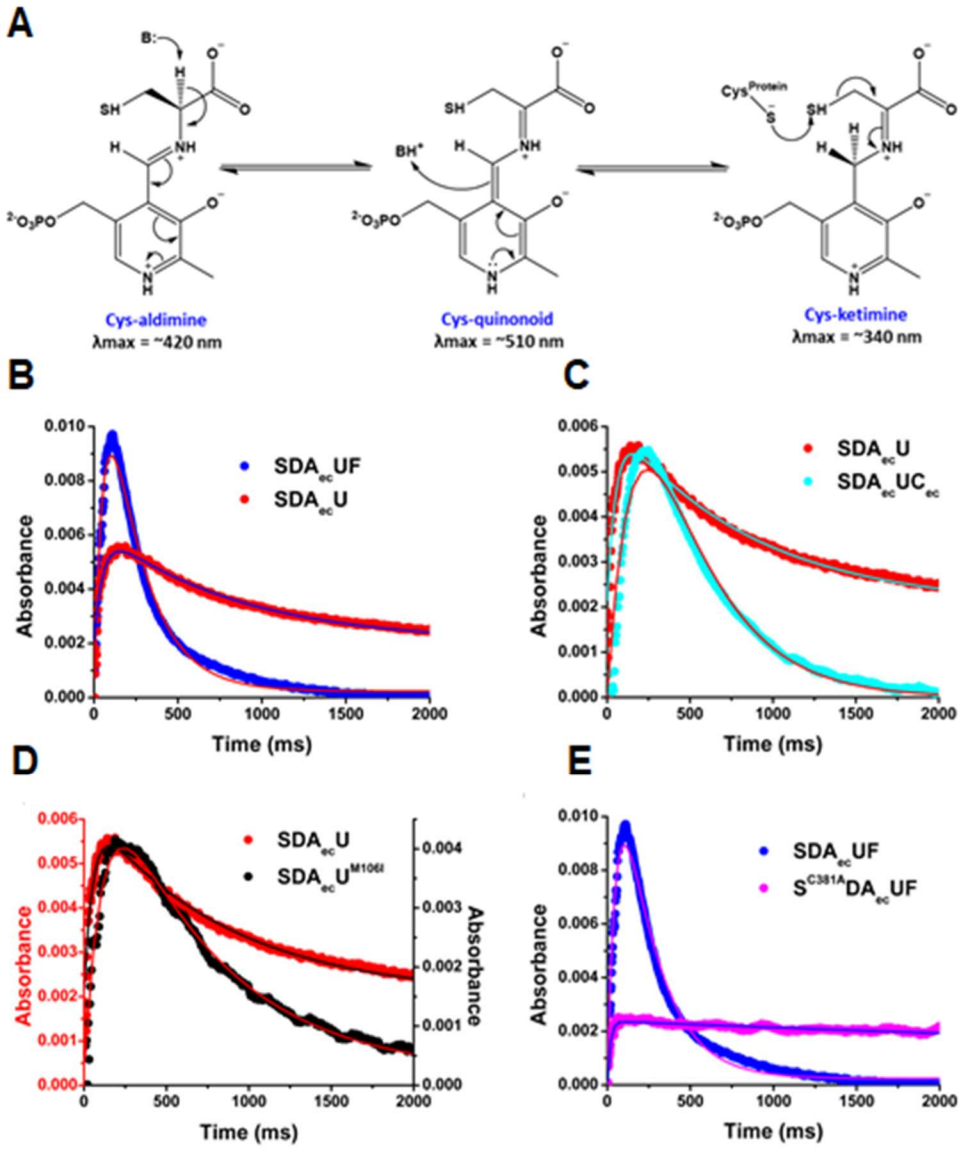

Figure 4.5. FXN accelerates the decay of quinonoid intermediate. A) Scheme showing steps of PLP chemistry that leads to C-S bond cleavage and persulfide formation on the mobile loop cysteine (NFS1-SSH). Stopped-flow kinetics for the cis-quinonoid decay of B) $SDA_{ec}U$ and $SDA_{ec}UF$ complexes, C) $SDA_{ec}U$ and $SDA_{ec}UC_{ec}$ (includes *E. coli* FXN homolog CyaY), D) $SDA_{ec}U$ and $SDA_{ec}U^{M106I}$ and E) $SDA_{ec}UF$ and $S^{C381A}DA_{ec}UF$. The traces are an average of three independent experiments. The rates for the development and decay of the quinonoid intermediate were obtained by nonlinear regression analysis (solid lines).

(Fig. 4.5B and Table 4.1). Interestingly, the decay rate of this cys-quinonoid intermediate was increased by a factor of four in the presence of FXN. Correspondingly, the formation of a species that absorbs at 340 nm, which was assigned to the cys-ketimine intermediate [75], was also enhanced by the addition of FXN. We next found that addition of the bacterial homolog of FXN (CyaY) to the $SDA_{ec}U$ complex also increased the decay rate (2.4 fold greater) of the cys-quinonoid intermediate (Fig. 4.5C), consistent with the ability of CyaY to activate the human cysteine desulfurase complex [46]. Finally, $ISCU2^{M106I}$ was tested for its ability to mimic FXN and affect steps in the PLP chemistry of NFS1. Stopped flow kinetics of the $SDA_{ec}U^{M106I}$ complex showed slower development and slightly faster decay kinetics (1.2 fold greater) for the cys-quinonoid intermediate compared to the native $SDA_{ec}U$ complex (Fig. 4.5D and Table 4.1). These stopped-flow experiments suggest that FXN, and to a smaller extent CyaY, affects the ability of NFS1 to accelerate the decay of the cys-quinonoid intermediate and generate the cys-ketimine species that is attacked by the mobile S-transfer loop during cysteine turnover.

We then tested whether the mobile S-transfer loop influences the decay kinetics of the cys-quinonoid intermediate in addition to its critical role in carbon-sulfur bond cleavage of the cys-ketimine intermediate to generate the NFS1 persulfide species. The conversion of the quinonoid intermediate to the ketimine species requires protonation at the C4' position (Fig. 4.5A). In bacterial cysteine desulfurases, the mobile S-transfer loop cysteine is thought to be the proton donor for this step of the mechanism [74, 75]. We therefore generated the $NFS1^{C381A}$ variant to test if the mobile S-transfer loop cysteine of NFS1 functions as the general acid for quinonoid decay in the SDA_{ec} complex. Stopped

flow kinetics for the $S^{C381A}DA_{ec}UF$ complex revealed that the quinonoid intermediate does not decay to generate the ketimine species (Fig. 4.5E), consistent with a proton donation role for C381. Overall, these results indicate FXN affects reactions associated with the NFS1 mobile S-transfer loop, which functions as a general acid, nucleophile, and sulfur transfer agent in Fe-S cluster biosynthesis.

Discussion

A direct link between the *FXN* gene and the neurodegenerative disease Friedreich's ataxia (FRDA) was established in a seminal 1996 study [84]. Typical FRDA patients have lower wild-type FXN expression levels (4-36% of controls) [166-170], suggesting a threshold level of FXN is required for normal function. FXN depletion results in the loss of activity for Fe-S cluster enzymes, increased iron accumulation in mitochondria, and enhanced sensitivity to oxidative stress [42]. Strategies to treat FRDA have focused on iron chelators, antioxidants, and mechanisms to increase FXN levels [171, 172]. Unfortunately, FRDA remains incurable. An alternate approach to generating a FRDA treatment is to first determine the biological role of FXN in Fe-S cluster biosynthesis and then replace or bypass that function.

An initial hypothesis was promoted that FXN functions as a chaperone that provides iron for Fe-S cluster assembly. This assignment was based on FXN depletion studies, which reveal a disruption of iron homeostasis and accumulation of iron in the mitochondria, and the lack of a designated iron chaperone for the Fe-S assembly pathway coupled to the presence of an iron-binding patch of carboxylate residues on FXN. However, FXN has weak iron binding affinity towards ferrous iron (55 μM), which is the

substrate for Fe-S cluster biosynthesis, and the iron-binding carboxylate patch residues are only semi-conserved [43, 44, 85, 86, 154, 157-160, 173]. Moreover, a similar iron overload phenotype is generated upon depletion of other members of the mitochondrial Fe-S assembly system [174], indicating that this phenotype is linked to loss of Fe-S clusters and not necessarily the ability to donate iron for this pathway. Furthermore, FRDA clinical variants for FXN have been identified on a region distinct from the carboxylate patch. These FRDA variants are not iron-binding residues and exhibit diminished ability to bind and activate the Fe-S assembly complex. Finally, the presence of ~150 μM labile iron pool in mitochondria could function as a feedstock for iron-containing proteins and raises the question as to whether a designated iron chaperone is even required for the Fe-S cluster biosynthetic pathway [175]. Despite these concerns, many investigators still champion an iron donor role for FXN.

More recently, much stronger evidence has been provided that supports a role for FXN in facilitating sulfur-based chemistry required for Fe-S cluster biosynthesis [31, 33, 49, 81, 89, 99, 161, 163, 176, 177]. Here, we have extended these FXN functional studies to include stopped-flow interrogation of the eukaryotic cysteine desulfurase reaction and functional assays that incorporate both synthesis of the Fe-S cluster intermediate and transfer of the cluster to an acceptor protein. We provide a stepwise analysis of the role of FXN in (*i*) the PLP-associated formation of intermediates for the cysteine desulfurase NFS1; (*ii*) the kinetics of sulfur accumulation on NFS1; (*iii*) the kinetics of interprotein sulfur transfer to the scaffold protein ISCU2; (*iv*) the rate of Fe-S cluster intermediate

formation on ISCU2; and (*v*) the kinetics of [2Fe-2S] cluster transfer from ISCU2 to the monothiol glutaredoxin GRX5 (Figs. 4.5A and 4.2).

FXN accelerates steps associated with the mobile S-transfer loop of NFS1. Stopped-flow experiments revealed a clear role for FXN in accelerating the decay of the cys-quinonoid intermediate for the $SDA_{ec}U$ complex (Fig. 4.5). The transformation of the cys-quinonoid intermediate to the cys-ketimine species requires protonation at the C4' position. Substitution of the mobile S-transfer loop cysteine (C381A) of NFS1 compromised the ability to advance to the ketimine intermediate. This result is consistent with NFS1 residue C381 functioning as a general acid for this step in the mechanism, consistent with the prokaryotic cysteine desulfurases [74, 75]. Radiolabeling studies revealed that FXN also accelerates the rate of persulfide formation on NFS1, which results from attack of the deprotonated mobile S-transfer loop cysteine on the cys-ketimine intermediate, and the rate of interprotein sulfur delivery from the mobile S-transfer loop cysteine of NFS1 to ISCU2 (Fig. 4.3 and Table 4.1). These enhanced rates of sulfur transfer also manifested in increased rates for the formation of [2Fe-2S] cluster intermediates on ISCU2 and in complete reactions in which [2Fe-2S] clusters were synthesized and transferred to GRX5.

In addition, we determined how human $ISCU2^{M106I}$, which is analogous to $Isu1^{M107I}$ [142, 162], is able to bypass the function of FXN and stimulate Fe-S cluster biosynthesis. $ISCU2^{M106I}$ was unable to replace FXN and affect the cysteine desulfurase kinetic parameters of the SDA_{ec} complex (Table 4.1) and only had a minor stimulatory effect on the rate of Fe-S cluster formation on ISCU2. Consistent with this result, a recent

crystal structure indicates that this ISCU2^{M106I} substitution is unlikely to affect the mobile S-transfer loop of NFS1 [178]. Instead, we show that ISCU2^{M106I}, unlike FXN, accelerates the rate of intact [2Fe-2S] cluster transfer from ISCU2 to GRX5 (Fig 4.2C). Further analysis indicates that the ISCU2^{M106I} substitution does not affect cluster stability on ISCU2 but appears to affect the [2Fe-2S] cluster binding equilibrium between ISCU2 and GRX5 (Fig. 4.2D). We hypothesize that substitutions on the scaffold protein that are capable of bypassing FXN (including the substitution of Isu1 M107 with residues that have a higher hydropathy index such as valine or isoleucine) [142] favor hydrophobic protein-protein interactions that drive the cluster transfer reaction from ISCU2 to GRX5. Stimulation of different steps by FXN and ISCU2^{M106I} is further supported by the additive effect that was observed in complete synthesis and transfer assays.

The eukaryotic SDA$_{ec}$U complex has unusually low activity for a cysteine desulfurase enzyme (k_{cat} < 10% of prokaryotic IscS) and requires FXN binding to stimulate activity and approach the catalytic turnover of IscS [31, 49]. CyaY, which is the prokaryotic homolog of FXN, does not activate IscS and, instead, inhibits *in vitro* Fe-S cluster biosynthesis [90]. Swapping protein components between the prokaryotic and eukaryotic systems reveals that these activation/inhibition effects were surprisingly independent of the FXN and ISCU2 homologs, but dependent on the cysteine desulfurase [46]. A recently determined structure of the SDA$_{ec}$ complex revealed an incomplete substrate binding site with a solvent exposed PLP cofactor, and an overall architecture in which ISD11 molecules mediate interactions between NFS1 subunits [49]. Quaternary interactions between NFS1 subunits for the SDA$_{ec}$ complex are quite different than its

prokaryotic homologs IscS, which have contributions from each subunit to the active site channel of the other subunit [48, 179]. The Cory SDA_{ec} architecture provides a rationale for the essential nature of ISD11 in eukaryotes, the low basal levels of cysteine desulfurase activity for the SDA_{ec} or $SDA_{ec}U$ complex, and the stimulation of sulfur-based chemistry upon FXN homolog binding to the eukaryotic cysteine desulfurases.

In our model, the $SDA_{ec}U$ is a low activity form of the Fe-S assembly complex with an incomplete substrate binding site and a mobile S-transfer loop that occupies a primarily non-productive conformation (Fig. 4.6). FXN functions as an allosteric activator and upon binding completes the substrate binding site and favors productive conformations for the mobile S-transfer loop cysteine. This alteration of the mobile S-transfer loop trajectory results in an acceleration of proton donation, which is necessary for advancing the cys-quinonoid intermediate, and an increased rate of persulfide formation on NFS1 and sulfur transfer to ISCU2. A role in binding and excluding non-productive conformations is further supported by the ability of the FXN homolog CyaY, which shares a mere 20% sequence identity with the human form, to impart the same effects on the cys-quinonoid decay (Fig. 4.5C) and on the cysteine desulfurase activity [46]. Although the FXN-induced stimulation of the mobile S-transfer loop reactions are relatively small (Table 4.1; 3 to 30 fold), this may be sufficient to reach the modest *in vivo* activity threshold that supports Fe-S cluster biosynthesis and mitochondrial function. The incorporation of ISD11/ACP into the eukaryotic Fe-S cluster biosynthetic pathway is thereby a mechanism to integrate FXN as an activity control element or regulator that drives sulfur chemistry. Overall, these results provide new insights into FXN function and

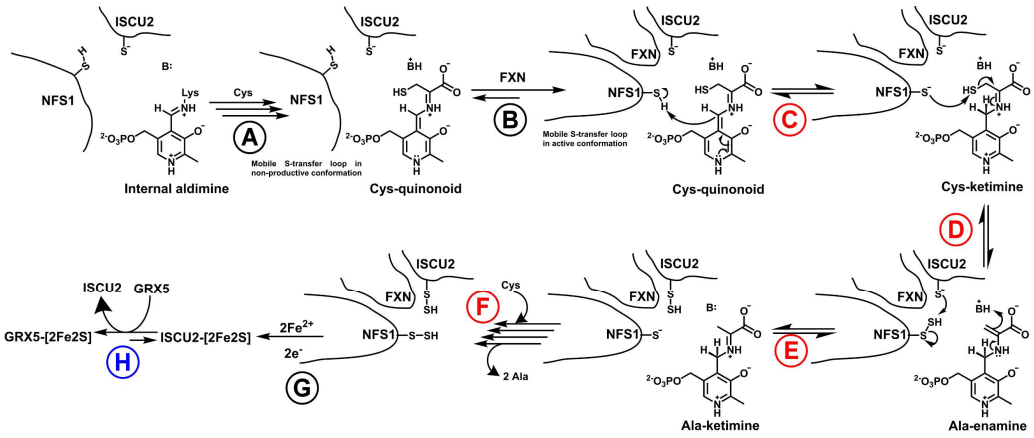

Figure 4.6. Model for how FXN and FXN bypass variant accelerate Fe-S cluster biosynthesis. A) Cysteine binding to NFS1 generates the Cys-quinonoid intermediate. B) In the absence of FXN, the NFS1 mobile S-transfer loop exists primarily in a non-productive conformation. FXN binding favors the active conformation. C) The FXN promoted conformation of the S-transfer loop allows its cysteine to function as a general acid and accelerate the decay of the cys-quinonoid intermediate. D) The deprotonated cysteine of the S-transfer loop nucleophilically attacks the cys-ketimine intermediate to generate a persulfide intermediate on NFS1 (NFS1-SSH). E) FXN favors the appropriate trajectory to deliver sulfur and produce a persulfide species on ISCU2 (ISCU2-SSH). F) A second cysteine turnover generates the NFS1-SSH ISCU2-SSH intermediate. G) Incorporation of ferrous iron and electrons generates the [2Fe-2S] intermediate on ISCU2. H) The [2Fe-2S] cluster is transferred to the apo acceptor GRX5. Steps labels in red are accelerated by FXN. Steps labeled in blue are accelerated by the ISCU2^{M106I} bypass variant.

suggest strategies to replace (exclude non-productive mobile S-transfer loop conformations) or bypass FXN function (facilitate Fe-S cluster transfer from ISCU2) and provide potential new mechanisms to treat FRDA.

Materials and Methods

Protein purification. Plasmids containing human NFS1 (Δ1-55) and ISD11 (pZM4) were generously provided by S. Leimkuhler [100]. The NFS1 and ISD11 plasmids were transformed into *E. coli* strain BL21(DE3) cells and copurified with the bacterial ACP (ACP_{ec}) as the SDA_{ec} complex [49]. Human ISCU2 (Δ1-35) and FXN (Δ1-55) were separately expressed and purified as previously described [31]. The spontaneous conversion of Δ1-55 FXN to the truncated form was confirmed by SDS-PAGE [31]. The QuikChange protocol (Agilent) was used to introduce the M106I point mutation into the *ISCU2-pET11a* plasmid [31] and the C381A point mutation into the *NFS1-pET15b* plasmid [100]. The protein sequence numbering for the M106I variant does not include the ISCU2 signal sequence to be consistent with the literature for the bacterial and yeast homologs. The MEGAWHOP [180] method was used to substitute human *GRX5* for *FDX* in the *pHis-GFP-TEV-FDX* plasmid [67] and produce *pHis-GFP-TEV-GRX5*. Sequences were confirmed by the Gene Technologies Lab (Texas A&M University).

The *pHis-GFP-TEV-GRX5* plasmid was transformed into Rosetta (DE3) cells (VWR). The cells were grown in LB media (VWR) at 37 °C until the OD_{600} reached 0.5 and then β-D-1-thiogalactopyranoside (IPTG) was added to a final concentration of 0.5 mM. The temperature was decreased to 16 °C and the cells were grown for an additional ~16 h. The harvested cell pellets were resuspended in Buffer A (50 mM Tris and 250 mM

2NaCl at pH 7.5) with 5 mM imidazole and lysed by sonication (Branson sonifier 450). The soluble fraction was loaded on a Ni-NTA column (5 mL; GE Life Sciences) and the his-GFP-TEV-GRX5 fusion was eluted using Buffer A and a linear gradient between 5 and 500 mM imidazole. The green fractions were combined and dialyzed into Buffer B (50 mM Tris, pH 7.5). The sample was then incubated overnight at room temperature with TEV protease (1:50 molar ratio of protease to fusion protein). The cleaved material was then loaded onto an anion exchange column (27 mL; 16 mm × 13.5 cm, POROS HQ 50) and eluted with Buffer B and a linear gradient from 0 to 1 M NaCl. The GRX5 fractions were concentrated and loaded onto a 26/60 Sephadex 100 column (GE Life Sciences) equilibrated with 50 mM HEPES and 150 mM NaCl at pH 7.5. Monomeric fractions with > 96% purity were concentrated, frozen in liquid nitrogen and stored at −80 °C. Unless otherwise stated, all protein manipulations and reactions were carried out in an anaerobic glove box (MBRAUN; maintained at ~14 °C with O_2 < 1 ppm). Protein concentrations were estimated using the following extinction coefficients: SDA_{ec} using 10.9 $mM^{-1}cm^{-1}$ at 420 nm, ISCU2 using 8490 $M^{-1}cm^{-1}$ at 280 nm, FXN using 26030 $M^{-1}cm^{-1}$ at 280 nm, and GRX5 using 17780 $M^{-1}cm^{-1}$ at 280 nm [31, 181]. Protein variants were assumed to have the same extinction coefficient as the native proteins.

Complete Fe-S cluster synthesis and transfer reactions. The complete reaction assays included 0.5 μM SDA_{ec}, 20 μM ISCU2 (or $ISCU2^{M106I}$), 20 μM (or 0 μM) FXN, 40 μM GRX5, and 400 μM $Fe(NH_4)_2(SO_4)_2$ and Buffer C (50 mM HEPES, 150 mM KCl and 10 mM $MgCl_2$ at pH 7.5). The reactions were initiated by the addition of 100 μM L-cysteine and 10 mM GSH. Cluster formation on GRX5 was then measured for $SDA_{ec}U$, $SDA_{ec}UF$,

$SDA_{ec}U^{M106I}$ and $SDA_{ec}U^{M106I}F$ by monitoring the ellipticity change at 450 nm using a Chirascan circular dichroism (CD) spectrometer (Applied Photophysics). Cuvettes (1 cm path length) were sealed with a rubber septa and electrical tape in a glove box. The kinetic data were fit to an exponential rise equation ([$y=y_0+A_0*(1 - \exp(-k*t))$] where the *k* is the apparent rate of cluster formation on GRX5) using Kaleidagraph (Synergy Software, Reading, PA).

Fe-S cluster assembly reactions on ISCU2. Fe-S assembly reactions on ISCU2 contained 10 μM SDA_{ec}, 30 μM ISCU2 (or $ISCU2^{M106I}$), 30 μM FXN (when added), 400 μM $Fe(NH_4)_2(SO_4)_2$ and Buffer C. The reactions were initiated with 1 mM L-cysteine. The formation of [2Fe-2S] clusters was monitored by the change in ellipticity at 330 nm [163]. The initial increase in ellipticity was plotted with time and fit to a linear equation (R^2 values ≥ 0.97) using Kaleidagraph.

Cysteine desulfurase activity measurements. Cysteine desulfurase activities were measured for each complex using a slightly modified methylene blue assay [31, 101]. Protein complexes were generated with final concentrations of 0.5 μM SDA_{ec}, 1.5 μM ISCU2 (or $ISCU2^{M106I}$), and 1.5 μM FXN (when included). The complexes were combined with 4 mM D,L-DTT and incubated for 15 min anaerobically on a heating block at 37 °C. Different concentrations of L-cysteine were added, incubated for 6 min, and quenched with 20 mM *N,N′*-diphenyl-*p*-phenylenediamine (DPD) (in 7.2 M HCl) and 30 mM $FeCl_3$ (in 1.2 M HCl). The samples were centrifuged after 20 min and the absorbance was measured at 670 nm. The amount of sulfide produced was determined for each data

point using a standard curve. Rates ($[S^{2-}]$/([NFS1]*min)) were plotted against the amount of L-cysteine added and fit to the Michaelis-Menten equation using Kaleidagraph.

[2Fe-2S] cluster transfer reactions from enzymatic and chemically reconstituted ISCU2 to GRX5. Clusters were enzymatically generated on ISCU2 (or $ISCU2^{M106I}$) using 0.5 μM SDA_{ec}, 20 μM ISCU2 (or $ISCU2^{M106I}$), and 400 μM $Fe(NH_4)_2(SO_4)_2$ and Buffer C. The reactions were initiated with of 100 μM L-cysteine and 10 mM GSH. After 160 min, the enzymatic formation of [2Fe-2S] clusters appeared to be complete based on the lack of changes in ellipticity at 450 nm. A solution containing 40 μM GRX5 (with or without 20 μM FXN) was then injected with an air-tight syringe into the sealed cuvette to initiate the transfer reactions. The change in ellipticity was plotted with time and fit to a linear equation with Kaleidagraph (R^2 values ≥ 0.97).

[2Fe-2S] clusters were chemically generated on ISCU2 (or $ISCU2^{M106I}$) by reacting 30 μM of apo protein with 600 μM ferric ammonium citrate, 600 μM Na_2S and 10 mM D, L-DTT for an hour. DTT and the excess iron and sulfide were then removed with a desalting column (5 mL, GE Healthcare) equilibrated in Buffer C. Iron was quantitated with the ferrozine assay (extinction coefficient of 28,000 $M^{-1}cm^{-1}$ at 562 nm) [102] and sulfide was quantitated using a methylene blue assay with an additional pre-treatment of the protein with NaOH and zinc acetate to release bound sulfide [182]. The protein concentration was determined using the Bradford assay. Chemically reconstituted ISCU2 had 2.1 ± 0.3 iron and 2.0 ± 0.6 sulfide atoms per protein, whereas $ISCU2^{M106I}$ had 1.9 ± 0.5 iron and 2.2 ± 0.1 sulfide atoms per protein. Cluster transfer reactions were

initiated by combining [2Fe-2S]-ISCU2 or [2Fe-2S]-ISCU2^{M106I} with 60 μM GRX5 and 10 mM GSH. Transfer reactions were monitored by the change in ellipticity at 450 nm.

[2Fe-2S] cluster extrusion assay. [2Fe-2S] clusters were assembled on 30 μM ISCU2 (or ISCU2^{M106I}) in the presence of 10 μM SDA_{ec}, 100 μM L-cysteine, 400 μM $Fe(NH_4)_2(SO_4)_2$ and 10 mM GSH. 4 mM D, L-DTT was added to the samples to initiate the cluster extrusion reaction, which was followed by the loss of ellipticity at 330 nm. The extrusion rates were determined by fits to a linear equation.

Protein separation and ^{35}S quantification for sulfur transfer reactions. L-[^{35}S]-cysteine (PerkinElmer, 10.2 μM, 1.00796 mCi) was diluted 50 times by non-radioactive L-cysteine to generate a 1 mM stock solution (final concentration of L-[^{35}S]-cysteine was 204 nM). Proteins from Fe-S assembly complexes (SDA_{ec} and ISCU2) were applied to a reverse phase C4 column (Waters) attached to a HPLC (1260 Infinity, Agilent Technologies) and separated using a gradient from either 0 to 100% or from 30% to 70% Buffer D (0.1 % TFA in water, pH 2.0) with the remainder of the composition made up of Buffer E (60% CH_3CN, 40% isopropanol, 0.1% TFA). Both the absorbance (diode array detector) and, after mixing with scintillation cocktail (BioCount 111182), the [^{35}S] signal (Model 5C β-RAM radio-HPLC detector, LabLogic) were recorded for the eluted proteins. The retention time of NFS1 (ISD11 and ACP_{ec} do not contain cysteine residues required for persulfide formation) was determined by reacting a 25 μL aliquot of the SDA_{ec} complex (37.5 μM) with 25 μL of L-[^{35}S]-cysteine (final concentration of 500 μM) for 30 min. The reaction was stopped by addition of 50 μL quenching solution and the proteins were separated under quench conditions. The quenching solution was made by mixing 1

volume of concentrated HCl with 4 volumes of 6 M guanidine hydrochloride (pH < 1). The retention time for ISCU2 was determined using absorbance or reaction of the $SDA_{ec}U$ complex with L-[^{35}S]-cysteine and comparison to the SDA_{ec} complex. Note that FXN, like ISD11 and ACP_{ec}, lacks cysteine residues needed to form a persulfide intermediate. To demonstrate that the quench solution inhibits sulfur transfer, labeled NFS1 was first generated by reacting the SDA_{ec} complex (30 μM) with L-[^{35}S]-cysteine (400 μM final concentration, 45 μl total reaction volume) for 30 min. The labeled NFS1 was either (*i*) incubated with ISCU2 (80 μM, 5 μL) for 30 min, followed by the addition of 50 μL quenching solution; or (*ii*) first combined with 50 μL quenching solution and then incubated with ISCU2 (80 μM, 5 μL) for 30 min. Samples were analyzed by a reverse phase chromatography under quench conditions. NFS1Data collection and analysis were performed with Laura software (LabLogic). To quantitate the amount of persulfide associated with the peak, the area under the scintillation curve (in CPM) was converted into a [^{35}S] concentration using a standard curve generated from known amounts of L-[^{35}S]-cysteine and then multiplied by the dilution factor (unlabeled / labeled L-cysteine = 4901.96).

Assays for monitoring persulfide formation and decay. For the persulfide formation and decay assays, 30 μM SDA_{ec} and 30 μM ISCU2 were combined to generate the $SDA_{ec}U$ complex, which was converted to the $SDA_{ec}UF$ complex by the addition of 75 μM FXN. The $SDA_{ec}U$ and $SDA_{ec}UF$ complexes were reacted with either 30, 200, or 600 μM cysteine (0.0204% [^{35}S]-cysteine), incubated at 37°C for different lengths of time (30 sec to 1 h), and diluted 4-fold into the quenching solution described above. The amount of

persulfide associated with NFS1 and ISCU2 was calculated as described above, plotted against time, and fit to a reaction scheme (see below) using KinTek software (KinTex Corporation, Austin, TX). To determine which cysteine residues were labeled with persulfide species, the $SDA_{ec}U$ complex was combined with 300 μM L-cysteine, incubated at 37 °C for 30 min, and quenched with concentrated HCl. The sample was digested with pepsin (100:1 sample:pepsin based on concentration in mg/mL) at 22 °C for 30 min and subjected to LC/MS/MS analysis (Center for Mass Spectrometry (CMS) at Texas A&M University).

Pulse chase experiments were conducted by first reacting the $SDA_{ec}U$ and $SDA_{ec}UF$ complexes (30 μM SDA_{ec}, 30 μM ISCU2, with or without 75 μM FXN) with 30 μM [^{35}S]-cysteine for 40 min (the amount of label maximized after 10-20 min) to generate radiolabeled NFS1 and ISCU2. Next, we added a final concentration of 1 mM non-radioactive L-cysteine to the samples and then diluted 4-fold into the quenching solution at various times. The amount of residual persulfide labels on NFS1 and ISCU2 were determined and fit to an exponential decay equation [$y=y_0+A_0*\exp(-k*x)$] using Kaleidagraph, where the k value gives the apparent rate of persulfide loss.

Validation of data fitting for persulfide formation kinetics. The data were fitted to a simulated mechanism according to the reaction scheme (Fig. 4.3E) using KinTek software. The estimation of error was determined by FitSpace confidence contour analysis. FitSpace determines the goodness of the fit by measuring the dependence of the sum of square errors (SSE) on each pair of parameters while all other parameters were varied. The confidence interval of all the fitted parameters were constrained by χ^2 threshold values of

0.99 and 0.997 for the $SDA_{ec}U$ and $SDA_{ec}UF$ data, respectively. These thresholds indicate that varying the parameter within the confidence interval would not increase the χ^2 value more than 1% ($SDA_{ec}U$) and 0.3% ($SDA_{ec}UF$) from the minimum χ^2 (χ^2_{min}) value, which represents the best fit. Confidence contour plots are provided that indicate well-defined regions determined by χ^2 threshold values (red colored patches).

Stopped flow kinetics for cysteine desulfurase reaction. 100 μM $SDA_{ec}U$ (100 μM SDA_{ec} + 100 μM ISCU2) or 100 μM $SDA_{ec}UF$ (100 μM SDA_{ec} + 100 μM ISCU2 + 100 μM FXN) in assay buffer (50 mM HEPES, 250 mM NaCl, pH 7.5) was placed in one of the syringes of the stopped flow apparatus (KinTek Corporation). The other syringe contained 10 mM L-cysteine. The samples were mixed by simultaneously pressing both syringes. Formation of the aldimine, quinonoid, and ketimine intermediates were followed by monitoring changes in absorbance at 410, 508 and 340 nm, respectively. For the aldimine and quinonoid kinetics, traces monitored at 410 nm and 508 nm with time were fitted with Origin software (OriginLab) to a consecutive B equation [$y = y_0 + (k_1*[A]_0/(k_2-k_1))*(\exp(-k_1*t)-\exp(-k_2*t))$], where k_1 and k_2 are rate constants of the formation and decay of intermediates respectively. The ketimine kinetics could not be adequately fit using a consecutive B equation.

CHAPTER V

REAL TIME KINETIC PROBES SUPPORT MONOTHIOL GLUTAREDOXINS AS INTERMEDIATE CARRIERS IN FE-S CLUSTER BIOSYNTHETIC PATHWAYS[7]

Introduction

Iron-sulfur clusters (Fe-S) are found throughout all of the kingdoms of life, where they serve a wide variety of critical functions [183]. Fe-S clusters are involved in electron transport[13, 184-186], catalysis of biological reactions [187-189], and regulation of cellular responses to oxidative stress [55, 190]. It is not surprising that defects in the biosynthesis and transfer of Fe-S clusters are associated with numerous human diseases [71, 191, 192]. Despite the importance of these cofactors, many mysteries remain regarding their biosynthesis and insertion into their target proteins.

In bacterial and eukaryotic mitochondria, the ISC biosynthetic machinery is responsible for cluster biosynthesis [21]. The ISC pathway utilizes a core complex consisting of a cysteine desulfurase (IscS) and a scaffold protein (IscU) [21]. IscS catalyzes the conversion of cysteine to alanine and a persulfide [32]. IscU serves as the site for cluster assembly. The persulfide that is formed on IscS can be transferred to IscU, where it is combined with ferrous iron and two electrons to form a [2Fe-2S] cluster [33, 34].

---

[7] Reprinted with permission from "Real-Time Kinetic Probes Support Monothiol Glutaredoxins As Intermediate Carriers in Fe−S Cluster Biosynthetic Pathways" by James Vranish, Deepika Das, David P. Barondeau, 2016. *ACS Chemical Biology*, 11, 3114-3121. Copyright 2016 American Chemical Society.

The cluster that is formed on IscU must then be transferred to a variety of apo target proteins in the cell. Several proteins have been implicated in the process of transferring clusters, including the chaperone/co-chaperone pair of HscA/HscB [109], IscA [59] and the monothiol glutaredoxins (Grxs). The role of the glutaredoxins has been quite mysterious. Grxs come in two varieties, the monothiol and dithiol glutaredoxins, with their respective names indicating the number of cysteine residues present in the active site of these enzymes. The Grxs are so named due to their ability to catalyze disulfide reduction reactions on molecules such as ribonucleotide reductase in a process that utilizes reduced glutathione (GSH) [109]. While similar to thioredoxins, they are uniquely able to reduce S-glutathionylated proteins [109, 171]. Interestingly, both classes of Grxs also possess the ability to bind an Fe-S cluster [109, 171, 178-180]. Curiously, this binding requires two monomers of Grx that both provide a single cysteine ligand to opposite iron atoms of the cluster with the other two ligands coming from two molecules of non-covalently bound GSH. Even more intriguing is the observation that the ligating cysteine is the residue that is required for Grxs thiol reduction function [109]. Additionally, there is evidence from crystal structures that the form of the cluster that is bound to monothiol Grxs is a [2Fe-2S] cluster. However, other studies have demonstrated the ability of this class of Grxs to bind both linear [3Fe-4S] and traditional [4Fe-4S] clusters [41]. The physiological relevance of these cluster forms remains a matter of debate, the monothiol Grxs can also bind clusters in heterodimeric complexes with BolA/Fra2, forming complexes with perturbed cluster properties and specific regulatory functions [52, 53, 55, 109, 171].

In Fe-S cluster biosynthesis, glutaredoxins have been proposed to function as intermediate cluster carriers for transfer processes or as cluster storage proteins based on *in vivo* and *in vitro* studies [178, 179]. Holo-monothiol and dithiol glutaredoxins have been shown to transfer their clusters to ferredoxin (Fdx), but *in vivo* data more strongly links the monothiol Grxs to Fe-S cluster biosynthesis [109, 171, 178]. Additionally, the monothiol glutaredoxins have been shown to be able to transfer clusters to IscA and to aconitase [41, 60]. Clusters bound to monothiol glutaredoxins are generally regarded as more labile than clusters bound to dithiol Grxs [109]. Additionally, the monothiol glutaredoxins have also been shown to accept a cluster from holo-IscU, in a chaperone enhanced fashion [109]. In the presence of chaperones, the measured rates of transfer from IscU to monothiol glutaredoxin and then glutaredoxin to ferredoxin was determined to occur faster than the transfer from IscU to ferredoxin alone, providing the first kinetic evidence for the role of glutaredoxin as an intermediate cluster carrier [109]. However, it is important to note that several of these transfer steps include DTT, which has been shown to artificially enhance the rates of cluster transfer reactions. Furthermore, these rates were measured without any determination of K_m values and didn't allow for competition between glutaredoxin and ferredoxin for a common cluster source, thus calling into question the relevance of these findings in a biological setting that includes all three proteins at much lower protein concentrations. Additionally, these studies utilized a [2Fe-2S]-IscU dimer species as the cluster source, despite the fact that it has never been established to be a kinetically competent intermediate of the cluster biosynthetic pathway.

Finally, the ability of monothiol glutaredoxins to act as intermediate carriers has not been kinetically investigated for other terminal target proteins other than Fdx and aconitase.

We demonstrated the ability of fluorescent Fe-S cluster binding proteins to report of their cluster content in mixtures containing other chromophores [67]. Here we extend the utility of this assay to investigate enzymatic cluster formation on *E. coli* IscU and monothiol Grx4. We directly investigate the transfer of clusters from IscS/IscU to Grx4 in the presence of a possible downstream target protein and thereby determine the ability of Grx4 to function as an intermediate cluster carrier. This study shows the power of this technique to detect pathway intermediates and directly investigate the complex network of cluster transfer reactions.

Results

Grx4 and DTT accelerate Fe−S Cluster transfer reactions to Fdx. We initially designed *in vitro* experiments monitored by CD spectroscopy, which is currently the preferred methodology for tracking Fe−S cluster transfer, to evaluate whether the *E. coli* monothiol glutaredoxin, Grx4 (also known as GrxD), can function as an intermediate [2Fe−2S] cluster carrier species in biosynthetic pathways. Apo-ferredoxin (apo-Fdx), which is a terminal [2Fe−2S] cluster binding protein, was chosen as an initial target. Here, a terminal cluster binding protein is defined as one that utilizes its Fe−S cluster for function, such as electron transfer, and is not an intermediate in the cluster distribution pathway. [2Fe−2S] clusters bound to proteins typically produce significant ellipticity features in the visible region of the spectrum, which are probably due to S → Fe charge transfer transitions. A negative ellipticity feature at 515 nm was selected to monitor the

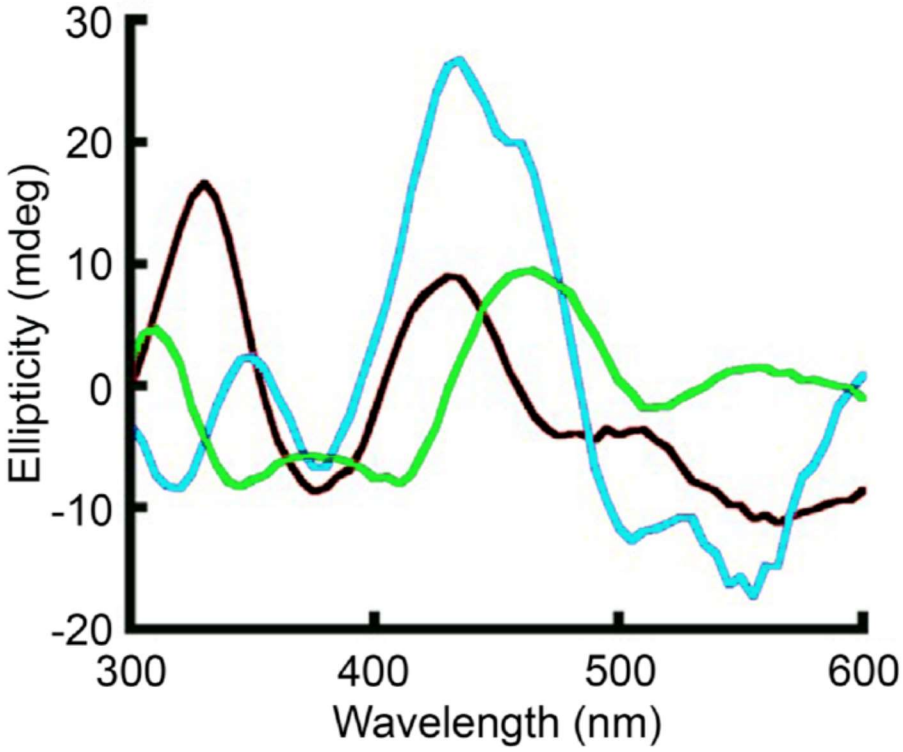

Figure 5.1. CD spectra of [2Fe-2S]-IscU, [2Fe-2S]-Grx4 and [2Fe-2S]-Fdx are distinctive. CD spectra of 25 μM [2Fe-2S]-IscU (black), 30 μM [2Fe-2S]-Grx4 (green), and 40 μM [2Fe-2S]-Fdx (cyan). [2Fe-2S]-IscU was generated by enzymatic reconstitution (0.5 μM IscS, 400 μM Fe2+, and 1 mM Lcysteine) and was 80% occupied with cluster. [2Fe-2S]- Fdx and [2Fe-2S]-Grx4 were isolated as holo-proteins from *E. coli* and were 90% occupied with cluster.

kinetics of [2Fe−2S] cluster binding to Fdx, as this feature is much larger for cluster-bound Fdx than for either IscU or Grx4, whereas a positive feature at 330 nm was used to monitor [2Fe−2S] cluster binding to IscU (Fig. 5.1). Clusters were synthesized anaerobically in situ from $Fe^{2+,}$ L-cysteine, and GSH by the IscS−IscU complex. Control reactions that lacked Grx4 and Fdx fully developed a [2Fe−2S]−IscU signal in about 30 min (Fig. 5.2A). The addition of the apo-acceptor Fdx resulted in the slow development of the 515 nm CD signal from [2Fe−2S]−Fdx that was not complete even after 6 h (Fig. 5.2B, D).Identical reactions that also included Grx4 developed this 515 nm signal at a ∼2.4-fold faster rate (Fig. 5.2C, D). Initial rate data were fit to linear equations) to obtain crude estimates of the second order rate constants for the transfer of cluster to Fdx from IscU (Fig. 5.3, k_3 = 194(3) M^{-1} min^{-1}) and Grx4 (Fig. 5.3, k_2 = 920(2) M^{-1} min^{-1}). Next, the ability of the non-physiological reagent DTT to substitute for or enhance Grx4 function was tested. A Grx4-containing cluster assembly reaction was spiked with DTT after 50 min, which was sufficient time to generate [2Fe−2S]−IscU (Fig. 5.2A) and allow testing of the role of DTT in subsequent cluster transfer reactions. The resulting development of the 515 nm signal was greatly accelerated compared to the sample without DTT (Fig. 5.2D). Note that [2Fe−2S] clusters bound to small molecule thiolates such as GSH and DTT do not contribute to this region of the CD spectrum. These results demonstrate that both Grx4 and DTT accelerate the rate of [2Fe−2S] cluster accumulation on Fdx and illustrate the need to exclude DTT in experiments aimed at interrogating the role of Grx4 in cluster transfer. Difficulties in resolving the individual component CD spectra at intermediate time points and, more importantly, limited assay sensitivity led us to apply newly

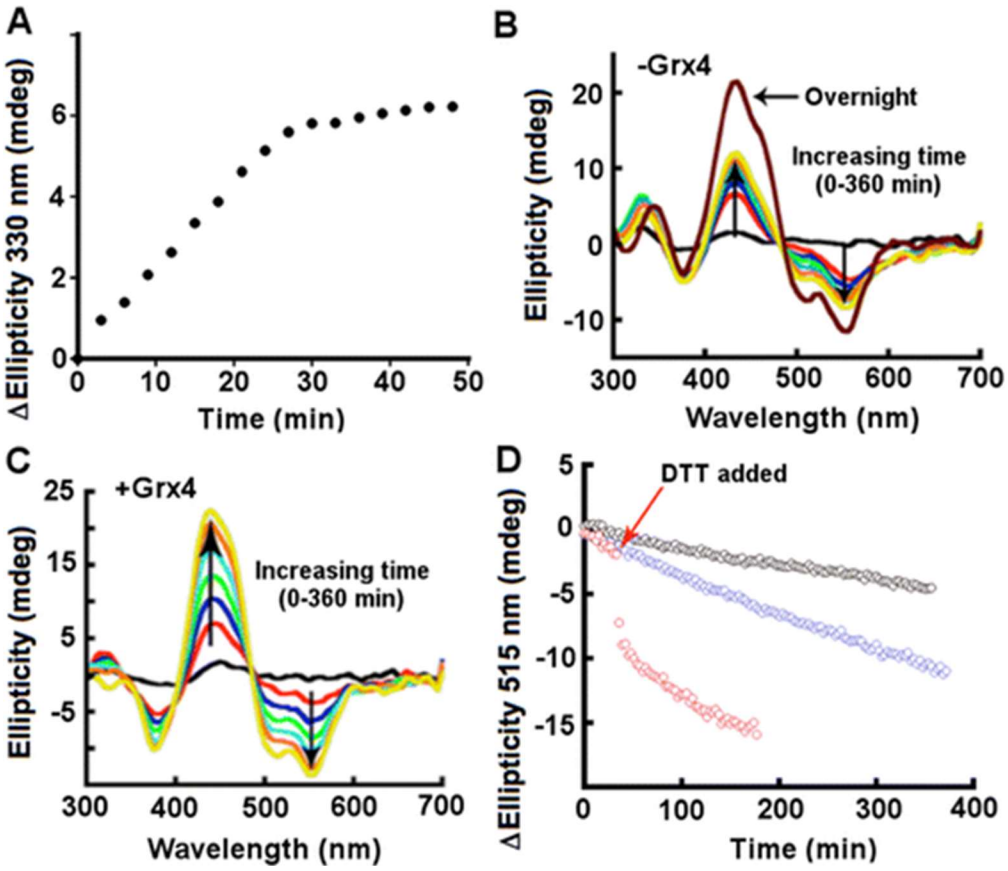

Figure 5.2. Both Grx4 and DTT accelerate cluster transfer reactions to apo-Fdx. Complete reactions contained 0.5 μM IscS, 10 μM IscU, 20 μM Grx4, 40 μM apo-Fdx, 400 μM Fe2+, 100 μM L-cysteine, and 10 mM GSH. For reactions lacking both Grx4 and Fdx, [2Fe−2S] cluster formation on IscU was monitored by the change in CD ellipticity at 330 nm (A). CD spectra are shown for Fdx-containing reactions that lack (B) or contain (C) Grx4 after 0 (black), 60 (red), 120 (blue), 180 (green), 240 (cyan), 300 (orange), and 360 (yellow) min. An additional spectrum (brown) was recorded after overnight incubation without Grx4 (panel B) that showed fully reconstituted [2Fe−2S]−Fdx. (D) The change in ellipticity at 515 nm is shown in black and blue for panels B and C, respectively. A separate complete reaction identical to panel C was spiked after 50 min with 5 mM DTT (red).

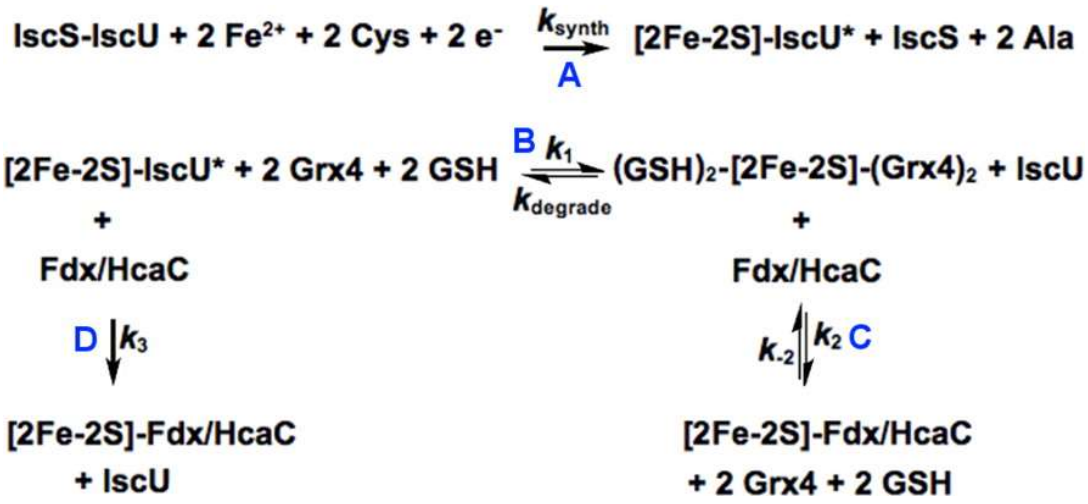

Figure 5.3. Fe−S cluster synthesis and transfer reactions. Overall scheme with different steps in the process of cluster biosynthesis are depicted.

developed fluorescent reporter method- biosynthesis and transfer reactions. Advantages of a fluorophore reporter to track Fe−S cluster content include the ability to use lower and broader concentration ranges and the capability to selectively monitor cluster-binding events by using labeled Fe−S proteins in biosynthetic assays.

Cluster transfer is the rate-limiting step in [2Fe− 2S]−Grx4 formation. Grx4 was labeled with a sulforhodamine B reporter ($Grx4_{Rho}$) to probe its role in Fe−S cluster biosynthetic networks. First, control reactions were performed to ensure that fluorescence quenching of $Grx4_{Rho}$ was due to [2Fe−2S] cluster binding. $Grx4_{Rho}$ exhibited little change in fluorescence intensity upon the addition of biosynthetic reagents (or reaction side-products) L-cysteine, Fe^{2+}, GSH, or sulfide (data not shown), similar to results for control reactions using Fdx_{Rho}. Additional control experiments revealed $Grx4_{Rho}$ could be used to monitor Fe−S biosynthetic reactions. Separate CD and fluorescence assays were used to monitor the in situ development of the [2Fe−2S]−Grx4 species (Fig. 5.3, Reactions A and B). These reactions lack any terminal acceptor such as Fdx or HcaC. For the CD assay, a positive feature at 455 nm was used to monitor cluster transfer, as this wavelength is diagnostic of [2Fe−2S]−Grx4 and has little intensity for [2Fe−2S]−IscU (Fig. 5.1). The rate of cluster accumulation on Grx4 was also measured using the fluorescence intensity for $Grx4_{Rho}$, which exhibits [2Fe−2S] cluster dependent quenching. The fluorescence intensity was corrected for the inner filter effect and for loss of signal due to photobleaching or adhesion to the plate. Biosynthetic assays using the IscS−IscU complex to generate clusters revealed similar pseudo-first-order generated by taking the difference between the sample at the beginning and end of the fluorescenc experiment was highly

similar to the [2Fe−2S]−Grx4 control (Fig. 5.4). Size exclusion chromatography verified multimerization, likely dimerization, of Grx4 during the reaction with the generation of very little, if any, aggregated material. Control reactions that include DTT exhibited decreased amounts of [2Fe−2S] cluster binding based on the lack of $Grx4_{Rho}$ quenching. Control reactions without IscU showed a low level of transient fluorescence quenching that occurred on a slower time scale than reactions with IscU. These results suggest the clusters formed on $Grx4_{Rho}$ in full biosynthetic assays were generated through an IscU-dependent enzymatic process rather than a chemical Fe−S reconstitution process (favored by non-enzymatic sulfide generation). Moreover, a similar extent of quenching at different ratios of $Grx4_{Rho}$ to Grx4 indicated minimal contribution of homo-FRET to the overall quenching. These control studies reveal the fluorescence of $Grx4_{Rho}$ is sensitive to the binding of IscS:IscU derived Fe−S clusters, and off pathway Fe−S minerals or protein aggregates contribute little to the changes in the fluorescence intensity. We further explored the mechanism of [2Fe−2S] cluster transfer to Grx4 by determining the concentration dependence of GSH and apo- $Grx4_{Rho}$. A lag phase for $Grx4_{Rho}$ quenching was observed at lower GSH concentrations that is shorter or absent at 10 mM GSH (Fig. 5.5A). The initial linear rates of quenching (following any lag phase) were converted to cluster transfer rates. Interestingly, the resulting cluster transfer rates varied linearly with concentration of GSH, implicating a single GSH molecule in rate-limiting cluster transfer to Grx4 (Fig. 5.3, Reaction B). This rate dependence is consistent with the GSH ligation requirement for [2Fe−2S] cluster binding to $Grx4_{Rho}$. The simplest explanation for the lag phase is that GSH also participates in cluster synthesis (Fig. 5.3, Reaction A), possibly

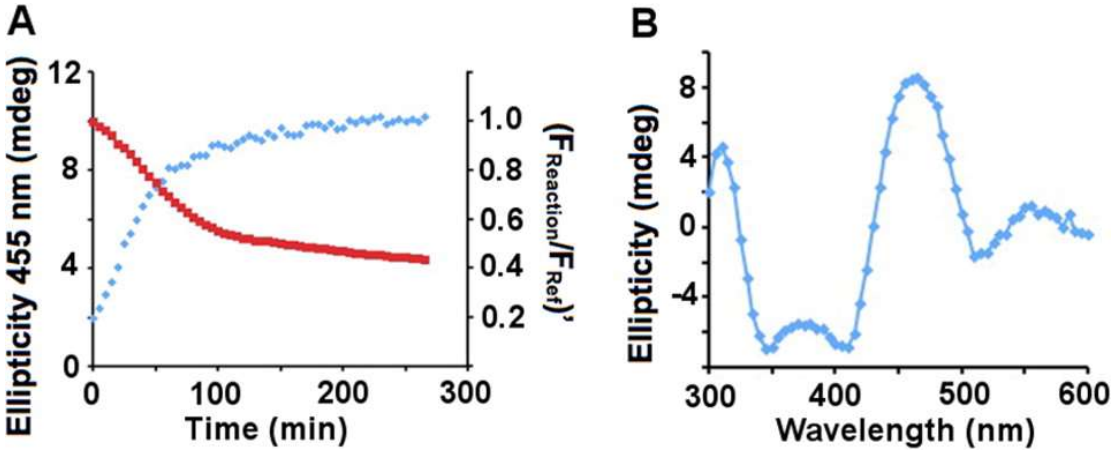

Figure 5.4. IscS–IscU mediated [2Fe–2S] cluster formation on Grx4. (A) The rate of cluster assembly on $Grx4_{Rho}$ was monitored using CD (blue) and fluorescence (red) spectroscopy. Fluorescence was measured using 550 nm excitation and 600 nm emission wavelengths. $(F_{Reaction}/F_{ref})'$ is the fluorescence of the reaction compared to a reference well (see Methods). CD ellipticity was measured at 455 nm. Reactions contained 10 mM GSH, 100 μM Fe^{2+}, 2 μM IscS, 10 μM IscU, 20 μM fluorescently labeled (red) or unlabeled (blue) Grx4, and 100 μM L-cysteine. (B) Difference CD spectrum obtained for the reaction containing $Grx4_{Rho}$ (red in panel A) by subtracting the 0 min from the 265 min spectra.

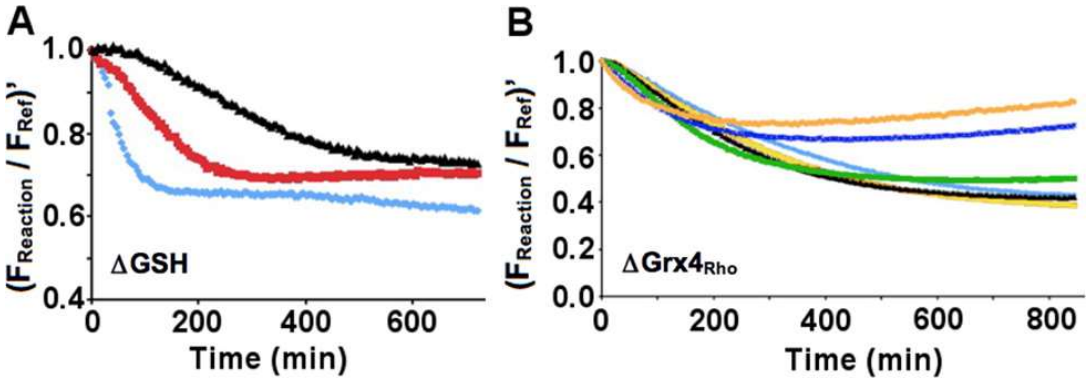

Figure 5.5. Rate of [2Fe–2S] cluster formation on Grx4 increases with higher GSH and $Grx4_{Rho}$ concentrations. Fluorescence quenching was monitored for $Grx4_{Rho}$ in reactions containing 5 μM IscU, 100 μM Fe^{2+}, and 100 μM L-cysteine. (A) Reactions contain 0.5 μM IscS, 2 μM $Grx4_{Rho}$, and either 1 mM (black), 3 mM (red), or 10 mM (cyan) GSH. (B) Reactions also included 100 nM IscS, 10 mM GSH, and either 1 μM (orange), 2 μM (blue), 6 μM (green), 15 μM (black), 30 μM (yellow), or 50 μM (cyan) $Grx4_{Rho}$.

as an electron source, under these conditions. The cluster transfer rate also depends on the apo-Grx4Rho concentration. The fluorescence assay measures the quenching rate or, stated another way, the time-dependent fraction of [2Fe−2S] cluster bound to $Grx4_{Rho}$ (Fig. 5.5B). The overlaid quenching rates indicate the cluster transfer rate increases with increasing acceptor levels. Interestingly, [2Fe−2S]−Grx4 appears unstable at concentrations of 2 μM or less, which might reflect the physiological dimerization/cluster binding constant. Again, the initial linear rates of quenching were converted to cluster transfer rates. A plot of cluster transfer rate as a function of apo- $Grx4_{Rho}$ concentration best fit to the Michaelis−Menten equation. Even though the substrate concentration was insufficient to reach saturation, we estimate a Km of 50 ± 10 μM and Vmax of 0.19 ± 0.03 μM cluster/min. On the basis of these results, we conclude that cluster transfer from IscU to Grx4 was at least partially rate limiting under these conditions and that GSH likely plays a functional role in this cluster transfer process.

$Grx4_{Rho}$ directly transfers clusters to apo-Fdx and apo-HcaC. We next investigated Grx4-dependent cluster exchange reactions by measuring transfer rates from [2Fe−2S]− $Grx4_{Rho}$ to Fdx and HcaC. [2Fe−2S]− $Grx4_{Rho}$ was first produced by an overnight cluster synthesis reaction catalyzed by the IscS−IscU complex. The quenched [2Fe−2S]− $Grx4_{Rho}$ reaction mixture was then diluted into wells containing varying concentrations of GSH and apo-Fdx or apo-HcaC (Fig. 5.6). The fluorescence quenching did not recover at a significant rate for reactions lacking an apo-acceptor protein (Fig. 5.6A and B, black line), indicating that [2Fe−2S]− $Grx4_{Rho}$ is stable upon dilution. The addition of either apo-Fdx

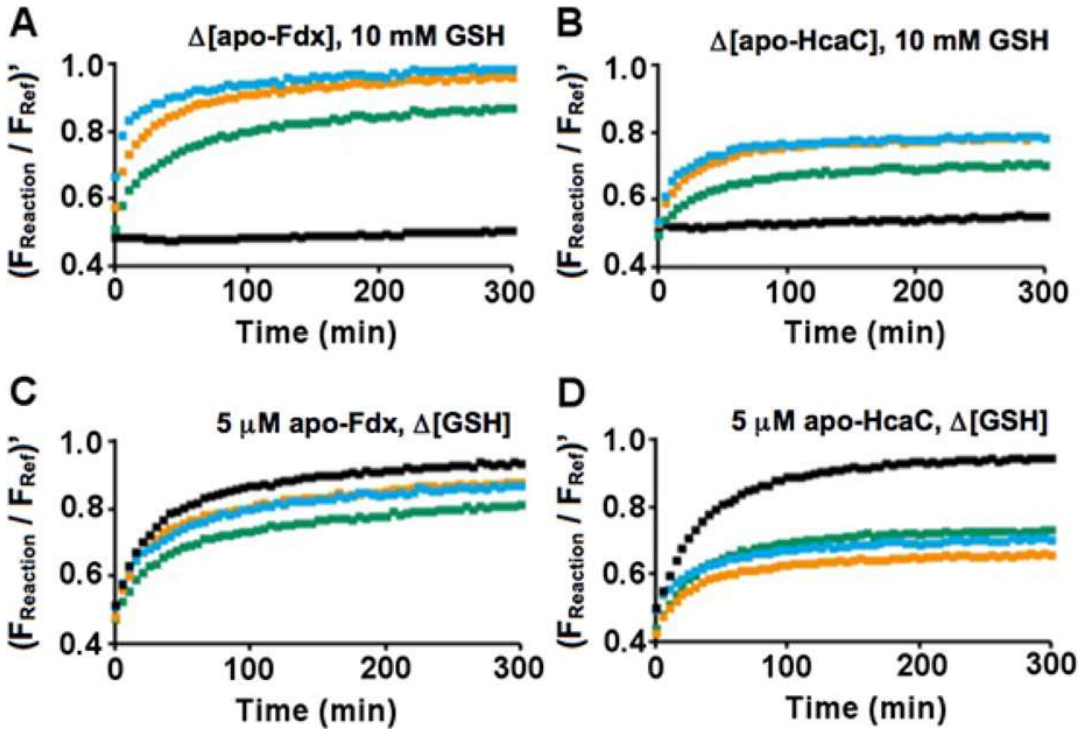

Figure 5.6. Direct cluster transfer from Grx4 to apo-acceptors. 2.5 μM [2Fe–2S] - $(Grx4_{Rho})_2$ was diluted into reactions containing 10 mM GSH and (A) apo-Fdx or (B) apo-HcaC. Acceptor protein concentrations were 0 μM (black), 5 μM (green), 10 μM (orange), and 20 μM (cyan). Similar cluster transfer reactions were performed using 0.7 mM (black), 2 mM (green), 5 mM (orange), and 10 mM (cyan) GSH and either (C) apo-Fdx (5 μM) or (D) apo-HcaC (5 μM).

or apo-HcaC to quenched [2Fe−2S]− $Grx4_{Rho}$ resulted in an increase in fluorescence (Fig. 5.6A and B), consistent with cluster transfer to acceptor proteins and recovery of the quenched fluorescence. The fluorescence intensity approached that of apo- $Grx4_{Rho}$ for reactions with high apo-Fdx concentrations but leveled off at lower values for apo-HcaC. The rate of increase in fluorescence was strongly dependent on the concentration of apo-acceptor protein. Moreover, the fluorescence of [2Fe−2S]− $Grx4_{Rho}$ failed to fully recover in some reactions, suggesting a reversible equilibrium between Fdx/HcaC and Grx4 for binding clusters.To test this hypothesis, the four curves from reactions containing 10 mM GSH were fit to models (Fig. 5.3, reaction C) for irreversible and reversible cluster transfer from [2Fe−2S]−Grx4 to Fdx. The reversible model (Grx4−Fdx-2) better fit the cluster transfer data (Table 5.1) than the irreversible model (Grx4−Fdx-1). A cluster degradation step (Fig. 5.3, $k_{degrade}$) was also included in the fits (Table 5.1). The very slow rates for $k_{degrade}$ further support the conclusion that [2Fe−2S]− $Grx4_{Rho}$ is stable upon dilution. The second order rate constant for [2Fe−2S] cluster transfer from Grx4 to Fdx (k_2 in Fig. 5.3 and Table 5.1) is 2-fold larger than the rate constant for the equivalent reaction with HcaC (model Grx4− HcaC-1 in Table 5.1). Interestingly, the rate constant for the reverse reaction (k−2) revealed the back reaction is 10-fold greater for cluster transfer from [2Fe−2S] − HcaC to apo-Grx4 compared to the analogous reverse reaction from [2Fe−2S]−Fdx. Analysis of cluster transfer at different GSH concentrations revealed that the rate and extent of cluster transfer from [2Fe−2S] −Grx4 to acceptor proteins increases at the lowest GSH concentrations (Fig. 5.6C and D), suggesting a GSH independent or direct [2Fe−2S] cluster transfer mechanism from Grx4 to Fdx/HcaC. Collectively, these

Table 5.1 Global fit kinetic parameters for cluster transfer reactions

Cluster transfer from [2Fe-2S]-Grx4$_{Rho}$ to apo-acceptors

model	$k_{degrade}$ (min^{-1})	k_2($M^{-1}min^{-1}$)	k_{-2}($M^{-1}min^{-1}$)	$K_{transfer}$	RMS error
Grx4-Fdx-1	0.000156(9)	1660(30)	n.a.	n.a.	0.22
Grx4-Fdx-2	0.000161(5)	3180(60)	970(30)	3.3	0.13
Grx4-HcaC-1	0.000306(5)	1590(5	11400(400)	0.14	0.11

Biosynthetic reactions on apo-acceptors monitored by Grx4$_{Rho}$ (Figures 5.6 and 5.7)

model	k_{synth} ($M^{-1}min^{-1}$)	k_1 ($M^{-1}min^{-1}$)	k_2 ($M^{-1}min^{-1}$)	k_{-2} ($M^{-1}min^{-1}$)	$k_{transfer}$ ($M^{-1}min^{-1}$)	k_3 ($M^{-1}min^{-1}$)	RMS error
IscU-Fdx-1	n.a.	1431(4)	1080(10)	n.a.	n.a.	n.a.	0.43
IscU-Fdx-2	n.a.	1286(5)	1150(10)	n.a.	n.a.	238(7)	0.39
IscU-Fdx-3	1,300 (40)	1540(10)	1080(10)	n.a.	n.a.	370(10)	0.35
IscU-Fdx-4[a]	n.a.	1339(4)	2440(90)	770(50)	3.2	n.a.	0.39
IscU-Fdx-5[a]	n.a.	1320(5)	1830(50)	350(30)	5.2	77(9)	0.39
IscU-Fdx-6[a]	870(30)	1770(20)	2030(60)	640(30)	3.2	n.a.	0.35
IscU-Fdx-7[a]	910(30)	1730(20)	1900(50)	490(40)	3.9	60(10)	0.35
IscU-HcaC-1		1260(3)	1700(300)[b]	11000(2000)[b]	0.15[b]	0(4)	0.23

[a]values for k_2 were restrained below 5000 $M^{-1}min^{-1}$. [b]Parameters were restrained near values derived from cluster transfer experiments from [2Fe-2S]- Grx4$_{Rho}$ to HcaC.

results indicate that transfer reactions from [2Fe−2S] −Grx4 are reversible with large differences in apparent equilibrium constants (Table 5.1), Ktransfer (k_2/k_{-2}), which results in a cluster stability ranking of Fdx > Grx4 > HcaC.

Grx4 functions as an intermediate [2Fe−2S] cluster carrier. Here, an IscS:IscU biosynthetic reaction was used to simultaneously generate [2Fe−2S] clusters and transfer these clusters to acceptor proteins (Fig. 5.3, Reactions A−D). In these reactions, Fdx or HcaC were allowed to directly compete with $Grx4_{Rho}$ for clusters generated by the IscS:IscU complex. Cluster binding to $Grx4_{Rho}$ results in quenching of the fluorescence, whereas cluster binding to unlabeled Fdx or HcaC is not expected to affect the fluorescence intensity of $Grx4_{Rho}$ (assuming the fraction of [2Fe−2S]−$Grx4_{Rho}$ does not change). The rhodamine fluorescence was converted to [2Fe−2S]−$(Grx4_{Rho})_2$ concentration and plotted as a function of time (Fig. 5.7). When apo-Fdx was added into a reaction mixture with $Grx4_{Rho}$, the time dependence of the fluorescence quenching was greatly perturbed. At higher concentrations of apo-Fdx, an initial formation of [2Fe−2S]−$Grx4_{Rho}$ was observed, followed by a steady state leveling as clusters are both accepted by Grx4 and donated to apo-Fdx. At later time points, the supply of apo-Fdx was depleted and quenching of $Grx4_{Rho}$ proceeded to completion. In the case of HcaC, rapid formation of [2Fe−2S]− $Grx4_{Rho}$ was observed followed by leveling off at different values that were dependent on the concentration of apo-HcaC (Fig. 5.8). This behavior further supports the observation that Grx4 and HcaC exhibit equilibrium cluster binding. Notably, the majority of reactions containing either Fdx or HcaC exhibit unperturbed initial kinetics of [2Fe−2S]

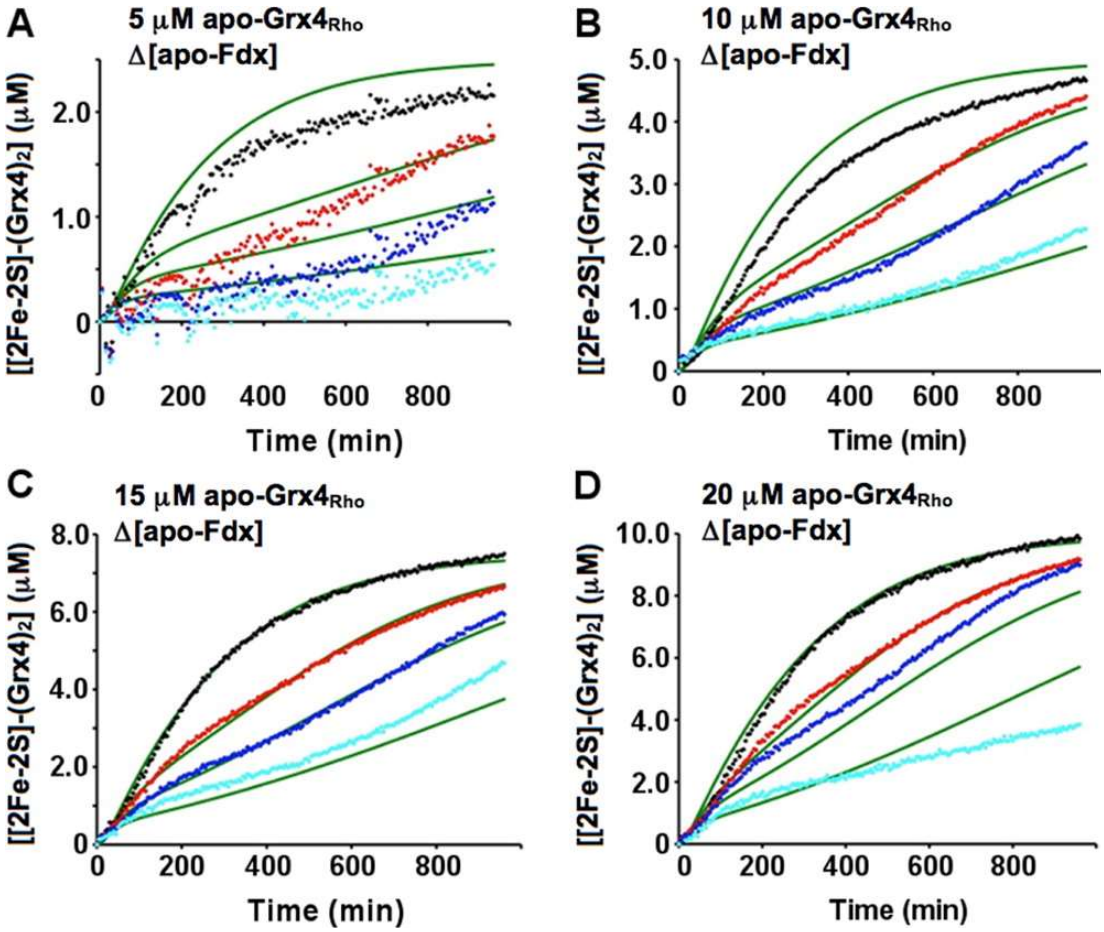

Figure 5.7. Cluster transfer to $Grx4_{Rho}$ in the presence of apo-Fdx. Cluster transfer reactions contained 10 mM GSH, 100 μM Fe^{2+}, 0.1 μM IscS, 5 μM IscU, 100 L-cysteine, and either 0 μM (black), 5 μM (red), 10 μM (blue), or 20 μM (cyan) apo-Fdx. The $Grx4_{Rho}$ concentrations were (A) 5 μM, (B) 10 μM, (C) 15 μM, and (D) 20 μM. The best fit from the global kinetic modeling (Table 5.1) is shown as green lines.

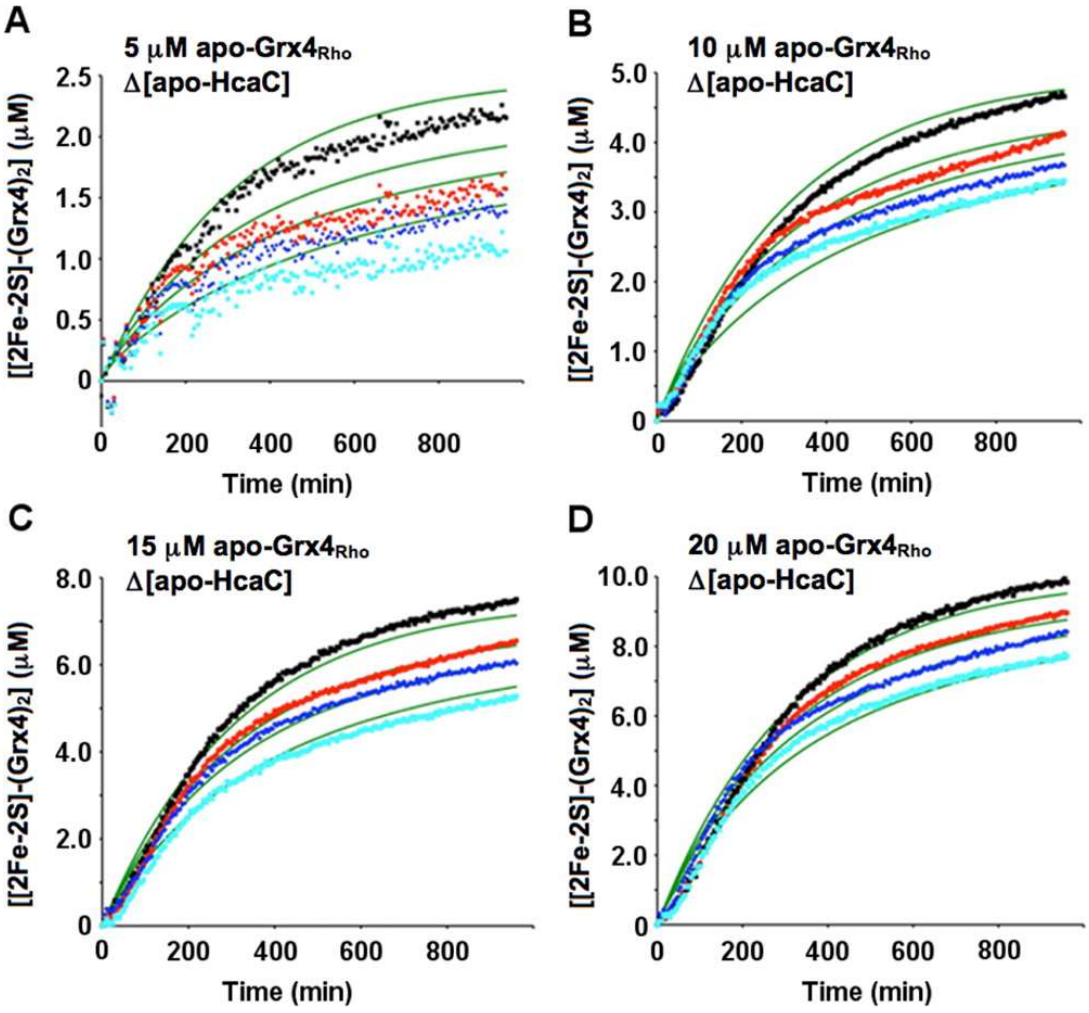

Figure 5.8. Cluster transfer to $Grx4_{Rho}$ in the presence of apo-HcaC. Cluster transfer reactions contained 10 mM GSH, 100 μM Fe^{2+}, 0.1 μM IscS, 5 μM IscU, 100 μM L-cysteine and either 0 μM (black), 5 μM (red), 10 μM (blue), or 20 μM (cyan) apo-HcaC. The $Grx4_{Rho}$ concentrations were (A) 5 μM, (B) 10 μM, (C) 15 μM, and (D) 20 μM. Green lines show the best fit to the kinetic modeling (Table 5.1).

-$Grx4_{Rho}$ formation upon addition of the apo-acceptor, suggesting that $Grx4_{Rho}$ is an early cluster transfer intermediate and hence successfully outcompetes terminal apo-targets for IscU-bound cluster. We used global fit kinetic analysis of the cluster transfer reactions to $Grx4_{Rho}$ in the presence of acceptor protein to define the cluster biosynthesis pathway. Multiple kinetic models were evaluated, and the kinetic parameters are provided in Table 5.1. The observation that the rate-limiting step of the reactions was cluster transfer rather than cluster synthesis allowed the reactions to be modeled (in some cases) with a fixed concentration of [2Fe−2S]−IscU. Additionally, fluorescence quenching data and results from other groups [50, 83] suggest that cluster transfer from IscU to either Grx4 or Fdx is irreversible, so all transfer steps from [2Fe−2S]−IscU were modeled as irreversible processes with only a forward rate constant (Fig. 5.3, steps k_1 for Reaction B and k_3 for Reaction D). Including Michaelis complexes for transfer reactions from [2Fe−2S] −IscU did not substantially improve the fit and failed to converge for V_{max} and K_m (data not shown). An initial model for cluster transfer to Fdx that contained only the linear transfer pathway from IscU to Grx4 to Fdx (Model IscU−Fdx-1; Fig. 5.3, k_1 and k_2) was improved by incorporating the ability of IscU to donate a cluster directly (Fig. 5.3, k_3) to the terminal target protein (Model IscU−Fdx-2). Limiting the amount of cluster in the model by including a cluster biosynthesis reaction (Fig. 5.3, k_{synth}) further improved the fit (model IscU−Fdx-3). Inclusion of reversible cluster transfer reactions (Fig. 5.3, k_{-2}) from Grx4 to Fdx with or without cluster synthesis (k_{synth}) and/or direct IscU−Fdx transfer (k_3) slightly improved fits (models IscU−Fdx-4 to IscU−Fdx-7) compared to the equivalent irreversible model and produced. $K_{transfer}$ values that ranged from 3.2 to 5.2. These values are in good

agreement with the results from the holo-Grx4 transfer experiments, supporting the reversibility of this reaction. In all cases, the addition of direct transfer (k_3) and cluster biosynthesis (k_{synth}) steps into the model had only minor effects on the k_1 and k_2 kinetic parameters. The observation that k_3 is substantially less than k_1 or k_2 implies that cluster transfer to Fdx proceeds through a [2Fe−2S] −Grx4 intermediate. We used a similar global fit kinetic analysis for the cluster transfer reactions to $Grx4_{Rho}$ in the presence of apo-HcaC. The inclusion of a reversible transfer from [2Fe−2S] −Grx4 to HcaC produced a model (IscU−HcaC-1) that closely approaches the observed data (Fig. 5.8 and Table 5.1). In this fit, k_2 and k_{-2} were constrained to values obtained from the [2Fe−2S] −Grx4 to HcaC transfer experiment since it was more sensitive to those rate constants and attempts to relieve the constraints resulted in unstable values. Including a pathway from [2Fe−2S] −IscU directly to HcaC produced k_3 values that converged on zero and did not improve the fit. A scan of curve fit error vs k_3 shows that k_3 is likely <100 M^{-1} min^{-1}, which is an order of magnitude lower than k_1 or k_2. Thus, cluster transfer to HcaC also appears to proceed through a [2Fe−2S] −Grx4 intermediate. These results support the hypothesis that monothiol glutaredoxins are intermediate cluster carriers that transport clusters from IscU to multiple target proteins.

Discussion

Fe−S cluster biosynthesis is an elaborate process in which multiple protein complexes are assembled and disassembled to form Fe−S clusters. These synthesized Fe−S clusters are distributed by a branched network of intermediate cluster carrier and apo-target proteins. In addition, the Fe−S assembly pathway also appears to include cluster storage and

conversion proteins, chaperones that accelerate at least some cluster transfer reactions, and the participation of non-protein [2Fe− 2S]−GSH intermediates. A major challenge in investigating these Fe−S cluster biosynthetic networks and assigning roles to the different proteins is the lack of spectroscopic probes to monitor kinetics of cluster synthesis and transfer reactions. Here, we apply newly developed fluorescent reporter methodology to track cluster synthesis and transfer. The fluorescence of $Grx4_{Rho}$, Fdx_{Rho}, and $HcaC_{Rho}$ have all previously been shown to be sensitive to Fe−S cluster binding. We further show that in biosynthetic assays $Grx4_{Rho}$ exhibits nearly identical time courses for fluorescence quenching and changes in CD spectroscopy due to [2Fe−2S] cluster formation. Additional experiments show that quenching of $Grx4_{Rho}$ is dependent on IscU and not due to DTT-dependent aggregation or homo-FRET. These fluorescent reporters are uniquely suited to deconvolute the complex kinetic processes of Fe−S assembly pathways by coupling real-time detection of the cluster content of a single protein in a reaction mixture of cluster binding proteins with high throughput plate reader assays and global fit analysis. This fluorescent reporter methodology was first applied to examine the mechanism of cluster transfer from IscU to $Grx4_{Rho}$. Importantly, these studies use the IscS−IscU assembly complex as the cluster source rather than an uncomplexed [2Fe−2S] −IscU dimeric species, which has not been established as a kinetically competent intermediate in the biosynthetic pathway. The rate of cluster formation was dependent on the concentration of apo- $Grx4_{Rho}$ and GSH, which is a cluster ligand for [2Fe−2S] −Grx4, implying that cluster transfer is at least partially rate-limiting in these combined cluster biosynthesis/transfer reactions. Interestingly, extrapolation of the Grx4 curve to the higher

concentrations that have been used previously in the literature [50] (45 μM cluster = 90 μM Grx4) results in a formation rate of 0.12 μM clusters/min, which corresponds to a second order rate constant of 1.1×10^3 M^{-1} min^{-1}. This is in good agreement with the rate of cluster formation we observed on Fdx in the presence of Grx4 derived from CD spectroscopy of 920 M^{-1} min^{-1} (note: the rate-limiting step should be cluster transfer from IscU to Grx4 at these concentrations) and the rate of $1.3- 1.7 \times 10^3$ M^{-1} min^{-1}derived from kinetic modeling. Notably, this rate is much higher than values previously determined using purified [2Fe−2S] −IscU dimer as the cluster source inthe absence of chaperones (30 M^{-1} min^{-1}) and is more similar to rates measured with chaperones (2×10^4 M^{-1} min^{-1}). This may indicate that the [2Fe−2S] −IscU dimer is not a relevant transfer species and that chaperones function in promoting or regenerating the active transfer species that is formed during complete biosynthetic reactions. Alternatively, this may reflect differences in homologous proteins from different species, reaction conditions, or saturation of assays. More studies will be needed to fully address this discrepancy. The ability of Grx4 to mediate cluster transfer from IscU to apo-target proteins was then investigated. First, preformed and fluorescently quenched [2Fe−2S] $-Grx_{Rho}$ was incubated with apo-acceptor proteins Fdx and HcaC. The fluorescence signal increased rapidly, indicating that Grx4 is capable of transferring clusters to these target proteins. The rate of the transfer reaction increased with a higher concentration of acceptor protein and decreased with increasing GSH concentrations. This implies that the cluster transfer reaction from Grx4 involves ligand exchange with a residue from the apo-acceptor rather than proceeding through a GSH-cluster intermediate. Second, combined IscS:IscU mediated cluster

biosynthesis and transfer reactions were carried out with $Grx4_{Rho}$ and apo-acceptor Fdx or HcaC. For the Fdx reactions, $Grx4_{Rho}$ exhibited clear intermediate-like behavior. Fitting of the kinetic traces showed that even when competing pathways for cluster transfer from IscU directly to Fdx/HcaC were included in the model, these rate constants were significantly lower than transfer through Grx4. This is in contrast to previous results that suggest that Grxs only act as intermediate carriers in the presence of chaperones. We also show that DTT is highly efficient at accelerating the cluster transfer reaction between IscU and Fdx (even in the presence of Grx4), suggesting previous studies that include DTT need to be reevaluated.

Moreover, cluster transfer reactions from Grx4 to Fdx or HcaC were found to be dynamic and reversible. The equilibrium slightly favored the products ([2Fe−2S]−Fdx, apo-Grx4, and GSH; $K_{transfer} \sim 3-5$) for Fdx and the reactants ([2Fe−2S]−Grx4 and apo-HcaC; $K_{transfer} \sim 0.15$) for HcaC. The apparent cluster stability (Fdx > Grx4 > HcaC) can be rationalized by the better coordination ability of cysteine compared to histidine. In summary, these results demonstrate the benefit of using fluorescent probes to interrogate enzymatic Fe−S cluster assembly. These probes allowed direct monitoring of the development and decay of [2Fe−2S]−Grx4 intermediates in biosynthetic reactions. These studies suggest that cluster transfer from Grx4 to terminal target proteins proceeds via direct ligand exchange, rather than a GSH mediated process. The rates of cluster transfer to Grx4 using the IscS−IscU complex suggest that the role of the chaperone protein in cluster transfer may need to be reevaluated. Furthermore, kinetic modeling strongly supports Grx4 as an intermediate carrier that accepts Fe−S clusters from IscU and transfers

them to multiple acceptor proteins. The Grx4-dependent transfer reactions were highly reversible, and the back reaction was even favored under some conditions, suggesting that cluster transfer networks are much more dynamic than previously thought. Future studies that determine the fraction of Grxs bound with clusters under varied growth conditions and exposure to oxidative stress may shed light on the functional dynamics of Grxs *in vivo*. Overall, the sensitivity of the fluorescent reporterand ability to monitor a labeled protein in the presence of unlabeled Fe−S proteins have the potential to be transformative for investigating the enzymology of Fe−S cluster biosynthetic networks.

Materials and Methods

Preparation of proteins and fluorescent labeling. *Escherichia coli* proteins were used for all studies. IscS, IscU, and Fdx were purified as previously described. The genes for Grx4 and HcaC were cloned into the Fdx expression vector that encoded N-terminal His-tag, GFP, and TEV protease cleavage sequences. Mature Grx4 and HcaC were generated using the proteolysis and purification procedure described for Fdx.*2* $Grx4_{Rho}$ was purified and fluorescently labeled with efficiencies of 0.76(4)-0.89(2). Apo-proteins were prepared by treatment with DTT and TCA, followed by washing with water and dissolving in 50 mM HEPES, 150 mM KCl pH 7.2 buffer.*2* Ferrous ammonium sulfate was used as the Fe^{2+} source for all experiments.

Fe-S cluster transfer reactions monitored by CD spectroscopy. Samples were prepared in an anaerobic glovebox and sealed in a 1 cm pathlength cuvette with a rubber septum and electrical tape. Reactions were performed in 50 mM HEPES, 150 mM KCl, and 10 mM MgCl2 at pH 7.5 and recorded at 25 °C on a CD spectrometer (Applied Photophysics

Chirascan). Formation of [2Fe-2S]-Fdx was monitored by the change in ellipticity at 515 nm, the CD ellipticity was measured starting at 90 min after the reaction was initiated (to minimize contributions from cluster synthesis on IscU and Grx4) and fit to a linear equation using Kaleidagraph (Synergy Software) to determine the cluster transfer rates from Grx4 to Fdx. The Grx4 ellipticity at 515 nm was converted to concentration by a determined extinction coefficient of 7580 M^{-1} min^{-1}, which is consistent with previous measurements.

Fe-S cluster reactions using $Grx4_{Rho}$. Kinetic assays with $Grx4_{Rho}$ were performed in 50 mM Tris with 150 mM KCl at pH 7.2 (Buffer A). Rhodamine fluorescence was measured using an excitation wavelength of 550 nm and emission wavelength of 600 nm using a fluorescent plate reader located inside an anaerobic glovebox (mBraun, O_2 < 1 ppm). Fluorescence data were corrected for the inner-filter effect and plotted as a ratio relative to a reference well that did not contain IscS or cysteine. Fluorescence data were reported as ($F_{Reaction}/F_{Ref}$)', which is the ratio of the corrected fluorescence intensities of the reaction well relative to a reference well. The oligomeric state of $Grx4_{Rho}$ was analyzed after completion of the reaction (the fluorescence had plateaued). The sample was loaded onto a Superdex 200 column (10 x 300 mm) equilibrated with Buffer A and 1 mL fractions were collected. The concentration dependence of $Grx4_{Rho}$ was determined (Fig. 5.4B) for cluster transfer reactions from IscU to Grx4. The fluorescence quenching data between 30 min and 75 min (to avoid the lag phase present in some samples) was fit to a linear equation. The slope was converted to a rate of cluster transfer by assuming the minimum observed fluorescence (for all concentrations of $Grx4_{Rho}$) corresponded to 100% cluster

transfer and then scaling the fluorescence percentage based on the added concentration of apo-fluorescent protein. For direct cluster transfer experiments from $Grx4_{Rho}$ to Fdx and HcaC, [2Fe-2S] clusters were generated on $Grx4_{Rho}$ (Fig. 5.5) using an overnight reaction that included 100 μM Fe^{2+}, 100 nM IscS, 5 μM IscU, 40 μM $Grx4_{Rho}$, 10 mM GSH, and 100 μM L-cysteine. Reaction progress was monitored by fluorescence quenching as described above. [2Fe-2S]- $Grx4_{Rho}$ samples were then diluted into mixtures containing varying concentrations of GSH and apo-Fdx or apo-HcaC.

Kinetic modeling. Copasi kinetic modeling software was used to fit the data (Table 5.1) using evolutionary programming with a population size of >100 and >300 generations. Fluorescence data were converted into [[2Fe-2S] -($Grx4_{Rho})_2$] concentrations by assuming that the minimum fluorescence for the data set corresponded to 100% cluster transfer. The fluorescence ratio was corrected by equation [1] to give [[2Fe-2S] -($Grx4_{Rho})_2$]. Kinetic data were modeled assuming a constant concentration of [2Fe-2S] -$(IscU)_2$ except when otherwise stated. Cluster transfer to glutaredoxin was modeled as being first order in glutaredoxin concentration since second order models failed to adequately fit the data (data not shown). The boundary limits of the variables were adjusted as needed to give optimal fits, but in general were kept at least an order of magnitude away from the observed final rate constants. Parameter scans were also carried out using Copasi, where one variable was systematically varied and the others were optimized using evolutionary programming. The sum of squares was obtained as a function of the rate constant that was varied.

CHAPTER VI

CHAPERONE-MEDIATED ACCELERATION OF CLUSTER DELIVERY TO APO-ACCEPTORS IS GLUTAREDOXIN-DEPENDENT

Introduction

Iron sulfur cluster biogenesis is one of the most ubiquitous pathways found in all life forms from eukaryotes to prokaryotes because of iron-sulfur clusters functioning as essential protein cofactors in many critical life processes namely oxidative respiration, DNA replication and repair, and photosynthesis [2]. There are four pathways in cells that are used for assembling and delivering iron-sulfur clusters known as SUF, NIF, ISC and CIA pathways. NIF and SUF pathways are specialized pathways. The NIF (Nitrogen Fixation Pathway) is required for cluster biosynthesis on nitrogenase [7] whereas SUF (Sulfur mobilization pathway) often operates in prokaryotes under oxidative stress conditions [8]. The CIA (cytosolic Iron sulfur protein assembly pathway) functions in eukaryotic cytosol and nucleus for iron-sulfur cluster maturation [9]. The ISC pathway is commonly the house-keeping pathway under normal growth conditions for prokaryotes and is the exclusive pathway in eukaryotic mitochondria [190]. Hence, several studies are ongoing to achieve a deeper mechanistic understanding of the pathway.

Cluster biogenesis consists of two major events, cluster assembly on the scaffold protein followed by transfer of the assembled cluster to different targets. The assembly process involves the formation of persulfide on cysteine desulfurase [32], transfer of the persulfide to scaffold protein, IscU, and assembly of the cluster on IscU in the presence of iron and electrons [23]. The next event is cluster transfer from the scaffold protein to

different protein targets. The transfer process needs to be well-orchestered as it involves the allocation of clusters synthesized on the scaffold protein to a wide array of different cluster targets including [2Fe-2S], [4Fe-4S] and [3Fe-4S]. Monothiol glutaredoxins have been shown to bind different forms of clusters, including [2Fe-2S], [4Fe-4S], [3Fe-4S] etc. [41] and function as an intermediate cluster carrier that transfers clusters to apo-acceptors such as ferredoxin and HcaC [109]. Glutaredoxin can also transfer cluster to IscA [57] which has been shown to be involved in maturation of [4Fe-4S] proteins [59]. Cluster transfer from holo-IscU to apo-Grx4 has been shown to be accelerated by the chaperones HscA and HscB in an ATP-dependent manner [50]. However, it is still unknown if chaperones or any other proteins are involved in the cluster transfer from glutaredoxin to downstream targets like apo-Fdx. The possibility is fueled by the observations that HscA interacts with apo-Fdx, glutaredoxin and apo-BioB [65, 66]. Further, several studies in the literature demonstrate that direct cluster transfer from holo-IscU to apo-Fdx is accelerated in the presence of chaperones [39, 83], however these experiments were performed in the presence of DTT which may mimic Grx4 and mediate thiol-dependent cluster redistribution on proteins [67].

We have previously shown that glutaredoxin serves as an intermediate in the cluster transfer from IscU to apo-acceptors [109]. Here, our objectives were to further study the generality of glutaredoxin mediated cluster transfer to apo-acceptors. Towards that goal, we investigated (1) interaction of holo-IscU with apo-acceptors in absence of Grx4, (2) whether chaperone mediated direct cluster transfer from holo-IscU to apo-Fdx in the DTT-independent reaction serves as an alternative pathway that bypasses

glutaredoxin and (3) the effect of chaperones on cluster transfer downstream to that of glutaredoxin.

Our results indicate that the acceleration of transfer from holo-IscU to apo-Fdx was detected only when DTT, chaperones and MgATP were present together. In the absence of chaperones, the transfer occurs but is much slower [109]. Our results support DTT as a functional mimic of glutaredoxin. In addition, cluster assembly rates on apo-Fdx were accelerated in the presence of chaperones and glutaredoxin in a one-pot cluster delivery assay consistent with our hypothesis. However, the rate of cluster transfer from holo-Grx4 to apo-Fdx was not affected by chaperones. We also provide evidence for interaction between holo-IscU and apo-acceptors and propose the formation of an encounter complex that does not appear to mediate cluster transfer. The physiological significance of these non-transferring complexes is unclear.

Results

Holo-Iscu interacts with terminal apo-acceptors without cluster transfer. Glutaredoxin has been shown to act as intermediate cluster carrier in the ISC pathway [109]. We wanted to further study the generality of glutaredoxin as an intermediate cluster carrier by fluorophore labeling IscU (Rho-IscU) and monitoring the fluorescence quenching and recovery during cluster assembly in the presence and absence of different apo-acceptors such as Grx4, apo-Fdx and HcaC. The presence of an Fe-S cluster quenches fluorescence. Previously we had shown minimal cluster transfer from holo-IscU to apo-Fdx monitored by CD spectroscopy [109]. We therefore expected similar quenching patterns of Rho-IscU in presence and absence of terminal apo-acceptors (apo-Fdx and apo-

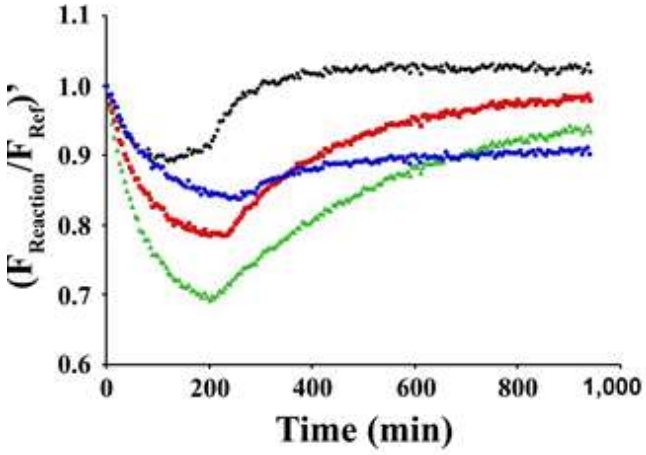

Figure 6.1. Cluster assembly on Rho IscU in the presence or absence of apo-acceptors. Reactions contained 10 mM GSH, 30 µM Fe2+, 0.5 µM IscS, 5 µM $IscU_{Rho}$, 30 µM cysteine (blue). Other reactions also contained apo-target proteins: 40 µM Grx4 (black), 20 µM Fdx (red), or 20 µM HcaC (green).

HcAc) consistent with a lack of cluster transfer. However, we observed two distinct differences in the presence of terminal apo-acceptors. First, the initial rate of quenching in the presence of terminal apo-acceptors (Fig. 6.1, red and green) appeared to be faster than IscU by itself (Fig. 6.1, blue) or in the presence of Grx4 (Fig. 6.1, black). Moreover, the extent of quenching in presence of apo-acceptors like Fdx and HcaC is much higher as compared to IscU by itself where they were expected to be comparable. Second, the recovery of fluorescence quenching in the presence of terminal acceptors appeared much slower as compared to IscU by itself. We hypothesized that during cluster transfer from holo-IscU, an intermediate complex between holo-IscU and apo-acceptor is formed (Fig. 6.2, step b). The faster rate of quenching in the presence of apo-acceptors can be explained by comparing the relative rates of the steps involved in the above process (Fig. 6.2, steps b and c). Since the cluster transfer (step c, Fig. 6.2) is very slow in the absence of glutaredoxin, there is an accumulation of the intermediate complex leading to apparent faster rates of quenching. For Grx4, the hetero-complex is very short-lived leading to rapid cluster transfer from holo-IscU to apo-Grx4 resulting in faster recovery of Rho-IscU fluorescence. However, for apo-Fdx and HcaC, the process of cluster transfer is much slower [109]. This would account for the faster fluorescence quenching of Rho-IscU in presence of apo-Fdx and HcaC. The apparent slower rate of fluorescence recovery in presence of apo-acceptors as compared to IscU only can be explained by hypothesizing that encounter-complex between holo-IscU and apo-Fdx is more-stable as compared to holo-IscU alone and hence a slower rate of cluster-loss.

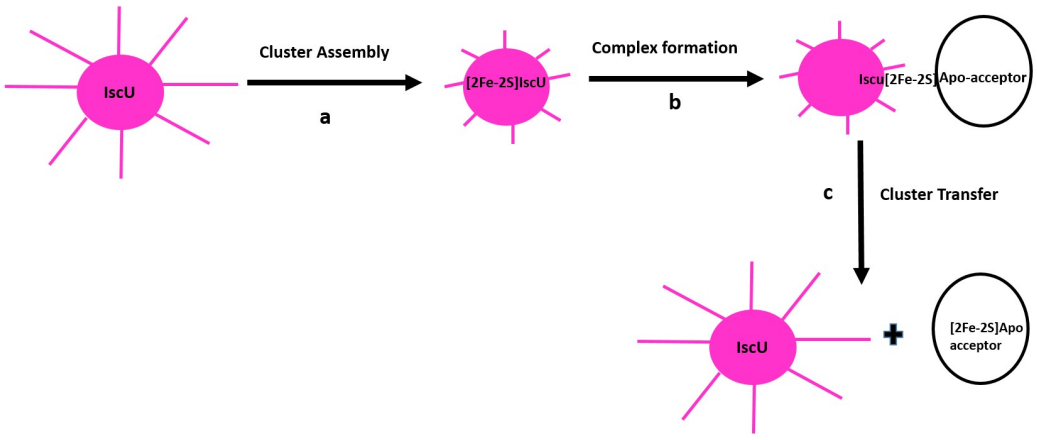

Figure 6.2. Events during cluster assembly on Rho-IscU in the presence of apo-acceptors. Step a is the cluster assembly on IscU. Step b is the formation of an intermediate complex and step c involves the cluster transfer to the apo-acceptor.

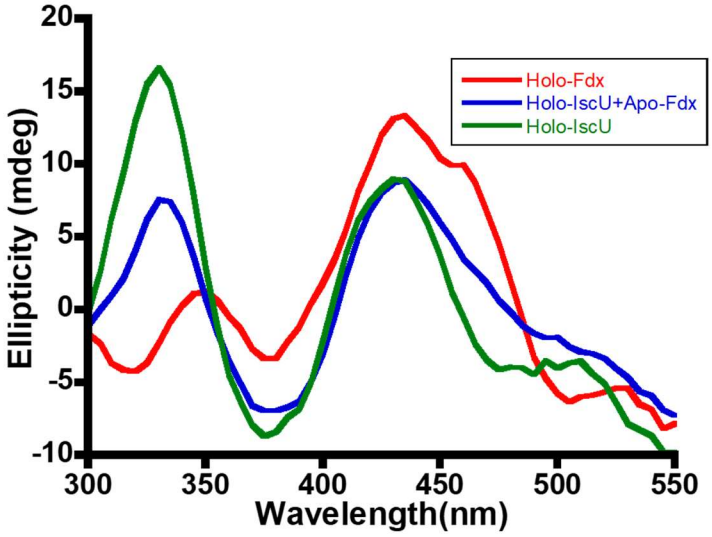

Figure 6.3. CD spectra for holo-IscU (green), holo-Fdx (red) and encounter complex between holo-IscU and apo-Fdx (blue). The CD spectra formed on addition to holo-IscU is distinct from holo-Fdx and holo-IscU. Green spectra is the final spectra after the cluster assembly reaction on 30 µM IscU in the presence of 0.5 µM IscS, iron and Cysteine. Blue spectrum is generated on addition of of 40 µM apo-Fdx to the above reaction. The red spectra is CD spectra for 40 µM Holo-Fdx as isolated from *E.coli* for comparison purposes.

Apo-Fdx interacts with holo-IscU to form complex with CD signature distinct from holo-IscU or holo-Fdx. We decided to further characterize the interaction between holo-IscU and apo-Fdx using CD spectroscopy. Cluster assembly reaction was performed on IscU followed by addition of apo-Fdx to the holo-IscU generated *in situ*. Immediate formation of a new species with CD spectrum distinct from either holo-IscU or holo-Fdx (Fig. 6.3) was observed. The CD spectrum remains unchanged even after 2h (Fig. 6.4). A complete cluster transfer to Fdx is observed only after an overnight incubation (Fig. 6.3).

Rho-labeled Fdx undergoes fluorescence quenching in the presence of holo-IscU. The interaction of Holo-IscU and apo-Fdx was also monitored using Fdx labeled with a fluorophore. When Rho-Fdx was added to holo-IscU, the fluorescence of Rho-Fdx was immediately quenched even though no cluster transfer was observed during the timescale while monitoring the same reaction via CD spectroscopy (Fig. 5.1, Chapter V). This observation would also be consistent with the formation of intermediate complex between holo-IscU and apo-Fdx. The fluorescence quenching could be attributed to a possible complex formation between apo-Fdx and holo-IscU.

Cluster transfer from IscU to apo-Fdx is accelerated by chaperones and ATP only in the presence of DTT. Chaperones accelerate direct cluster transfer from holo-IscU to apo Fdx [26]. We tested the DTT dependence of this pathway. We also wanted to test the effect of chaperones on the proposed intermediate complex formed between holo-IscU and apo Fdx. Surprisingly, it was observed that cluster transfer from holo-IscU to apo-Fdx was accelerated only in the presence of chaperones, ATP and DTT (Fig. 6.5). The accelerated

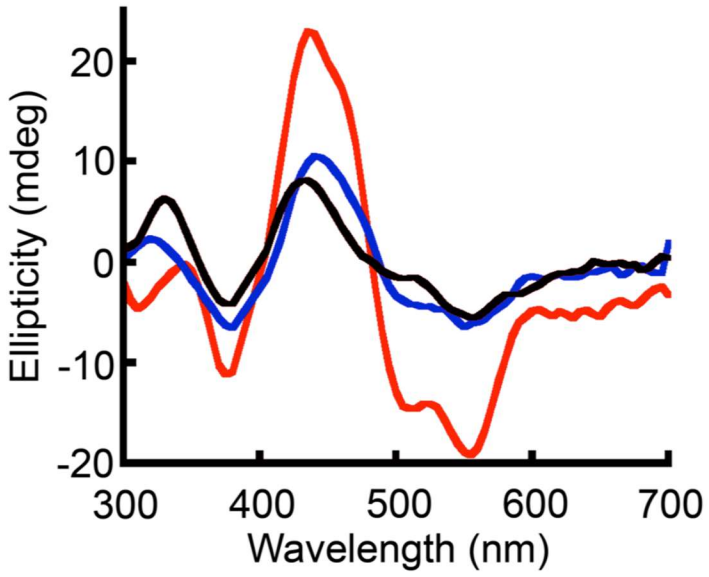

Figure 6.4 CD spectra of Fe-S cluster transfer reactions at an intermediate time point. CD spectra before apo-Fdx addition (black) to a completed reaction of cluster assembly on 30 μM IscU, after 120 min of the addition (blue). The red is spectrum for holo-Fdx as isolated from *E.coli* for comparison purposes.

cluster transfer was not observed with: i) Chaperones and ATP (Fig. 6.5) ii) Chaperones and DTT and iii) ATP and DTT (data not shown). When apo-Fdx was added to holo-IscU, intermediate complex with a distinct CD signature was formed without any cluster transfer (Fig. 6.3). No further change was observed on addition of chaperones and MgATP to the reaction. Immediate cluster transfer to Fdx occurs when DTT is added to the reaction as evident from the shift in the peak to 355 nm from 330 nm, the latter being characteristic of holo-IscU (Fig. 6.5). The observation that the cluster transfer from holo-IscU to apo-Fdx did not occur in presence of DTT when chaperones were absent indicated that DTT does not initiate solution chemistry in this reaction. It was hence hypothesized that DTT here is likely a mimic of a physiological molecule.

Cluster transfer from IscU to apo-Fdx undergoes chaperone-dependent acceleration in the presence of Grx4. Grx4 functions as an Fe-S cluster carrier in transfer reactions from IscU to terminal apo-acceptors like Fdx and HcaC [109]. Johnson and co-workers demonstrated that the cluster transfer from holo-IscU to Grx4 is accelerated in the presence of chaperones [50]. So, we hypothesized that Grx4 is the physiological molecule mimicked by DTT and tested whether chaperones accelerate the rate of cluster transfer from IscU to apo-Fdx in the presence of Grx4. Hence, we set up a complete assembly and transfer reaction containing IscU, IscS, Grx4, apo-Fdx and chaperones. The reaction was initiated by the addition of GSH and MgATP. Fe-S cluster formation reactions on Fdx were monitored by the loss of ellipticity at 350 nm. The cluster assembly on Fdx was significantly faster in the presence of chaperones (Fig. 6.6).

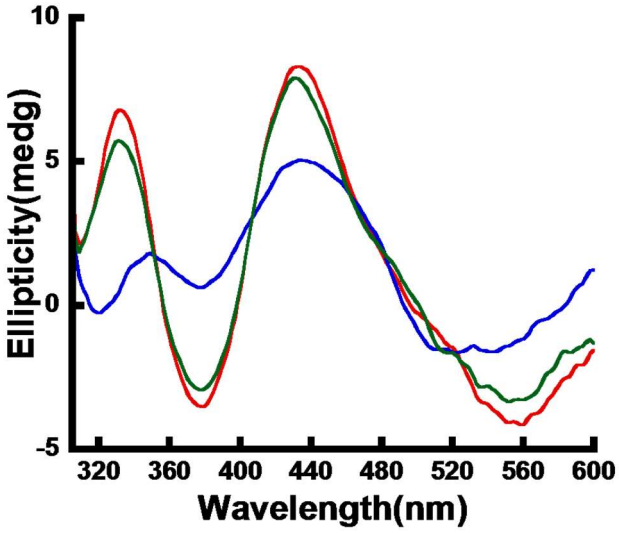

Figure 6.5. DTT is required for chaperone dependent cluster transfer from holo-IscU to apo-Fdx. Reaction contains 30 µM Iscu, 1µM IscS, 400 µMFe^{2+}, 100 µM cysteine and 10 mM GSH. Red spectrum is recorded after cluster assembly on IscU is complete as monitored by the saturation of ellipticty at 330 nm. 40µM apo-Fdx was added to the above reaction and the spectra was recorded (red) immidiatey. No further change in the spectra was recorded for next 30 minutes. 20 µM HscA & HscB and 3 mM MgATP were then added to the above reaction (green) with no change in spectra till 15 min. 2 mM DTT addition was then added followed by recording the spectra (blue).

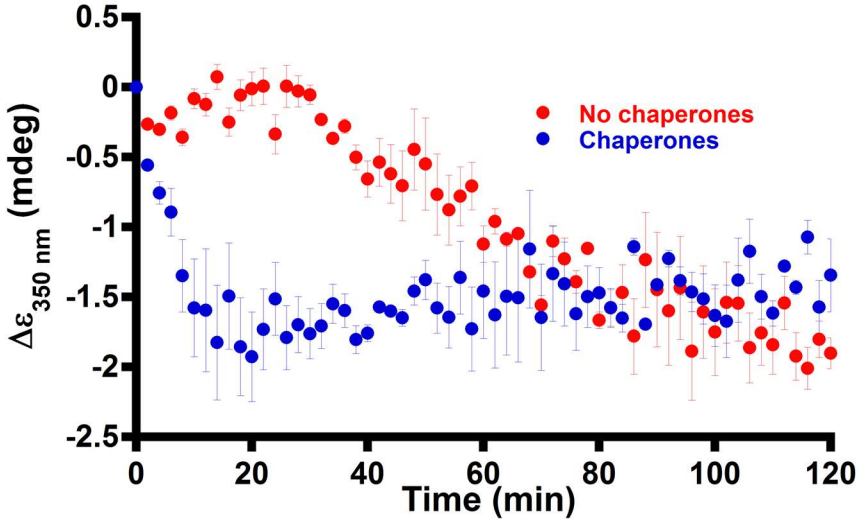

Figure 6.6. One-pot cluster assembly on apo-Fdx is accelerated by chaperones. Assay contained 20 µM IscU, 0.5 µM IscS, 40 µM Grx4, 400 µM $Fe(NH_4)_2(SO_4)_2$, 40 µM HscA , 40 µM HscB, 50 µM apo-Fdx and 100 µM cysteine and the reaction is initiated by the addition of 10 mM GSH and 3mM MgATP.

Chaperones do not affect the rate of cluster transfer from holo-Grx4 to apo-Fdx. We found that the rate of Fe-S cluster assembly and transfer to Fdx in the presence of glutaredoxin was accelerated by chaperones. The acceleration could be attributed to two possible effects. The first possibility is that the faster cluster assembly on Grx4 in the presence of chaperones led to an increased concentration of holo-Grx4 and faster cluster transfer to apo-Fdx. The second possibility is that the chaperones accelerate cluster transfer from holo-Grx4 to apo-Fdx. A combination of these effects is also conceivable. To distinguish between these possibilities, the effect of chaperones on cluster transfer from holo-Grx4 to apo-Fdx was studied. First, holo-Grx4 was isolated from *E. coli* was used. Second, the cluster transfer from holo-Grx4 to Fdx was monitored by recording the change in ellipticity at 315 nm due to minimal contribution of holo-Fdx at that wavelength (Fig. 6.7). The rate of cluster transfer from Holo-Grx4 to apo-Fdx was observed to remain unchanged in the presence of chaperones. Hence, we concluded that the accelerated rate of the complete cluster assembly and transfer reaction on Fdx is due to chaperone-assisted faster cluster assembly on Grx4 and not due to faster transfer from holo-Grx4 to apo-Fdx.

Discussion

Cluster transfer is the slow step in Fe-S cluster biogenesis and mechanistic details of this process are poorly understood. We have demonstrated that Grx4 functions as an intermediate cluster carrier in cluster transfer reactions from IscU to Fdx. However, those experiments were done in absence of chaperones. The next question is whether Grx4 is also an obligate intermediate in the cluster transfer from IscU to apo-acceptors like ferredoxin in the presence of chaperones or do chaperones open up an alternate direct

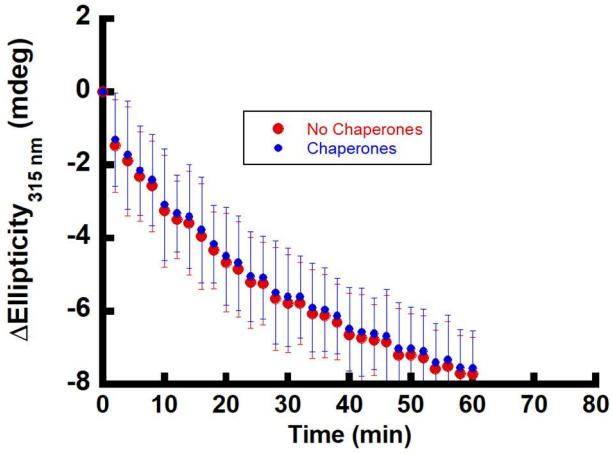

Figure 6.7. Chaperones do not affect the rate of cluster transfer from holo-Grx4 to apo-Fdx. The reaction contained 20 μM holo-Grx4 and 10 mM GSH and was initiated by addition of 30 μM Apo-Fdx.The change in ellipticity at 315 nm for cluster transfer from holo-Grx4 to apo-Fdx in the presence and absence of chaperones remains unchanged.

pathway from IscU to apo-Fdx. A chaperone-mediated direct pathway is supported by acceleration of cluster transfer from holo-IscU to apo-Fdx in the absence of glutaredoxin [26]. Here, we found that the acceleration in reactions in the absence of Grx4. We suggest that DTT mimics Grx4's function as an intermediate cluster carrier, as they can bind clusters with two coordinating thiols. We also demonstrated that cluster assembly and transfer reaction on apo-Fdx is accelerated in the presence of chaperones and glutaredoxin. This is the first time that the effect of chaperones has been tested in a one-pot biosynthetic reaction to ferredoxin. This is significant as there is a lack of consensus as to the identity of physiologically relevant cluster-bound scaffold protein. Three possible candidates are [2Fe-2S]-bound IscU dimer, monomeric [2Fe-2S]-IscU and the cluster bound IscU-IscS complex. By letting the reaction proceed with all the proteins present, we are likely to circumvent possible formation of off-path intermediates and monitor the correct physiological course of the reaction. Now, the observed acceleration of cluster assembly on apo-Fdx in presence of chaperones and glutaredoxin could be due to faster cluster assembly to Grx4 or a faster cluster transfer from holo-Grx4 to apo-Fdx or both.

The model of chaperone-mediated acceleration is that HscB, the co-chaperone recruits holo-IscU to the chaperone HscA. HscA binds IscU via LPPVK recognition motif [38] in a nucleotide-dependent manner. ATP-bound HscA binds IscU with a lower affinity. ATP hydrolysis to ADP results in conformational change on HscA leading to a stronger binding of IscU which facilitates the cluster transfer from holo-IscU to acceptors. However, HscA belongs to Hsp70 class of chaperones that are known to be involved in protein folding [37]. Hence, it is possible that chaperones accelerate cluster transfer to

apo-acceptors not only by facilitating the release of cluster from IscU via a conformational change but also by interacting with apo-acceptors and pre-organizing the unfolded apo-acceptors. Studies showing an interaction of HscA with apo-Grx4, apo-Fdx and apo-BioB lent support to this possibility but a functional relevance of these observations has not been explored yet. Hence, we compared the rates of cluster transfer from holo-Grx4 to apo-Fdx in presence and absence of chaperones and found the rates comparable. Therefore, we still do not have a functional explanation for the interaction of HscA and apo-acceptors. We also evaluated whether holo-IscU and apo-acceptors like ferredoxin interact in the absence of glutaredoxin. Our observations are consistent with formation of non-transferring complex formation between holo-IscU and apo-Fdx. Further studies are required to confirm if the observation is an artefact or has functional significance in the process of cluster transfer like pre-folding the apo-protein thereby facilitating cluster delivery to the targets.

Materials and Methods

Preparation of proteins and fluorescent labeling. *Escherichia coli* proteins were used for all studies. IscS, IscU, IscU-intein fusion and Fdx were purified as previously described [46, 67]. IscU was labeled with rhodamine fluorophore following the established protocol [67].

Fe-S cluster reactions using IscU-Rho. Kinetic assays with IscU-Rho were performed in 50 mM Tris with 150 mM KCl at pH 7.2 (Buffer A). Rhodamine fluorescence was measured using an excitation wavelength of 550 nm and emission wavelength of 600 nm using a fluorescent plate reader located inside an anaerobic glovebox (mBraun, $O_2 < 1$

ppm). Fluorescence data were corrected for the inner-filter effect and plotted as a ratio relative to a reference well that did not contain IscS or cysteine. Fluorescence data were reported as ($F_{Reaction}/F_{Ref}$)', which is the ratio of the corrected fluorescence intensities of the reaction well relative to a reference well. Cluster assembly reaction on 5 μM Rho-IscU was performed using 30 μM $Fe^{2+,}$ 0.5 μM IscS, 30 μM cysteine and 10 mM GSH. The reaction was repeated in the presence of 40 μM Grx4, 20 μM Fdx and 20 μM HcaC.

CD spectroscopy. CD spectra were recorded using a 1 cm path length cuvette on a Chirascan CD spectrometer (Applied Photophysics). Cuvettes were sealed with a rubber septa and electrical tape in a glove box. The assays were run in 50 mM HEPES, 150 mM KCl, and 10mM $MgCl_2$ (pH 7.5).

Cluster assembly assay on IscU and reaction with apo-Fdx. The assay constituted 30 μM IscU, ,0.5 μM IscS, 400 μM $Fe(NH_4)_2(SO_4)_2$, and 100 μM cysteine. The reaction was initiated with 10 mM GSH. The formation of holo-IscU was studied using CD spectroscopy via monitoring ellipticity at 330 nm. 40 μM apo-Fdx was added using air-tight syringe after the level of holo-IscU saturated and the change in the CD signal was recorded.

Cluster transfer from Holo-IscU to apo-Fdx in presence of chaperones. Holo-IscU was assembled following the above procedure using 30 μM IscU, 0.5 μM IscS, 400 μM $Fe(NH_4)_2(SO_4)_2$, 100 μM cysteine and 10 mM GSH and monitored using CD spectroscopy. 40 μM apo-Fdx was then added to the reaction and the spectra was recorded. Next, 30 μM HscA and HscB and 3 mM MgATP followed by addition of 2 mM DTT using an-air tight syringe. The transfer of cluster from holo-IscU to apo-Fdx was detected

by the peak-shift to 355 nm from 330 nm which is characteristic of holo-IscU but has minimal contribution for holo-Fdx.

One pot cluster assembly on apo-Fdx in the presence of chaperones and DTT. The assay contained 20 μM IscU, 0.5 μM IscS, 40 μM Grx4, 400 μM $Fe(NH_4)_2(SO_4)_2$, 40 μM HscA, 40 μM HscB, 50 μM apo-Fdx and 100 μM cysteine and the reaction is initiated by the addition of 10 mM GSH and 3mM MgATP. Cluster formation on apo-Fdx was then measured by monitoring the ellipticity at 350 nm over time. The control reactions lacked chaperones and MgATP.

Cluster transfer reaction from Holo-Grx4 to apo-Fdx in presence of chaperones. Assay contained 30 μM holo-Grx4 (as isolated from *E.Coli*), 40 μM HscA and 40 μM HscB and 10 mM GSH. The reaction was initiated by addition of 40 μM apo-Fdx and 3 mM MgATP. The cluster transfer from holo-Grx4 to apo-Fdx was monitored by change in ellipticity at 315 nm.

CHAPTER VII

SUMMARY AND CONCLUSIONS

This work has been directed towards achieving a better understanding of the mechanism of iron-sulfur cluster biogenesis in the ISC pathway via in-vitro analysis. In particular, we first focused on re-examining the traditional *in vitro* iron-sulfur cluster assembly assays and re-optimized them to minimize off-path solution chemistry so that they selectively report on physiological processes. We also developed one-pot cluster-delivery assays on terminal apo-acceptors where the iron-sulfur clusters were assembled on scaffold protein followed by transfer to the intermediate carrier and then delivered to terminal targets. The assays were not biased in any way by using pre-isolated intermediates and hence were more likely to follow the physiological path and report more accurately on the effects of different components on the course of reaction. We then used these assays and other spectroscopic techniques to study the role of different proteins like CyaY, ISCU2(M106I), Grx4 and HscA-HscB in ISC pathway.

Dithiothreitol (DTT) has been traditionally used as an electron source for *in vitro* iron-sulfur cluster formation assays. DTT was used as an electron source for monitoring the cluster assembly on scaffold protein, ISCU2 in the presence of cysteine desulfurase complex, SD and allosteric activator, FXN but the nature of cluster formed had not been characterized. In chapter II, we used CD spectroscopy and observed that [4Fe-4S]-like clusters not bound to proteins were generated under this condition. These species were then characterized via Mössbauer spectroscopy as high Molecular Weight Species

(HMWS) with spectral character similar to mineral species like pyrites. We identified that DTT-mediated generation of sulfide from persulfide-cleavage and interception of other [2Fe-2S] cluster-intermediates were the primary pathways that led to the formation of HMWS. We re-optimized the assay condition using cysteine as our electron source and showed that the clusters generated under the assay condition are [2Fe-2S] bound to scaffold protein. Using this assay, we demonstrated that FXN that had been previously shown by our group to function as allosteric activator of cysteine desulfurase complex SD in presence of scaffold protein ISCU2 also accelerates the rate of cluster-assembly on ISCU2.

In chapter III, we aimed to study the role of CyaY in the process of iron-sulfur cluster biogenesis process. CyaY is known to inhibit the rate of iron-sulfur cluster assembly on ISCU2 whereas its eukaryotic homolog, FXN, functions as an allosteric activator of cysteine desulfurase. However, the mechanism of this inhibition is not yet known. Moreover, there have not been any studies conducted to test if the inhibitory effect of CyaY translates to a slower delivery of clusters on apo-proteins. Using stopped flow experiments, we demonstrated that CyaY inhibits the rate of cluster-formation on IscU by inhibiting the rate of persulfide transfer from IscS to IscU. We also used one-pot cluster formation assay to show that CyaY slows down the rate of cluster delivery on glutaredoxin. We confirmed the inhibition to be a downstream effect of slow cluster assembly on IscU by showing that CyaY has no effect on cluster transfer from holo-IscU to apo-Grx4 in a separate experiment.

Frtataxin (FXN) functions as an allosteric inhibitor of cysteine desulfurase. A genetic mutation that lowers expression of frataxin causes Friedreich's ataxia, a recessive autosomal disease that results in progressive damage to nervous system. An interesting breakthrough was made with the discovery that a point mutation on scaffold protein, ISCU2(M106I) could bypass the FXN deletion in yeast under in-vivo conditions. In chapter II, we demonstrated that FXN accelerates the cluster assembly on scaffold protein, ISCU2 by accelerating the sulfur transfer step but the molecular details were still not understood. The mechanistic understanding of the activation would facilitate rational drug design for Friedreich's ataxia. Evaluation of the effect of M106I mutation on ISCU2 under in-vitro conditions for human system would also contribute towards the same goal. In chapter IV, we studied the mechanism of FXN activation and FXN-bypass by ISCU2(M106I). Using a novel persulfide assay and stopped flow experiments, we demonstrated that FXN accelerates the formation of persulfide on cysteine desulfurase (NFS1) as well as sulfur transfer to ISCU2 by accelerating cys-aldimine formation and quinonoid decay respectively. Using CD spectroscopy, we carried out one-pot cluster assembly assays on GRX5 with FXN and ISCU2(M106I) respectively and found the rates to be comparable and hence confirmed ISCU2(M106I) can bypass FXN under in-vitro conditions for human system. We demonstrated that mechanism of FXN bypass to be accelerated rate of cluster transfer from holo-ISCU2 to GRX5 and concluded that ISCU2(M106I) and FXN activate different steps of cluster biogenesis, contrary to current model in literature. We further confirmed the observation using one-pot cluster delivery

assay on GRX5 in presence of both FXN and ISCU2(M106I) and found the rate to be higher than either for FXN or ISCU2(M106I) taken individually.

In chapter V, we studied the role of monothiol glutaredoxin in the process of cluster transfer using a combination of one-pot cluster assay and novel fluorescence quenching assay developed in our group. We were able to demonstrate that the cluster transfer from IscU to apo-Fdx was accelerated in the presence of Grx4 and show that Grx4 can act as an intermediate cluster carrier in cluster transfer from IscU to apo-acceptors like Fdx and HcaC with rate constants for transfer that proceed through Grx4 being comparable or larger than the rate constants for direct cluster transfer from IscU to apo-protein.

Chaperones accelerate the direct cluster transfer from IscU to Fdx in ATP-dependent manner. They are also shown to accelerate the cluster transfer from IscU to Grx4. In chapter VI, we tested if the chaperone-based direct cluster transfer from IscU to apo-Fdx is an alternative pathway to the glutaredoxin mediated cluster transfer that we observed in chapter V. We observed that the chaperone-dependent accelerated cluster transfer from IscU to apo-Fdx was DTT dependent and concluded that DTT acts as a mimic to glutaredoxin in that reaction. We demonstrated that the chaperone-accelerated cluster transfer rate from IscU to apo-Fdx is independent of DTT in presence of glutaredoxin. We also studied the effect of chaperones on cluster transfer steps downstream to that of glutaredoxin and observed that the rate of cluster transfer from holo-Grx4 to apo-Fdx is unchanged in the presence of chaperones. Hence, we conclude that the chaperone-based acceleration of cluster delivery to terminal apo-acceptors like Fdx is a result of faster cluster assembly on the intermediate cluster carrier, Grx4.

To conclude, in spite of all the recent discoveries made in the field of iron-sulfur cluster biosynthesis pathways, a lot of questions regarding the mechanism of cluster formation and transfer remain unanswered. In particular, there is very little known about the 4Fe-4S cluster synthesis and delivery pathways including the mechanism for partitioning of 2Fe-2S and 4Fe-4S cluster synthesis. Though, IscA had been shown to be able to bind 4Fe-4S cluster, the result needs re-evaluation in the light of recent findings. Further studies are also required to confirm the generality of monothiol glutaredoxins in the process of cluster transfer to various targets and its involvement, if any, in transfer of 4Fe-4S iron-sulfur clusters. It would also be interesting to study how IscR, transcriptional regulator of iron-sulfur cluster biosynthesis in mitochondria represses the cluster synthesis. A combination of different *in vivo* and *in vitro* techniques would be required to address these questions.

REFERENCES

1. Russell, M.J. *The alkaline solution to the emergence of life: energy, entropy and early evolution.* Acta Biotheoretica, 2007, **55**, 133-79.
2. Johnson, D.C.; Dean, D.R.; Johnson, M.K. *Structure, function, and formation of biological iron-sulfur clusters.* Annual Review of Biochemistry, 2005, **74**, 247-81.
3. Rouault, T.A. *Mammalian iron-sulphur proteins: novel insights into biogenesis and function.* Nature Reviews Molecular Cell Biology, 2015, **16**, 45-55.
4. Johnson, M.K. *Iron-sulfur proteins: new roles for old clusters.* Current Opinion in Chemical Biology, 1998, **2**, 173-81.
5. Fontecave, M. *Iron-sulfur clusters: ever-expanding roles.* Nature Chemical Biology, 2006, **2**, 171-74.
6. Brzoska, K.; Meczynska, S.; Kruszewski, M. *Iron-sulfur cluster proteins: electron transfer and beyond.* Acta Biochimica Polonica, 2006, **53**, 685-91.
7. Jacobson, M.R.; Brigel, K.E.; Bennet, L.T.; Setterquiest, R.A.; Wilson, M.A.; Cash, V.L.; Benyon, J.; Newton, W.E.; Dean, D.R. *Physical and genetic map of the major nif gene cluster from Azotobacter vinelandii.* Journal of Bacteriology, 1989, **171**, 1017-27.
8. Takahashi, Y.; Tokumoto, A. *A third bacterial system for the assembly of iron-sulfur clusters with homologs in archaea and plastids.* Journal of Biological Chemistry, 2002, **277**, 28380-83.

9. Lill, R.; Muhlenhoff, U. *Iron-sulfur protein biogenesis in eukaryotes: components and mechanisms.* Annual Review of Cell and Developmental Biology, 2006, 457-86.

10. Terauchi, K.; Kitayama, Y.; Nishiwaki, T.; Kumika, M.; Murayama, Y.; Oyama, T.; Kondo, T. *ATPase activity of KaiC determines the basic timing for circadian clock of cyanobacteria.* Proceedings of the National Academy of Science USA, 2007, **104**, 16377-81.

11. Boer, J.L.; Mulrooney, S.B.; Hausinger, R.P. *Nickel-dependent metalloenzymes.* Archives of Biochemistry and Biophysics, 2014, **544**, 142-52.

12. Spatzal, T.; Aksoyoglu, M.; Zhang, L.; Andrade, S.L.A.; Schleicher, E.; Weber, S.; Rees, D.C.; Einsle, O. *Evidence for interstitial carbon in nitrogenase FeMo cofactor.* Science, 2011, **334**, 940.

13. Bruschi, M.; Guerlesquin, F. *Structure, function and evolution of bacterial ferredoxins.* FEMS Microbiology Reviews, 1988, **4**, 155-75.

14. Shisler, K.A.; Broderick, J.B. *Emerging themes in radical SAM chemistry.* Current Opinion in Structural Biology, 2012, **22**, 701-10.

15. Crack, J.C.; Hutchings, M.I.; Thomson, M.J.; Le Brun, N.E. *Bacterial iron–sulfur regulatory proteins as biological sensor-switches.* Antioxidants and Redox Signaling, 2012, **17**, 1215-31.

16. Rudolf, J.; Makrantoni, V.; Ingledew, W.J.; Stark, M.J.; White, M.F. *The DNA repair helicases XPD and FancJ have essential iron-sulfur domains.* Molecular Cell, 2006, **23**, 801-8.

17. Meyer, J. *Iron-sulfur protein folds, iron-sulfur chemistry, and evolution.* Journal of Biological Inorganic Chemistry, 2008, **13**, 157-70.

18. Rickard, D.; Luther, G.W. *Chemistry of iron sulfides.* Chemical Reviews, 2007, **107**, 514-62.

19. Kabil, O.; Vitvitsky, V.; Banerjee, R. *Sulfur as a signaling nutrient through hydrogen sulfide.* Annual Review of Nutrition, 2014, **34**, 171-205.

20. Sheftel, A.D.; Lill, R. *The power plant of the cell is also a smithy: the emerging role of mitochondria in cellular iron homeostasis.* Annals of Medicine, 2009, **41**, 82-99.

21. Zheng, L.; Cash, V.L.; Flint, D.H; Dean, D.R. *Assembly of iron-sulfur clusters: identification of an iscSUA-hscBA-fdx gene cluster from Azotobacter vinelandii.* Journal of Biological Chemistry, 1998, **273**, 13264-72.

22. Rouault, T.A.; Tong, W.H. *Iron-sulfur cluster biogenesis and human disease.* Trends in Genetics, 2008, **24**, 398-407.

23. Agar, J.N.; Krebs, C.; Frazzon, J.; Huynh, B.H.; Dean, D.R.; Johnson, M.K. *IscU as a scaffold for iron-sulfur cluster biosynthesis: sequential assembly of [2Fe-2S] and [4Fe-4S] clusters in IscU.* Biochemistry, 2000, **39**, 7856-62.

24. Kim, J.H. *[2Fe-2S]-Ferredoxin binds directly to cysteine desulfurase.* Journal of American Chemical Society, 2013, **135**, 8117-20.

25. Ding, H.; Clark, R.J.; Ding, B. *IscA mediates iron delivery for assembly of iron-sulfur clusters in IscU under the limited accessible free iron conditions.* Journal of Biological Chemistry, 2004, **279**, 37499-504.

26. Bonomi, F.; Lametti, S.; Morleo, A.; Ta, D.; Vickery, L.A. *Studies on the mechanism of catalysis of iron-sulfur cluster transfer from IscU[2Fe2S] by HscA/HscB chaperones.* Biochemistry, 2008, **47**, 12795-801.

27. Mettert, E.L.; Kiley, P.J. *Coordinate regulation of the Suf and Isc Fe-S cluster biogenesis pathways by IscR is essential for viability of Escherichia coli.* Journal of Bacteriology, 2014, **196**, 4315-23.

28. Kim, J.H.; Bothe, J.R.; Frederick, R.O.; Holder, J.C.; Markley, J.L. *Role of IscX in iron-sulfur cluster biogenesis in Escherichia coli.* Journal of American Chemical Society, 2014, **136**, 7933-42.

29. Pastore, C.; Adinolfi, S.; Huynen, M.A.; Rybin, V.; Martin, S.; Meyer, M.; Bukao, B.; Pastore, A. *YfhJ, a molecular adaptor in iron-sulfur cluster formation or a frataxin-like protein?* Structure, 2006, **14**, 857-67.

30. Couturier, J.; Przbyla-Toscano, J.; Roret, T.; Didierjean, C.; Rouhier, N. *The roles of glutaredoxins ligating Fe-S clusters: sensing, transfer or repair functions?* Biochimica et Biophysica Acta, 2015, **1853**, 1513-27.

31. Tsai, C.L.; Barondeau, D.P. *Human frataxin is an allosteric switch that activates the Fe-S cluster biosynthetic complex.* Biochemistry, 2010, **49**, 9132-39.

32. Urbina, H.D.; Silberg, J.J.; Hoff, K.G.; Vickery, L.E. *Transfer of sulfur from IscS to IscU during Fe/S cluster assembly.* Jounal of Biological Chemistry, 2001, **276**, 44521-26.

33. Bridwell-Rabb, J.; Fox, N.G.; Tsai, C.L.; Winn, A.M.; Barondeau, P. *Human frataxin activates Fe-S cluster biosynthesis by facilitating sulfur transfer chemistry.* Biochemistry, 2014, **53**, 4904-13.

34. Bonomi, F.; Lametti, S.; Morleo, A.; Ta, D.; Vickery, L.A. *Facilitated transfer of IscU-[2Fe2S] clusters by chaperone-mediated ligand exchange.* Biochemistry, 2011, **50**, 9641-50.

35. Shimomura, Y.; Wada, K.; Fukuyama, K.; Takahashi, Y. *The asymmetric trimeric architecture of [2Fe-2S] IscU: implications for its scaffolding during iron-sulfur cluster biosynthesis.* Journal of Molecular Biology, 2008, **383**, 133-43.

36. Marinoni, E.N.; de Oliveira, J.S.; Nicolet, Y.; Raulfs, E.C.; Amara, P.; Dean, D.R.; Fontecilla-Camps, J.C. *(IscS-IscU)2 complex structures provide insights into Fe2S2 biogenesis and transfer.* Angewandte Chemie International Edition England, 2012, **51**, 5439-42.

37. Mayer, M.P.; Bukau, B. *Hsp70 chaperones: cellular functions and molecular mechanism.* Cellular and Molecular Life Sciences, 2005, **62**, 670-84.

38. Hoff, K.G., Cupp-Vickery, J.R.; Vickery, L.E. *Contributions of the LPPVK motif of the iron-sulfur template protein IscU to interactions with the Hsc66-Hsc20 chaperone system.* Jounal of Biological Chemistry, 2003, **278**, 37582-9.

39. Hoff, K.G.; Silberg, J.J.; Vickery, L.E. *Interaction of the iron-sulfur cluster assembly protein IscU with the Hsc66/Hsc20 molecular chaperone system of Escherichia coli.* Proceedings of the National Academy of Science USA, 2000, **97**, 7790-5.

40. Rouhier, N.; Couturier, J.; Johnson, M.K.; Jacquot, J.P. *Glutaredoxins: roles in iron homeostasis.* Trends in Biochemical Sciences, 2010, **35**, 43-52.

41. Zhang, B.; Bandyopadhyay, S.; Shakamuri, P.; Naik, S.G.; Huynh, B.H.; Couturier, J.; Rouhier, N.; Johnson, M.K. *Monothiol glutaredoxins can bind linear [Fe3S4]+ and [Fe4S4]2+ clusters in addition to [Fe2S2]2+ clusters: spectroscopic characterization and functional implications.* Journal of American Chemical Society, 2013, **135**, 15153-64.

42. Schmucker, S.; Puccio, H. *Understanding the molecular mechanisms of Friedreich's ataxia to develop therapeutic approaches.* Human Molecular Genetics, 2010, **19**, 103-10.

43. Bulteau, A.L.; O'neill, H.A.; Kennedy, M.C.; Ikeda-Saito, M.; Isaya, G.; Szweda, L.I. *Frataxin acts as an iron chaperone protein to modulate mitochondrial aconitase activity.* Science, 2004, **305**, 242-45.

44. Zhang, Y.; Lyver, E.R.; Knight, S.A.; Pain, D.; Lessuisse, E.; Dancis, A. *Mrs3p, Mrs4p, and frataxin provide iron for Fe-S cluster synthesis in mitochondria.* Journal of Biological Chemistry, 2006. **281**, 22493-502.

45. Gakh, O.; Park, S.; Liu, G.; Macomber, L.; Imlay, J.A.; Ferreira, G.C.; Isaya, G. *Mitochondrial iron detoxification is a primary function of frataxin that limits oxidative damage and preserves cell longevity.* Human Molecular Genetics, 2006, **15**, 467-79.

46. Bridwell-Rabb, J.; Ianuzzi, C.; Pastore, A.; Barondeau, P. *Effector role reversal during evolution: the case of frataxin in Fe-S cluster biosynthesis.* Biochemistry, 2012, **51**, 2506-14.

47. Adam, A.C.; Börnhovd, C.; Prokisch, H.; Neupert, W.; Hell, K. *The Nfs1 interacting protein Isd11 has an essential role in Fe/S cluster biogenesis in mitochondria.* Europian Molecular Biology Organization Journal, 2006, **25**, 174-83.

48. Cupp-Vickery, J.R.; Urbina, H.; Vickery, L.E. *Crystal structure of IscS, a cysteine desulfurase from Escherichia coli.* Journal of Molecular Biology, 2003, **330**, 1049-59.

49. Cory, S.A.; Vranken, J.G.V.; Brignole, E.J.; Patra, S.; Winge, D.R.; Drennan, C.L.; Rutter, J.; Barondeau, P. *Structure of human Fe-S assembly subcomplex reveals unexpected cysteine desulfurase architecture and acyl-ACP-ISD11 interactions.* Proceedings of the National Academy of Science USA, 2017, **114**, 5325-34.

50. Shakamuri, P.; Zhang, B.; Johnson, M.K. *Monothiol glutaredoxins function in storing and transporting [Fe2S2] clusters assembled on IscU scaffold proteins.* Journal of American Chemical Society, 2012, **134**, 15213-6.

51. Wang, L.; Ouyang, B.; Li, Y.; Feng, Y.; Jacquot, J.P.; Rouhier, N.; Xia, B. *Glutathione regulates the transfer of iron-sulfur cluster from monothiol and dithiol glutaredoxins to apo ferredoxin.* Protein Cell, 2012, **3**, 714-21.

52. Li, H.; Mapolelo, D.T.; Randeniya, S.; Johnson, M.K.; Outten, C.E. *Human glutaredoxin 3 forms [2Fe-2S]-bridged complexes with human BolA2.* Biochemistry, 2012, **51**,1687-96.

53. Yeung, N.; Gold, B.; Liu, N.L.; Prathapam, R.; Sterling, H.J.; Williams, E.R.; Butland, G. *The E. coli monothiol glutaredoxin GrxD forms homodimeric and heterodimeric FeS cluster containing complexes.* Biochemistry, 2011, **50**, 8957-69.

54. Willems, P.; Wanschers, B.F.; Esseling, J.; Szklarczyk, R.; Kudla, U.; Duarte, I.; Forkink, M.; Nooteboom, M.; Swarts, H.; Gloerich, J.; Nijtmans, L.; Koopman, W.; Huynen, M.A. *BOLA1 is an aerobic protein that prevents mitochondrial morphology changes induced by glutathione depletion.* Antioxidants and Redox Signaling, 2013, **18**, 129-38.

55. Poor, C.B.; Wgner, S.V.; Haoran, L.; Dlouhy, A.C.; Schuermann, J.P.; Sanishvili, R.; Hinshaw, J.R.; Riggs-Gelasco, P.J.; Outten, C.E.; He, C. *Molecular mechanism and structure of the Saccharomyces cerevisiae iron regulator Aft2.* Proceedings of the National Academy of Science USA, 2014, **111**, 4043-48.

56. Mapolelo, D.T.; Zhang, B.; Naik, S.G.; Huynh, B.H.; Johnson, M.K. *Spectroscopic and functional characterization of iron-sulfur cluster-bound forms of Azotobacter vinelandii (Nif)IscA.* Biochemistry, 2012, **51**, 8071-84.

57. Mapolelo, D.T.; Zhang, B.; Randeniya, S.; Albetel, A.N.; Li, H.; Couturier, J.; Outten, C.E.; Rouhier, N.; Johnson, M.K. *Monothiol glutaredoxins and A-type*

proteins: partners in Fe-S cluster trafficking. Dalton Transactions, 2013, **42**, 3107-15.

58. Tan, G.; Lu, J.; Bitoun, J.P.; Huang, H.; Ding, H. *IscA/SufA paralogues are required for the [4Fe-4S] cluster assembly in enzymes of multiple physiological pathways in Escherichia coli under aerobic growth conditions.* Biochemical Journal, 2009, **420**, 463-72.

59. Muhlenhoff, U.; Richter, N.; Pines, O.; Pierik, A.J.; Lill, R. *Specialized function of yeast Isa1 and Isa2 proteins in the maturation of mitochondrial [4Fe-4S] proteins.* Journal of Biological Chemistry, 2011, **286**, 41205-16.

60. Maio, N.; Singh, A.; Uhrigshardt, H.; Saxena, N.; Tong, W.H.; Rouault, T.A. *Cochaperone binding to LYR motifs confers specificity of iron sulfur cluster delivery.* Cell Metabolism, 2014, **19**, 445-57.

61. Iametti, S.; Barbiroli, A.; Bonomi, F. *Functional implications of the interaction between HscB and IscU in the biosynthesis of FeS clusters.* Journal of Biological Inorganic Chemistry, 2015, **20**, 1039-48.

62. Majewska, J.; Ciesielski, S.J.; Schilke, B.; Kominek, J.; Blenska, A.; Delewski, W.; Song, J.; Marszalek, J.; Craig, E.; Dutkiewicz, R. *Binding of the chaperone Jac1 protein and cysteine desulfurase Nfs1 to the iron-sulfur cluster scaffold Isu protein is mutually exclusive.* Journal of Biological Chemistry, 2013, **288**, 29134-42.

63. Puglisi, R.; Yan, R.; Adinolfi, S.; Pastore, A. *A new tessera into the interactome of the isc operon: a movel interaction between HscB and IscS.* Frontiers in Molecular Biosciences, 2016, **3**, 48.

64. Uzarska, M.A.; Dutkiewicz, R.; Freibert, S.A.; Lill, R.; Muhlenhoff, U. *The mitochondrial Hsp70 chaperone Ssq1 facilitates Fe/S cluster transfer from Isu1 to Grx5 by complex formation.* Molecular Biology of the Cell, 2013, **24**, 1830-41.

65. Reyda, M.R.; Fugate, C.J.; Jarrett, J.T. *A complex between biotin synthase and the iron-sulfur cluster assembly chaperone HscA that enhances in vivo cluster assembly.* Biochemistry, 2009, **48**, 10782-92.

66. Vranish, J.N.; Russell, W.K.; Yu, L.E.; Cox, R.M.; Russell, D.H.; Barondeau, P. *Fluorescent probes for tracking the transfer of iron-sulfur cluster and other metal cofactors in biosynthetic reaction pathways.* Journal of American Chemical Society, 2015, **137**, 390-98.

67. Johnson, D.C.; Unciuleac, M.C.; Dean, D.R. *Controlled expression and functional analysis of iron-sulfur cluster biosynthetic components within Azotobacter vinelandii.* Journal of Bacteriology, 2006, **188**, 7551-61.

68. Lill, R. *Function and biogenesis of iron-sulphur proteins.* Nature, 2009, **460**, 831-38.

69. Lill, R.; Muhlenhoff, U. *Maturation of iron-sulfur proteins in eukaryotes: mechanisms, connected processes, and diseases.* Annual Review of Biochemistry, 2008, **77**, 669-700.

70. Sheftel, A.; Stehling, O.; Lill, R. *Iron-sulfur proteins in health and disease.* Trends in Endocrinology & Metabolism, 2010, **21**, 302-14.

71. Beinert, H.; Holm, R.H.; Munck, E. *Iron-sulfur clusters: nature's modular, multipurpose structures.* Science, 1997, **277**, 653-59.

72. Fox, N.G.; Chakrabarti, M.; McCormick, S.; Lindahl, P.; Barondeau, D.P. *The human iron-sulfur assembly complex catalyzes the synthesis of [2Fe-2S] clusters on ISCU2 that can be transferred to acceptor molecules.* Biochemistry, 2015, **54**, 3871-9.

73. Zheng, L.; White, R.H.; Cash, V.L.; Dean, D.R. *Mechanism for the desulfurization of L-cysteine catalyzed by the nifS gene product.* Biochemistry, 1994, **33**, 4714-20.

74. Behshad, E.; Bollinger, J.M. *Kinetic analysis of cysteine desulfurase CD0387 from Synechocystis sp. PCC 6803: formation of the persulfide intermediate.* Biochemistry, 2009, **48**, 12014-23.

75. Behshad, E.; Parkin, S.E.; Bollinger, J.M. *Mechanism of cysteine desulfurase Slr0387 from Synechocystis sp. PCC 6803: kinetic analysis of cleavage of the persulfide intermediate by chemical reductants.* Biochemistry, 2004, **43**, 12220-26.

76. Schmucker, S.; Martelli, A.; Colin F.; Page, A.; Wattenhoffer-Donzzè, M.; Reutenauer, L.; Puccio, H. *Mammalian frataxin: an essential function for cellular viability through an interaction with a preformed ISCU/NFS1/ISD11 iron-sulfur assembly complex.* Public Library of Science One, 2011, **6**, 16199.

77. Wiedemann, N.; Urzica, E.; Gulard, B.; Mùller, H.; Lohaus, C.; Meyer, H.E.; Ryan, M.T.; et al. *Essential role of Isd11 in mitochondrial iron-sulfur cluster synthesis on Isu scaffold proteins.* European Molecular Biology Organization Journal, 2006, **25**, 184-95.

78. Shi, Y.; Ghosh, M.; Kovtunovych, G.; Crooks, D.R.; Rouault, T.A. *Both human ferredoxins 1 and 2 and ferredoxin reductase are important for iron-sulfur cluster biogenesis.* Biochimica et Biophysica Acta, 2012, **1823**, 484-92.

79. Sheftel, A.D.; Stehling, O.; Pierik, A.J.; Elsässer, H.P.; Muhlenhoff, U.; Webert, H.; Hobler, A.; Hannemann, F.; Bernhardt, R.; Lill, R. *Humans possess two mitochondrial ferredoxins, Fdx1 and Fdx2, with distinct roles in stroidogenesis, heme, and Fe/S cluster biosynthesis.* Proceedings of the National Academy of Science USA, 2010, **107**, 11775-80.

80. Webert, H.; Freibert, S.; Gallo, A.; Heidenreich, T.; Linne, U.; Amlacher, S.; Hurt, E.; Muhlenhoff, U.; Banci, L.; Lill, R. *Functional reconstitution of mitochondrial Fe/S cluster synthesis on Isu1 reveals the involvement of ferredoxin.* Nature Communications, 2014, **5**, 5013, 6013-23.

81. Vickery, L.E.; Cupp-Vickery, J.R. *Molecular chaperones HscA/Ssq1 and HscB/Jac1 and their roles in iron-sulfur protein maturation.* Critical Reviews in Biochemistry and Molecular Biology, 2007, **42**, 95-111.

82. Chandramouli, K.; Johnson, M.K. *HscA and HscB stimulate [2Fe-2S] cluster transfer from IscU to apoferredoxin in an ATP-dependent reaction.* Biochemistry, 2006, **45**, 11087-95.

83. Campuzano, V.; Montermini, L.; Moltó, M.D.; Pianese, L.; Cossèe, M.; et al. *Friedreich's atxia: autosomal recessive disease caused by an intronic GAA triplet repeat expansion.* Science, 1996, **271**, 1423-7.

84. Yoon, T.; Cowan, J.A. *Iron-sulfur cluster biosynthesis:.characterization of frataxin as an iron donor for assembly of [2Fe-2S] clusters in ISU-type proteins.* Journal of American Chemical Society, 2003, **125**, 6078-84.

85. Kondapalli, K.C.; Kok, N.M.; Dancis, A.; Stemmler, T.A. *Drosophila frataxin: an iron chaperone during cellular Fe-S cluster bioassembly.* Biochemistry, 2008, **47**, 6917-27.

86. Pandey, A.; Yoon, H.; Lyver, E.R.; Dancis, A.; Pain, D. *Identification of a Nfs1p-bound persulfide intermediate in Fe-S cluster synthesis by intact mitochondria.* Mitochondrion, 2012, **12**, 539-49.

87. Tsai, C.L.; Bridwell-Rabb, J.; Barondeau D.P. *Friedreich's ataxia variants I154F and W155R diminish frataxin-based activation of the iron-sulfur cluster assembly complex.* Biochemistry, 2011, **50**, 6478-87.

88. Colin, F.; Martelli, A.; Clèmancey, M.; Latour, J.; Gambarelli, S.; Zepierri, L.; Birck, C.; Page, A.; Puccio, H.; de Choudens, S.O. *Mammalian frataxin controls sulfur production and iron entry during de novo Fe4S4 cluster assembly.* Journal of American Chemical Society, 2013, **135**, 733-40.

89. Adinolfi, S.; Iannuzzi, C.; Prischi, F.; Pastore, C.; Iametti, S.; Martin, S.R.; Bonomi, F.; Pastore, A. *Bacterial frataxin CyaY is the gatekeeper of iron-sulfur*

cluster formation catalyzed by IscS. Nature Structural and Molecular Biology, 2009, **16**, 390-96.

90. Kim, J.H.; Tonelli, M.; Markley, J.L. *Disordered form of the scaffold protein IscU is the substrate for iron-sulfur cluster assembly on cysteine desulfurase.* Proceedings of the National Academy of Science USA, 2012, **109**, 454-59.

91. Huang, J.; Cowan, J.A. *Iron-sulfur cluster biosynthesis: role of a semi-conserved histidine.* Chemical Communications (Cambridge), 2009, **21**, 3071-73.

92. Gao, H.; Subramanian, S.; Couturier, J.; Naik, S.G.; Kim, S.; Leustek, T.; Knaff, D.B.; et al. *Arabidopsis thaliana Nfu2 accommodates [2Fe-2S] or [4Fe-4S] clusters and is competent for in vitro maturation of chloroplast [2Fe-2S] and [4Fe-4S] cluster-containing proteins.* Biochemistry, 2013, **52**, 6633-45.

93. Mansy, S.S.; Wu, G.; Sureus, K.K.; Cowan, J.A. *Iron-sulfur cluster biosynthesis. Thermatoga maritima IscU is a structured iron-sulfur cluster assembly protein.* Journal of Biological Chemistry, 2002, **27,** 21397-404.

94. Ryle, M.J.; Lanzilotta, W.N.; Seefeldt, L.C.; Scarrow, R.C.; Jensen, G.M. *Circular dichroism and x-ray spectroscopies of Azotobacter vinelandii nitrogenase iron protein. MgATP and MgADP induced protein conformational changes affecting the [4Fe-4S] cluster and characterization of a [2Fe-2S] form.* Journal of Biological Chemistry, 1996, **271**, 1551-57.

95. Qi, W.; Li, J.; Chain, C.Y.; Pasquevich, G.A.; Pasquevich, A.F.; Cowan, J.A. *Glutathione complexed Fe-S centers.* Journal of American Chemical Society, 2012, **134**, 10745-48.

96. Lanz, N.D.; Grove, T.L.; Gogonea, C.B.; Lee, K.; Krebs, C.; Booker, S.J. *RlmN and AtsB as models for the overproduction and characterization of radical SAM proteins.* Methods in Enzymology, 2012, **516**, 125-52.

97. Que, L.; Holm, R.H.; Mortenson, L.E. *Letter: extrusion of Fe2S2 and Fe4S4 cores from the active sites of ferredoxin proteins.* Journal of American Chemical Society, 1975, **97**, 463-64.

98. Pandey, A.; Gordon, D.M.; Pain, J.; Stemmler, T.L.; Dancis, A.; Pain D. *Frataxin directly stimulates mitochondrial cysteine desulfurase by exposing substrate-binding sites, and a mutant Fe-S cluster scaffold protein with frataxin-bypassing ability acts similarly.* Journal of Biological Chemistry, 2013, **288**, 36773-86.

99. Marelja, Z.; Stöcklein, W.; Nimtz, M.; Leimkühler, S. *A novel role for human Nfs1 in the cytoplasm: Nfs1 acts as a sulfur donor for MOCS3, a protein involved in molybdenum cofactor biosynthesis.* Journal of Biological Chemistry, 2008, **283**, 25178-85.

100. Siegel, L.M. *A direct microdetermination for sulfide.* Analytical Biochemistry, 1965, **11**, 126-32.

101. Fish, W.W. *Rapid colorimetric micromethod for the quantitation of complexed iron in biological samples.* Methods in Enzymology, 1988, **158**, 357-64.

102. Stookey, L.L. *Ferrozine-a new spectrophotometric reagent for iron.* Analytical Chemistry, 1970, **42**, 779-781.

103. Cowart, R.E.; Singleton, F.L.; Hind, J.S. *A comparison of bathophenanthrolinedisulfonic acid and ferrozine as chelators of iron(II) in reduction reactions.* Analytical Biochemistry, 1993, **211**, 151-55.

104. Py, B.; Barras, F. *Building Fe-S proteins: bacterial strategies.* Nature Reviews Microbiology, 2010, **8**, 436-46.

105. Jacobson, M.R.; Brigle, K.E.; Benett, L.T.; Setterquist, R.A.; Wilson, M.S.; Cash, V.L.; Beynon, J.; Newton, W.E.; Dean, D.R. *Physical and genetic-map of the major nif gene-cluster from Azotobacter-Vinelandii.* Journal of Bacteriology, 1989, **171**, 1017-1027.

106. Jacobson, M.R.; Cash, V.L.; Weiss, M.C.; Laird, N.F.; Newton, W.E.; Dean, D.R. *Biochemical and genetic-analysis of the Nifusvwzm cluster from Azotobacter-Vinelandii.* Molecular & General Genetics, 1989, **219**, 49-57.

107. Zheng, L.M.; Cash, V.L.; Flint, D.H.; Dean, D.R. *Assembly of iron-sulfur clusters - identification of an iscSUA-hscBA-fdx gene cluster from Azotobacter vinelandii.* Journal of Biological Chemistry, 1998, **273**, 13264-72.

108. Takahashi, Y.; Nakamura, M. *Functional assignment of the ORF2-iscS-iscU-iscA-hscB-hscA-fdx-ORF3 gene cluster involved in the assembly of Fe-S clusters in Escherichia coli.* Journal of Biochemistry, 1999, **126**, 917-26.

109. Tokumoto, U.; Takahashi, Y. *Genetic analysis of the isc operon in Escherichia coli involved in the biogenesis of cellular iron-sulfur protein.* Journal of Biochemistry, 2001, **130**, 63-71.

110. Takahashi, Y.; Tokumoto, U. *A third bacterial system for the assembly of iron-sulfur clusters with homologs in archaea and plastids.* Journal of Biological Chemistry, 2002, **277**, 28380-83.

111. Outten, F.W.; Djaman, O.; Storz, G. *A suf operon requirement for Fe-S cluster assembly during iron starvation in Escherichia coli.* Molecular Microbiology, 2004, **52**, 861-72.

112. Schwartz, C.J.; Djaman, O.; Imlay, J.A.; Kiley, P.J. *The cysteine desulfurase, IscS, has a major role in in vivo Fe-S cluster formation in Escherichia coli.* Proceedings of the National Academy of Sciences USA, 2000, **97**, 9009-14.

113. Agar, J.N.; Zheng, L.; Cash, V.L.; Dean, D.R.; Johnson, M.K. *Role of the IscU protein in iron-sulfur cluster biosynthesis: IscS-mediated assembly of a [Fe2S2] cluster in IscU.* Journal of the American Chemical Society, 2000, **122**, 2136-37.

114. Krebs, C.; Agar J.N.; Smith, A.D.; Frazzon, J.; Dean, D.R.; Huynh, B.H.; Johnson M.K. *IscA, an alternate scaffold for Fe-S cluster biosynthesis.* Biochemistry, 2001, **40**, 14069-80.

115. Yang, J.; Bitoun, J.P.; Ding, H. *Interplay of IscA and IscU in biogenesis of iron-sulfur clusters.* Journal of Biological Chemistry, 2006, **281**, 27956-63.

116. Ding, H.; Yang, J.; Coleman, L.C.; Yeung, S. *Distinct iron binding property of two putative iron donors for the iron-sulfur cluster assembly: IscA and the bacterial frataxin ortholog CyaY under physiological and oxidative stress conditions.* Journal of Biological Chemistry, 2007, **282**, 7997-8004.

117. Kim, J.H.; Fùzèry, A.K.; Tonelli, M.; Ta, D.T.; Westler, W.M.; Vickery, L.E.; Markley, J.L. *Structure and dynamics of the iron-sulfur cluster assembly scaffold protein IscU and its interaction with the cochaperone HscB.* Biochemistry, 2009, **48**, 6062-71.

118. Kim, J.H.; Tonelli, M.; Frederick, R.O.; Chow, D.C.F.; Markley, J.L. *Specialized Hsp70 chaperone (HscA) binds preferentially to the disordered form, whereas J-protein (HscB) binds preferentially to the structured form of the iron-sulfur cluster scaffold protein (IscU).* Journal of Biological Chemistry, 2012, **287**, 31406-13.

119. Knoell, H.E.; Knappe, J. *Escherichia coli ferredoxin, an iron-sulfur protein of the adrenodoxin type.* European Journal of Biochemistry, 1974, **50**, 245-52.

120. Yan, R.; Adinolfi, S.; Pastore, A. *Ferredoxin, in conjunction with NADPH and ferredoxin-NADP reductase, transfers electrons to the IscS/IscU complex to promote iron-sulfur cluster assembly.* Biochimica Et Biophysica Acta-Proteins and Proteomics, 2015, **1854**, 1113-17.

121. Roche, B.; Huguenot, A.; Barras, F.; Py, B. *The iron-binding CyaY and IscX proteins assist the ISC-catalyzed Fe-S biogenesis in Escherichia coli.* Molecular Microbiology, 2015, **95**, 605-23.

122. Campuzano, V.; Montermini, L.; Moltó, M D.; Pianese, L.; Cossèe, M.; Cavalcanti, F. *Friedreich's ataxia: autosomal recessive disease caused by an intronic GAA triplet repeat expansion.* Science, 1996, **271**, 1423-1427.

123. Filla, A.; de Michele, G.; Cavalcanti, F.; Pianese, L.; Montecelli, A.; Campanella, G.; Cocozza, S. *The relationship between trinucleotide (GAA) repeat length and*

clinical features in friedreich ataxia. American Journal of Human Genetics, 1996, **59**, 554-60.

124. Durr, A.; Cossee, M.; Agid, Y.; Campuzano, V.; Mignard, C.; Penet, C.; Mandel, J.C.; Brice, A.; Koenig, M. *Clinical and genetic abnormalities in patients with Friedreich's ataxia.* New England Journal of Medicine, 1996, **335**, 1169-75.

125. Babcock, M.; de Silva, D.; Oaks, R.; Davis-Kaplan, S.; Jiralerspong, S.; Montermini, L.; Pandolfo, M.; Kaplan, J. *Regulation of mitochondrial iron accumulation by Yfh1p, a putative homolog of frataxin.* Science, 1997, **276**, 1709-12.

126. Rotig, A.; de Lonlay, P.; Cheretien, D.; Foury, F.; Koenig, M.; Sidi, D.; Munnich, A.; Rustin, P. *Aconitase and mitochondrial iron-sulphur protein deficiency in Friedreich ataxia.* Nature Genetics, 1997, **17**, 215-17.

127. Li, D.S.; Ohshima, K.; Jiralerspong, S.; Bojanowski, M.W.; Pandolfo, M. *Knock-out of the cyaY gene in Escherichia coli does not affect cellular iron content and sensitivity to oxidants.* Federation of European Biochemical Societies Letters, 1999, **456**, 13-26.

128. Vivas, E.; Skovran, E.; Downs, D.M. *Salmonella enterica strains lacking the frataxin homolog CyaY show defects in Fe-S cluster metabolism in vivo.* Journal of Bacteriology, 2006, **188**, 1175-79.

129. Pohl, T.; Walter, J.; Stolpe, S.; Soufo, J.H.D.; Grauman, P.L.; Friedrich, T. *Effects of the deletion of the Escherichia coli frataxin homologue CyaY on the respiratory NADH:ubiquinone oxidoreductase.* BMC Biochemistry, 2007, **8**, 13-23.

130. Roche, B.; Agrebei, R.; Huguenot, A.; de Choudens, S.O.; Barras, F.; Py, B. *Turning Escherichia coli into a Frataxin-Dependent Organism.* PLOS Genetics, 2015, **11**, 1005314-36.

131. Iannuzzi, C.; Adinolfi, S.; Howes, B.D.; Garcia-Ferres, R.; Clèmancey, M.; Latour, J.; Smulevich, G.; Pastore, A. *The role of CyaY in iron sulfur cluster assembly on the E. coli IscU scaffold protein.* PLOS One, 2011, **6**, 21992.

132. di Maio, D.; Chandramouli, B.; Yan, R.; Brancato, G.; Pastore, A. *Understanding the role of dynamics in the iron sulfur cluster molecular machine.* Biochimica Et Biophysica Acta-General Subjects, 2017, **1861**, 3154-63.

133. Skovran, E.; Lauhon, C.T.; Downs, D.M. *Lack of YggX results in chronic oxidative stress and uncovers subtle defects in Fe-S cluster metabolism in Salmonella enterica.* Journal of Bacteriology, 2004, **186**, 7626-34.

134. Gralnick, J.A.; Downs, D.M. *The YggX protein of Salmonella enterica is involved in Fe(II) trafficking and minimizes the DNA damage caused by hydroxyl radicals - Residue Cys-7 is essential for YggX function.* Journal of Biological Chemistry, 2003, **278**, 20708-15.

135. Boyd, J.M.; Lewis, J.A.; Escalante-Semerena, J.C.; Downs, D.M. *Salmonella enterica requires apbC function for growth on tricarballylate: evidence of functional redundancy between apbC and iscU.* Journal of Bacteriology, 2008, **190**, 4596-602.

136. Boyd, J.M.; Pierik, P.; Netz, D.J.A.; Lill, R.; Downs, D.M. *Bacterial ApbC can bind and effectively transfer iron-sulfur clusters.* Biochemistry, 2008, **47**, 8195-202.

137. Boyd, J.M.; Drevland, R.M.; Downs, D.M.; Graham, D.E. *Archaeal ApbC/Nbp35 homologs function as iron-sulfur cluster carrier proteins.* Journal of Bacteriology, 2009, **191**, 1490-97.

138. Boyd, J.M.; Sondelski, J.L.; Downs, D.M. *Bacterial ApbC protein has two biochemical activities that are required for in vivo function.* Journal of Biological Chemistry, 2009, **284**, 110-18.

139. Kim, S.H.; Lee, B.Y.; Lau, G.W.; Cho, Y.H. *IscR modulates catalase A (KatA) activity, peroxide resistance, and full virulence of Pseudomonas aeruginosa PA14.* Journal of Microbiology and Biotechnology, 2009, **19**, 1520-26.

140. Yoon, H.; Golla, R.; Lesuisse, E.; Pain, J.; Donald, J.E.; Lyver, E.R.; Pain, D.; Dancis, A. *Mutation in the Fe-S scaffold protein Isu bypasses frataxin deletion.* Biochemical Journal, 2012, **441**, 473-80.

141. Yoon, H.; Knight, S.A.B.; Pandey, A.; Pain, J.; Turkarslan, S.; Pain, D.; Dancis, A. *Turning Saccharomyces cerevisiae into a frataxin-independent organism.* PLOS Genetics, 2015, **11**, 1005135-53

142. Vranish, J.N.; Das, D.; Barondeau, D.P. *Real-time kinetic probes support monothiol glutaredoxins as intermediate carriers in Fe-S cluster biosynthetic pathways.* American Chemical Society Chemical Biology, 2016, **11**, 3114-21.

143. Van Vranken, J.G.; Jeong, M.Y.; Wei, P.; Chen, Y.C.; Gygi, S.P.; Winge, D.R.; Rutter, J. *The mitochondrial acyl carrier protein (ACP) coordinates mitochondrial fatty acid synthesis with iron sulfur cluster biogenesis.* Elife, 2016, **5**, 17828-38

144. Shi, Y.; Ghosh, M.C.; Tong, W.; Rouault, T.A. *Human ISD11 is essential for both iron-sulfur cluster assembly and maintenance of normal cellular iron homeostasis.* Human Molecular Genetics, 2009, **18**, 3014-25.

145. Terali, K.; Beavill, R.L.; Pickersgill, R.W.; van der Giazen, M. *The effect of the adaptor protein Isd11 on the quaternary structure of the eukaryotic cysteine desulphurase Nfs1.* Biochemical and Biophysical Research Communications, 2013, **440**, 235-40.

146. Stehling, O.; Elsasser, H.P.; Brùckel, B.; Muhlenhoff, U.; Lill, R. *Iron-sulfur protein maturation in human cells: evidence for a function of frataxin.* Human Molecular Genetics, 2004, **13**, 3007-15.

147. Muhlenhoff, U.; Richhardt, N.; Ristow, M.; Kispal, G.; Lill, R. *The yeast frataxin homolog Yfh1p plays a specific role in the maturation of cellular Fe/S proteins.* Human Molecular Genetics, 2002, **11**, 2025-36.

148. Adamec, J.; Rusnak, F.; Owen, W.G.; Naylor, S.; Benson, L.M.; Gacy, A.M.; Isaya, G. *Iron-dependent self-assembly of recombinant yeast frataxin: implications for Friedreich ataxia.* Human Molecular Genetics, 2000, **67**, 549-62.

149. Schagerlof, U.; Elmlund, H.; Gakh, O.; Nordlund, G.; Hebert, H.; Lindahl, M.; Isaya, G.; Al-Karadaghi, S. *Structural basis of the iron storage function of frataxin*

from single-particle reconstruction of the iron-loaded oligomer. Biochemistry, 2008, **47**, 4948-54.

150. Schmucker, S.; Argentini, M.; Carelle-Calmels, N.; Martelli, A.; Puccio, H. *The in vivo mitochondrial two-step maturation of human frataxin.* Human Molecular Genetics, 2008, **17**, 3521-31.

151. Zaidi, A.; Singh, K.P.; Anwar, S.; Suman, S.S.; Equbal, A.; Singh, K.; Dikhit, K.R.; Bimal, S.; Pandey, K.; Das, P.; Ali, V. *Interaction of frataxin, an iron binding protein, with IscU of Fe-S clusters biogenesis pathway and its upregulation in AmpB resistant Leishmania donovani.* Biochimie, 2015, **115**, 120-35.

152. Gerber, J.; Muhlenhoff, U.; Lill, R. *An interaction between frataxin and Isu1/Nfs1 that is crucial for Fe/S cluster synthesis on Isu1.* European Molecular Biology Organization Reports, 2003, **4**, 906-11.

153. Aloria, K.; Schilke, B.; Andrew, A.; Craig, E.A. *Iron-induced oligomerization of yeast frataxin homologue Yfh1 is dispensable in vivo.* European Molecular Biology Organization Reports, 2004, **5**, 1096-101.

154. Li, H.; Gakh, O.; Smith, D.Y.; Isaya, G. *Oligomeric yeast frataxin drives assembly of core machinery for mitochondrial iron-sulfur cluster synthesis.* Journal of Biological Chemistry, 2009. **284**, 21971-80.

155. Cook, J.D.; Bencze, K.Z.; Jankovic, A.D.; Crater, A.K.; Busch, C.N.; Bradley, P.B.; Stemmler, A.J.; Spaller, M.R.; Stemmler, T.L. *Monomeric yeast frataxin is an iron-binding protein.* Biochemistry, 2006, **45**, 7767-77.

156. Yoon, T.; Dizin, E.; Cowan, J.A. *N-terminal iron-mediated self-cleavage of human frataxin: regulation of iron binding and complex formation with target proteins.* Journal of Biological Inorganic Chemistry, 2007, **12**, 535-42.

157. Huang, J.; Dizin, E.; Cowan, J.A. *Mapping iron binding sites on human frataxin: implications for cluster assembly on the ISU Fe-S cluster scaffold protein.* Jounal of Biological Inorganic Chemistry, 2008, **13**, 825-36.

158. Parent, A.; Elduque, X.; Cornu, D.; Belot, L.; Le Caer, J.; Grandas, A.; Toledano, M.B.; D'autrèaux, B. *Mammalian frataxin directly enhances sulfur transfer of NFS1 persulfide to both ISCU and free thiols.* Nature Communications, 2015, **6**, 5686-92.

159. Yoon, H.; Knight, S.A.B.; Pandey, A.; Pain, J.; Zhang, Y.; Pain, D.; Dancis, A. *Frataxin-bypassing Isu1: characterization of the bypass activity in cells and mitochondria.* Biochemistry, 2014, **459**, 71-81.

160. Bailey, T.S.; Zakharov, L.N.; Pluth, M.D. *Understanding hydrogen sulfide storage: probing conditions for sulfide release from hydrodisulfides.* Jornal of American Chemical Society, 2014, **136**, 10573-6.

161. Beinert, H. *Semi-micro methods for analysis of labile sulfide and of labile sulfide plus sulfane sulfur in unusually stable iron sulfur proteins.* Analytical Biochemistry, 1983, **131**, 373-78.

162. Johnson, D.C.; Dean, D.R.; Smith, A.D.; Johnson, M.K. *Structure, function, and formation of biological iron-sulfur clusters.* Annual Review of Biochemistry, 2005, **74**, 247-81.

163. Baradaran, R.; Berrisford, J.M.; Minhas, G.S.; Sazanov, L.A. *Crystal structure of the entire respiratory complex I.* Nature. 2013, **494**, 443-8.

164. Sun, F.; Huo, X.; Zhai, Y.; Wang, A.; Xu, J.; Su, D.; Bartlam, M.; Rao, Z. *Crystal structure of mitochondrial respiratory membrane protein complex II.* Cell, 2005, **121**, 1043-57.

165. Zhang, Z.; Huang, L.; Shulmeister, V.M.; Chi, Y.; Kim, K.K.; Hung, L.; Crofts, A.R.; Berry, E.A.; Kim, S. *Electron transfer by domain movement in cytochrome bc1.* Nature, 1998, **392**, 677-84.

166. Cicchillo, R.M.; Baker, M.A.; Schnitzer, E.J.; Newman, E.B.; Krebs, C.; Booker, S.J. *Escherichia coli L-serine deaminase requires a [4Fe-4S] cluster in catalysis.* Jornal of Biological Chemistry, 2004, **279**, 32418-25.

167. Lauble, H.; Kennedy, M.C.; Beinert, H.; Stout, C.D. *Crystal structures of aconitase with isocitrate and nitroisocitrate bound.* Biochemistry, 1992, **31**, 2735-48.

168. Shisler, K.A.; Broderick, J.B. *Emerging themes in radical SAM chemistry.* Current Opinion in Structural Biology. **22**, 701-10.

169. Crack, J.C.; Green, J.; Hutchings, M.I.; Thomson, A.J.; Le Brun, N.E. *Bacterial iron-sulfur regulatory proteins as biological sensor-switches.* Antioxidants & Redox Signaling, 2012, **17**, 1215-31.

170. Muhlenhoff, U.; Lill, R. *Biogenesis of iron-sulfur proteins in eukaryotes: a novel task of mitochondria that is inherited from bacteria.* Biochimica et Biophysica Acta, 2000, **1459**, 370-82.

171. Bonomi, F.; Iametti, S.; Ta, D.; Vickery, L.E. *Multiple turnover transfer of [2Fe2S] clusters by the iron-sulfur cluster assembly scaffold proteins IscU and IscA.* Journal of Biological Chemistry, 2005, **280**, 29513-18.

172 Tokumoto, U.; Takahashi, Y. *Genetic analysis of the isc operon in Escherichia coli involved in the biogenesis of cellular iron-sulfur proteins.* Journal of Biochemistry, 2001, **130**, 63-71.

173. Tan, G.; Lu, J.; Bitoun, J.P.; Huang, H.; Ding, H. *IscA/SufA paralogs are required for the [4Fe-4S] cluster assembly in enzymes of multiple physiological pathways in Escherichia coli under aerobic growth conditions.* Biochemical Journal, 2009, **420**, 463-72.

174. Angelini, S.; Gerez, C.; de Choudens, O.; Sanakis, Y.; Fontecave, M.; Barras, F.; Py, B. *NfuA, a new factor required for maturing Fe/S proteins in Escherichia coli under oxidative stress and iron starvation conditions.* Journal of Biological Chemistry, 2008, **283**, 14084-91.

175. Rodriguez-Manzaneque, M.T.; Ros, J.; Cabiscol, E.; Sorribas, A.; Herrero, E. *Grx5 glutaredoxin plays a central role in protection against protein oxidative damage in Saccharomyces cerevisiae.* Molecular Biology of the Cell, 2002, **13**, 1109-21.

176. Rodriguez-Manzaneque, M.T.; Tamarit, J.; Belli, G.; Ros, J.; Herrero, E. *Grx5 is a mitochondrial glutaredoxin required for the activity of iron/sulfur enzymes.* Molecular Biology of the Cell, 2002, **13**, 1109-21.

177. Holmgren, A. *Hydrogen donor system for Escherichia coli ribonucleoside-diphosphate reductase dependent upon glutathione.* Proceedings of the National Academy of Sciences USA, 1976, **73**, 2275-79.

178. Chrestensen, C.A.; Starke, D.W.; Mieyal, J.J. *Acute cadmium exposure inactivates thioltransferase (Glutaredoxin), inhibits intracellular reduction of protein-glutathionyl-mixed disulfides, and initiates apoptosis.* Journal of Biological Chemistry, 2000, **275**, 26556-65.

179. Davis, D.A.; Newcomb, F.A.; Starke, D.W.; Ott, D.E.; Mieyal, J.J.; Yarchoan, R. *Thioltransferase (glutaredoxin) is detected within HIV-1 and can regulate the activity of glutathionylated HIV-1 protease in vitro.* Journal of Biological Chemistry, 1997, **272**, 25935-40.

180. Couturier, J.; Ströher, E.; Albetel, A.N.; Roret, T.; Muthuramalingam, M.; Tarrago, L.; Seidel, T.; Tsan, P.; Jacquot, A.P.; Johnson, M.K.; Dietz, K.J.; Didierjean, C. Rouhier, N. *Arabidopsis chloroplastic glutaredoxin C5 as a model to explore molecular determinants for iron-sulfur cluster binding into glutaredoxins.* Journal of Biological Chemistry, 2011, **286**, 27515-27.

181. Iwema, T.; Picciocchi, A.; Traore, D.A.K.; Ferrer, J.; Chauvat, F.; Jacquamet, L. *Structural basis for delivery of the intact [Fe2S2] cluster by monothiol glutaredoxin.* Biochemistry, 2009, **48**, 6041-43.

182. Johansson, C.; Kavanagh, K.L.; Gileadi, O.; Oppermann, U. *Reversible sequestration of active site cysteines in a 2Fe-2S-bridged dimer provides a*

mechanism for glutaredoxin 2 regulation in human mitochondria. Journal of Biological Chemistry, 2007, **282**, 3077-82.

183. Johansson, C.; Roos, A.K.; Montano, S.J.; Sengupta, R.; Fillipakopoulus, P.; Guo, K.; et al. *The crystal structure of human GLRX5: iron-sulfur cluster co-ordination, tetrameric assembly and monomer activity.* Biochemical Journal, 2011, **433**, 303-11.

184. Rouhier, N.; Unno, H.; Bandopadhyay, S.; Masip, L.; Kim, S.; Hirasawa, M; et al. *Functional, structural, and spectroscopic characterization of a glutathione-ligated [2Fe-2S] cluster in poplar glutaredoxin C1.* Proceedings of the National Academy of Sciences USA, 2007, **104**, 7379-84.

185. Feng, Y.; Zhong, N.; Rouhier, N.; Hase, T.; Kusunoki, M.; Jacquot, J.; Jin, C.; Bin, Xia. *Structural insight into poplar glutaredoxin C1 with a bridging iron-sulfur cluster at the active site.* Biochemistry, 2006, **45**, 7998-8008.

186. Dhalleine, T.; Rouhier, N.; Couturier, J. *Putative roles of glutaredoxin-BolA holo-heterodimers in plants.* Plant Signaling & Behavior, 2014, **9**, 28564.

187. Li, H.; Mapolelo, D.T.; Dingra, N.N.; Naik, S.G.; Lees, N.S.; Hoffman, B.M.; Riggs-Jelasco, P.J.; Huynh, B.H.; Johnson, M.K.; Outten, C.E. *The yeast iron regulatory proteins Grx3/4 and Fra2 form heterodimeric complexes containing a [2Fe-2S] cluster with cysteinyl and histidyl ligation.* Biochemistry, 2009, **48**, 9569-81.

188. Shakamuri, P.; Zhang, B.; Johnson, M.K. *Monothiol glutaredoxins function in storing and transporting [Fe(2)S(2)] clusters assembled on IscU scaffold Proteins.* Journal of the American Chemical Society, 2012, **134**, 15213-16.

189. Muhlenhoff, U.; Gerber, J.; Richhardt, N.; Lill, R. *Components involved in assembly and dislocation of iron-sulfur clusters on the scaffold protein Isu1p.* European Molecular Biology Organization Journal, 2003, **22**, 4815-25.

190. Takahashi, Y.; Nakamura, M. *Functional assignment of the ORF2-iscS-iscU-iscA-hscB-hscA-fdx-ORF3 gene cluster involved in the assembly of Fe-S clusters in Escherichia coli.* Journal of Biochemistry, 1999, **126**, 917-26.

191. Nuth, M.; Cowan, J.A. *Iron-sulfur cluster biosynthesis: characterization of IscU-IscS complex formation and a structural model for sulfide delivery to the [2Fe-2S] assembly site*. Journal of biological inorganic chemistry, 2009, **14**, 829-839.

192. Yan, R.; Konarev, P.V.; Adinolfi, S.; Roche, B.; Kelly, G.; Simon L.;Martin, S.R.; Py, B.; et al. *Ferredoxin competes with bacterial frataxin in binding to the desulfurase IscS*. Journal of Biological Chemistry, 2013, **288**, 24777-87.

193. Bandyopadhyay, S.; Chandramouli, K.; Johnson, M.K. *Iron-sulfur cluster biosynthesis.* Biochemical Society Transactions, 2008, **36**, 1112-9.